MOUNTAIN-PLAINS CONSORTIUM

MPC 24-555 | R. Ghabchi and D. Datta

ELECTROSPUN RECYCLED POLYETHYLENE TEREPHTHALATE MICROFIBERS AS AN ASPHALT BINDER MODIFIER

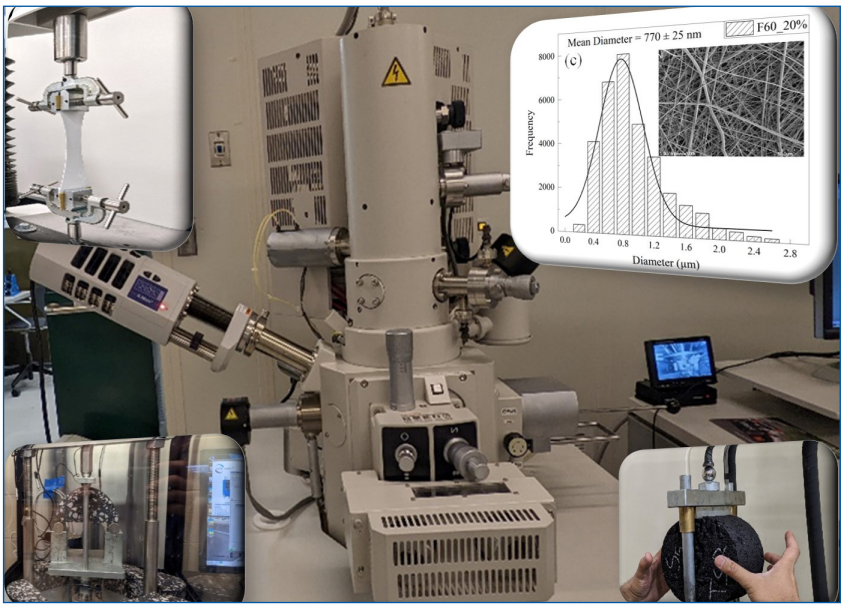

MOUNTAIN-PLAINS CONSORTIUM REGION 8

A University Transportation Center sponsored by the U.S. Department of Transportation serving the Mountain-Plains Region. Consortium members:

Colorado State University
North Dakota State University
South Dakota State University
University of Colorado Denver
University of Denver
University of Utah
Utah State University
University of Wyoming

Technical Report Documentation Page

1. Report No.	2. Government Accession No.	3. Recipient's Catalog No.
MPC-664		

4. Title and Subtitle	5. Report Date
Electrospun Recycled Polyethylene Terephthalate Microfibers as an Asphalt Binder Modifier	September 2024
	6. Performing Organization Code

7. Author(s)	8. Performing Organization Report No.
Rouzbeh Ghabchi, PhD, PE Debbrata Datta	MPC 24-555

9. Performing Organization Name and Address	10. Work Unit No. (TRAIS)
Department of Civil and Environmental Engineering South Dakota State University Brookings, SD 57007	11. Contract or Grant No.

12. Sponsoring Agency Name and Address	13. Type of Report and Period Covered
Mountain-Plains Consortium North Dakota State University PO Box 6050, Fargo, ND 58108	Final Report
	14. Sponsoring Agency Code

15. Supplementary Notes

Supported by a grant from the US DOT, University Transportation Centers Program

16. Abstract

Fibers are used in an asphalt mix to improve its durability and resistance against distresses, such as rutting and cracking. Consequently, accurate rheological and performance characterization of asphalt binders and mixes containing fibers is of vital importance. With increased concerns over the environmental disruptions resulting from disposing of end-of-life plastics in landfills and the need to improve the sustainability of construction materials, incorporating plastic in construction materials has always been considered an effective method for recycling and reducing waste sent to landfills. In this study, the end-of-life polyethylene terephthalate (PET) plastic obtained from bottled water containers was used to produce PET microfibers using the electrospinning technique. The electrospun PET microfibers (EPM) produced through various PET concentrations in electrospinning solutions were used as an asphalt additive. It was found that adding EPM to asphalt mixes improved their resistance to rutting, moisture-induced damage, and cracking compared to mixes that did not contain any EPM. At the asphalt binder level, an increase in EPM content resulted in an improvement in the binder's high-temperature PG grade, while different variations were observed in its low-temperature grade, depending on the EPM content. Overall, it was concluded that incorporating EPM in asphalt mixes can potentially be a feasible approach to reduce plastic landfills and improve the performance and sustainability of the ground transportation system.

17. Key Word	18. Distribution Statement
bituminous binders, cracking, elasticity (mechanics), nondestructive tests, plastics, recycled materials	Public distribution

19. Security Classif. (of this report)	20. Security Classif. (of this page)	21. No. of Pages	22. Price
Unclassified	Unclassified	69	n/a

Form DOT F 1700.7 (8-72) Reproduction of completed page authorized

ELECTROSPUN RECYCLED POLYETHYLENE TEREPHTHALATE MICROFIBERS AS AN ASPHALT BINDER MODIFIER

Rouzbeh Ghabchi, Ph.D., P.E.
Associate Professor
Department of Civil and Environmental Engineering
South Dakota State University
Brookings, SD 57007

Debbrata Datta
Graduate Research Assistant
Department of Civil and Environmental Engineering
South Dakota State University
Brookings, SD 57007

September 2024

Acknowledgment

The study presented herein was conducted with support from the Mountain-Plains Consortium (MPC), a University Transportation Center funded by the United States Department of Transportation through project MPC-664. The contributions of Ingevity Co., Bowes Construction Co., Jebro Co., Flint Hills Co., and GCC Ready Mix Co. are highly appreciated.

Disclaimer

This report's contents reflect the views of the authors, who are responsible for the facts and the accuracy of the information presented. This document is disseminated under the Department of Transportation's sponsorship, a University Transportation Centers Program, in the interest of information exchange. The U.S. Government assumes no liability for the contents or use thereof.

NDSU does not discriminate in its programs and activities on the basis of age, color, gender expression/identity, genetic information, marital status, national origin, participation in lawful off-campus activity, physical or mental disability, pregnancy, public assistance status, race, religion, sex, sexual orientation, spousal relationship to current employee, or veteran status, as applicable. Direct inquiries to: Vice Provost, Title IX/ADA Coordinator, Old Main 201, 701-231-7708, ndsu.eoaa@ndsu.edu.

ABSTRACT

Fibers are used in an asphalt mix to improve its durability and resistance against distresses, such as rutting and cracking. Consequently, accurate rheological and performance characterization of asphalt binders and mixes containing fibers is of vital importance. With increased concerns over the environmental disruptions resulting from disposing of end-of-life plastics in landfills and the need to improve the sustainability of construction materials, incorporating plastic in construction materials has always been considered an effective method for recycling and reducing waste sent to landfills. In this study, the end-of-life polyethylene terephthalate (PET) plastic obtained from bottled water containers was used to produce PET microfibers using the electrospinning technique. The electrospun PET microfibers (EPM) produced through various PET concentrations in electrospinning solutions were used as an asphalt additive. It was found that adding EPM to asphalt mixes improved their resistance to rutting, moisture-induced damage, and cracking compared to mixes that did not contain any EPM. At the asphalt binder level, an increase in EPM content resulted in an improvement in the binder's high-temperature PG grade, while different variations were observed in its low-temperature grade, depending on the EPM content. Overall, it was concluded that incorporating EPM in asphalt mixes can potentially be a feasible approach to reduce plastic landfills and improve the performance and sustainability of the ground transportation system.

TABLE OF CONTENTS

LIST OF TABLES

LIST OF FIGURES

EXECUTIVE SUMMARY

Despite attempts to recycle plastic waste into economically valuable products, approximately 25% of the total plastic waste undergoes recycling, leaving a significant amount in landfills, rivers, and oceans. To increase the amount of recycled plastic, incorporating waste plastic in construction materials is proven to be a feasible yet cost-effective method to boost construction sustainability and address a global environmental challenge. Asphalt mixes, one of the world's prominent paving materials, is a potential candidate for recycling plastics. Researchers have incorporated recycled polyethylene terephthalate (PET) plastics in asphalt mixes in two forms: (i) crushed (synthetic aggregate replacement) and (ii) chemically processed PET. For example, studies have recycled PET as a synthetic aggregate in asphalt mixes. However, it was not reported that PET aggregates significantly enhanced the performance of mixes compared to those that did not contain PET aggregates. Other studies in which micronized PET was used as an asphalt binder modifier have reported an improved resistance to rutting and cracking compared to those without micronized PET. The industry has yet to thoroughly explore the overall performance of asphalt binders and mixes containing PET. As a response to this need, a laboratory study was conducted to introduce electrospun PET microfiber (EPM) as an asphalt binder modifier and asphalt mix additive to increase the recycling rates and generate a value-added product from waste PET plastic bottles, mainly used in the beverage industry. For this purpose, a solution-based electrospinning method was employed in the laboratory to produce EPM by using different concentrations of PET in the solution and flow rates. Then, the effects of EPM as an additive on asphalt binder and mix properties were investigated. EPM was produced from a solution of PET in a mix of dichloromethane (DCM) and trifluoroacetic acid (TFA). Two PET concentrations were utilized, namely 15% and 20%, and various solution flow rates, namely 40, 50, 60, 120, and 250 μL/min. Fourier transform infrared (FTIR) spectroscopy, scanning electron microscopy (SEM), and tensile strength tests were conducted on EPMs to characterize their chemical composition, mechanical properties, and morphology. It was found that the electrospinning parameters and solution proportions did not alter the molecular structure of the PET. Also, the diameter of the EPMs decreased with a reduction in flow rates at constant PET concentrations. In addition, morphological examination of SEM micrographs suggested the most uniform and smooth fibers were consistently produced at the lowest flow rate. Increasing the flow rates resulted in forming fibers with rough textures, non-uniform in shape and size, and fractured. It was found the fibers having smaller diameters resulted in an enhancement in their mechanical properties. Given the findings pertinent to the EPM's chemical composition, morphological characteristics, mechanical properties, and fiber yield, electrospinning using a solution of 20% PET concentration and a flow rate of 60 μL/min resulted in EPMs of the highest mechanical and morphological properties. The EPM produced using the specified electrospinning method was used to modify the PG 58-28 asphalt binder and mix. For this purpose, different amounts of EPM, namely 0.2, 0.5, 0.7, and 1.0% (by asphalt binder weight), were blended with a PG 58-28 asphalt binder. Testing EPM-containing asphalt binders showed that an increase in EPM content increased resistance to rutting and fatigue and improved high-temperature PG grade compared to neat binders. It was concluded that using EPM as an asphalt binder modifier is an effective method for improving the mechanical properties of asphalt binders while addressing environmental concerns and preserving natural resources. The performance of asphalt mixes containing different amounts of EPM was also assessed by conducting tests on asphalt mixes. It was observed that adding EPM to asphalt mixes improved their resistance to rutting, cracking, and moisture-induced damage compared to the mixes without any EPM. Based on the findings of this study, incorporating EPM in asphalt mixes is a potentially feasible approach to reduce plastic landfills and improve the performance and sustainability of the ground transportation system.

1. INTRODUCTION

1.1 Problem Statement

Water bottle container production in the United States consumes more than 17 million barrels of petroleum annually. Out of this amount, more than 8.8 billion plastic bottles end up in landfills (Pacific Institute, 2007). It is expected that more than 80% of the Polyethylene Terephthalate (PET) water bottles in the United States will be landfilled and added to more than two million tons of existing landfilled waste PET bottles (Resource Recycling, 2012). In 2018, only 26.8% of PET bottles and jars were recycled in the United States (U.S. EPA, 2020). As a result, waste PET, widely used in beverage packaging and bottled water, has become an environmental challenge. Its high elasticity, highly stable polymer backbone, crystallinity, and hydrophobicity make PET a strong candidate for recycling in asphalt mixes. Due to its mechanical properties, incorporating an engineered form of PET in asphalt mixes can enhance their performance. PET has been recycled and used in asphalt mixes in two primary forms: (a) crushed PET and (b) chemically processed PET. While using recycled PET as synthetic aggregate in asphalt mixes has been found to be feasible (Hassani et al., 2005; Ahmadinia et al., 2012; Moghaddam et al., 2012; Modarres and Hamedi, 2014a,b), it was not reported to significantly improve the mix performance when compared to that of mixes containing no PET aggregates. In other studies in which micronized PET as an asphalt binder modifier was used, a meaningful improvement in the resistance of asphalt mixes to rutting and cracking was achieved (Ghabchi et al., 2021b; Almeida e Silva et al., 2015, 2018). However, PET-modified binders' storage stability issues, thermal incompatibility of the micronized PET with asphalt mix, and low efficiency of the milling process used for producing micronized PET were found to be several challenges associated with this recycling technique. In other studies in which chemical processing of PET was used to incorporate it in asphalt mixes (Merkel et al., 2020; Leng et al., 2018a,b), an improved resistance to rutting, fatigue, and low-temperature cracking as a result of using chemically-processed PET-modified asphalt binder compared to those of virgin binder was reported. While promising improvements in the performance of asphalt mixes by using chemically processed PET were observed, the amount of energy required for chemical reaction, the need for several chemicals, and toxic byproducts add to the cost and environmental concerns associated with this recycling technique. This study was conducted to address environmental concerns related to PET waste and overcome preceding challenges associated with existing methods for recycling PET in asphalt mixes. Also, this study aimed to integrate PET into the load-bearing structure of asphalt mix to benefit its performance from the superior mechanical properties of PET. These goals were achieved by producing microfibers from PET waste in the laboratory by applying electrospinning, a scalable and economically feasible technique. As a result, the Electrospun PET Microfiber (EPM) was produced in the laboratory. The structure and morphology of the produced EPM were characterized by applying different imaging techniques. Also, the effects of EPM modification of asphalt binders (with varying amounts of EPM) on their rheological, mechanical, and adhesion properties were studied by following a comprehensive laboratory testing program. Furthermore, the effects of EPM-modified asphalt binders in mixes on their resistance to cracking, rutting, and stripping were evaluated by testing laboratory-prepared specimens. The outcomes of this study are expected to be applied as a pathway and a novel approach for recycling PET waste in asphalt mixes, which, in turn, addresses a critical environmental challenge. In addition, an improvement in asphalt mix performance in terms of resistance to cracking, rutting, and moisture-induced damage was achieved as a result of using EPM-modified asphalt binders in mixes, which is expected to enhance sustainability, durability and economic feasibility of asphalt pavements and ground transportation system.

1.2 Research Objectives

The specific objectives of this study are as follows:

1. Produce PET microfibers in the laboratory by applying a solvent-based electrospinning technique using recycled PET as feedstock.
2. Determine the effect of electrospinning parameters, namely PET concentration and flow rate, on the electrospun PET microfibers (EPM) properties. More specifically, it aims to characterize the tensile strength, morphology, and chemical structure of the produced EPM by conducting tensile strength tests and applying scanning electron microscopy (SEM) and Fourier-transform infrared (FTIR) spectroscopy.
3. Incorporate 0%, 0.2%, 0.5%, 0.7%, and 1.0 % of EPM by the weight of binder in non-polymer modified PG 58-28 asphalt binder; and characterize EPM-modified PG 58-28 asphalt binder containing different amounts of EPM and neat PG 58-34, and PG 64-28 (as polymer-modified binder baselines) by conducting dynamic shear rheometer (DSR), bending beam rheometer (BBR), multiple stress creep and recovery (MSCR), and binder bond strength (BBS) tests.
4. Characterize the effect of using EPM on the resistance of asphalt mixes to cracking, rutting, and moisture-induced damage by conducting semicircular bend (SCB), Hamburg wheel tracking (HWT), and tensile strength ratio (TSR) tests, respectively.

1.3 Study Scope and Tasks

Specific tasks carried out in the study are as follows:

1. Prepare an electrospinning solution and produce EPMs at different flow rates using the static electrospinning technique.
2. Characterize the tensile strength, morphology, and chemical structure of the produced EPM by conducting tensile strength tests and applying SEM and FTIR spectroscopy.
3. Select the optimum flow rate and ground PET amount for the mass production of fibers based on the characteristics of the fibers produced and observations made during electrospinning.
4. Collect three types of asphalt binders, namely PG 58-28, PG 64-28, PG 58-34, and five types of aggregates stockpiles (commonly used for the production of asphalt mixes in South Dakota and elsewhere in the Upper Midwest region).
5. Determine the actual PG grade of the asphalt binders conducting dynamic shear rheometer (DSR) and bending beam rheometer (BBR) tests following AASHTO T315 (AASHTO, 2017) and AASHTO T313 (AASHTO, 2017) standard methods, respectively.
6. Conduct multiple-stress creep and recovery (MSCR) test and determine the MSCR grade of the asphalt binders following the AASHTO T350 (AASHTO, 2017) standard method.
7. Conduct binder bond strength (BBS) tests following AASHTO T361 (AASHTO, 2017) and assess the adhesion quality of the binder blends containing EPM.
8. Design a Superpave asphalt mix in the laboratory using the volumetric mix design method for a given aggregate structure.
9. Prepare asphalt mixes using the achieved mix design containing various amounts of EPM.

10. Determine the effect of EPM contents in HMA mixes on their resistance to rutting, cracking, and moisture-induced damage following AASHTO T 324 (AASHTO, 2011), ASTM D8044 (ASTM, 2017), and AASHTO T 283 (AASHTO, 2011) standard methods, respectively.
11. Analyze and report the test results and draw conclusions.

1.4 Report Organization

This report is organized in the following order:

Chapter 1: Introduction – This chapter includes the problem statement, research objectives, study scope and tasks, and the organization of the report.

Chapter 2: Background –This chapter summarizes the literature review, focusing on the methods used to characterize the effects of deicing agents and moisture-induced damage on asphalt mixes.

Chapter 3: Materials and Methods – This chapter describes the selection and collection of the materials, sample preparation in the laboratory, and methodologies used for the laboratory characterization of the asphalt mixes and binders containing EPM.

Chapter 4: Results and Discussions: This section summarizes and presents the results of testing EPM, asphalt binders, asphalt binder-aggregate systems, and asphalt mixes. More specifically, it presents the outcomes of the FTIR, SEM, DSR, BBR, BBS, SCB, HWT, and TSR tests.

Chapter 5: Conclusions and Recommendations– Important findings of this study and recommendations based on these findings are presented in this chapter.

2. BACKGROUND

2.1 Asphalt Industry: Pioneer in Recycling and Sustainability

The construction industry utilizes eco-friendly materials to reduce the environmental impact of human activities. These materials can either be made from recycled materials to conserve energy or be designed to minimize natural resource consumption. Multiple studies have shown that incorporating waste materials, such as coconut shells, coconut fibers, chitosan, lignin, date seed ash, bio-fuel byproducts, and ground tire rubber, among others, into asphalt pavement can enhance the mix's properties **(**Chen and Wong, 2013; Cheng and Wong, 2015; Sangiorgi et al., 2016; Ghabchi, 2022; Ghabchi and Castro, 2022; Ghabchi and Castro, 2021a,b; Ghabchi et al., 2021a,b). Sangiorgi et al. (2016) investigated the utilization of bentonite as a replacement for limestone fillers in asphalt mixes. The results demonstrated substituting bentonite for limestone did not significantly reduce air void and increased the ITS of the mix. Also, the addition of bleaching clay increased the indirect tensile stiffness modulus, but particle loss in the mixture was twice as high as in the reference mixture due to varying embrittlement. According to a study by Zhang et al. (2018), increasing the filler-to-binder ratio reduces particle loss and permeability, regardless of the filler type, due to blocking air voids. Chen et al. (2005) studied using fully recycled concrete aggregates (RCAs) in asphalt mixes. The study revealed RCAs have a high absorptive capacity due to their low density and high porosity, resulting in a high abrasion value. Nevertheless, the abrasion loss, drain-down value, and moisture susceptibility were within acceptable ranges. Chen and Wong (2017) reported that hybrid composites (78% RCA and 16% glass material) also have a high binder absorption rate, necessitating a higher binder content for adequate bonding. Mohammadinia et al. (2018) studied recycled ground tires in asphalt pavement. The results demonstrated that adding ground tires as aggregate replacement increased the asphalt mix rigidity by strengthening the interfacial bonds. Based on these findings, it was suggested both recycled concrete aggregates and recycled tires could be utilized in asphalt pavements without compromising their performance

2.2 Recycled Waste Plastic in HMA

Hot mix asphalt (HMA) is a composite material consisting of aggregates and asphalt binder primarily used to build roads and airport pavements. Asphalt mix is the primary material used in pavement construction, accounting for 93% of the 2.7 million miles of paved roads in the United States. Asphalt pavements may experience different distresses, such as rutting (permanent deformation), raveling, fatigue cracks, moisture-induced damage, and low-temperature (L-T) cracks, among other distresses. Consequently, to improve the quality and durability of asphalt pavements, the pavement industry continually researches materials and methods to enhance the engineering properties of asphalt binder and mix. For example, incorporating different types of additives, such as polymers, fibers, adhesion boosters, and asphalt recycling agents, into the HMA is known as an effective method to improve the engineering properties of asphalt binders and mixes. Various types of polymers and fibers used in asphalt binders as additives can enhance their resistance to rutting and cracking, extending their service life. For example, It was reported that incorporating fibers in asphalt mixes can potentially prevent asphalt binder bleeding (Serfass and Samanos, 1996; Hassan et al., 2005), improve its viscoelastic properties (Peltonen, 1991a; Huang and White, 1996), enhance creep compliance and resistance to rutting (Putman and Amirkhanian, 2004), and improve resistance to moisture-induced damage (Wu et al., 2008). It has also been reported that incorporating fibers in asphalt mixes reduced reflective cracks compared to mixes that did not contain fibers (Chen et al., 2004; Tapkin, 2008). Other studies have found fibers in asphalt mixes can help improve their resistance to low-temperature cracks, fatigue cracks, and overall enhanced durability (Huang, 2004; Maurer and Malasheskie, 1989; Lee et al., 2005; Freeman et al., 1989). Several other properties of asphalt mixes, including wear resistance (Hassan et al., 2005), toughness, tensile strength, dynamic modulus (Wu et al., 2007), and elasticity (Peltonen, 1991b) are reported to improve as a result of

incorporating fibers in the HMA. However, adding fiber may increase the need for additional compaction efforts to attain the same density of the HMA without any fiber (Peltonen, 1991a). Two methods are used to incorporate fibers in HMA: (i) modification of the asphalt binder (terminal blending) and (ii) addition of fibers to asphalt mix (plant mixing). Currently, a variety of fibers, including lignin, cellulose, basalt, and polyester fibers, are successfully incorporated into asphalt (Ghabchi and Castro, 2021b; Xiong et al., 2015).

PET, with its high melting point, thermal stability, tensile strength, stiffness, and chemical resistance (Dhaka et al., 2022; Ben Zair et al., 2021; Miao et al., 2021; and Ma et al., 2018) is widely utilized for various applications, including protective gear, membranes, vascular grafts, tissue scaffolding, filtration and packaging in beverage industries (Strain et al., 2015; Zander et al., 2016). Single-use PET plastics, such as beverage bottles, are frequently discarded in the environment, leading to serious environmental concerns (Koo et al., 2014). For example, researchers observed that as a form of microplastics, PET could enter the food chain, consumption of which can result in a decrease in the migration and proliferation of human mesenchymal stem cells in the bone marrow and endothelial progenitor cells (Dhaka et al., 2022). To mitigate the PET waste problem, research on the natural decomposition of plastics using specific bacterial micro-organisms is underway (Vo et al., 2018). Despite ongoing efforts, PET is still considered a non-biodegradable material (Ben Zair et al., 2021). In addition, the disposal of PET in landfills or burning it in the open air poses significant environmental and health risks (Chavan and Rao, 2016). Due to its single-use nature and the increase in the production of PET bottles year by year (NAPCOR, 2019), recycling and repurposing this stream of plastic waste should be an environmental and economic priority. Therefore, incorporating PET fiber in asphalt pavement is a potential solution to the plaswaste. However, before this can be achieved, it is important to explore the feasibility of using different forms of PET plastic in asphalt mixes. Some studies suggested that the addition of PET to asphalt mixes has the potential to improve its overall performance. Several researchers have previously introduced waste PET in asphalt as a form of asphalt binder modifier, partial replacement of asphalt binder, and partial or full aggregate replacement in asphalt mixtures. Researchers have incorporated recycled PET in asphalt mixes in two forms: as crushed PET (aggregate replacement) or as chemically processed PET. For example, some studies used recycled PET as a synthetic aggregate in asphalt mixes. However, it was not reported that the use of PET aggregates significantly enhanced the performance of mixes when compared to those that did not contain PET aggregates (Hassani et al., 2005; Ahmadinia et al., 2012; Moghaddam et al., 2012; Modarres and Hamedi, 2014a;2014b). Other studies in which micronized PET (PET) was used as an asphalt binder modifier have reported an improved resistance to rutting and cracking as compared to those without any PET (Ghabchi et al., 2021b; Silva et al., 2018). Additionally, incorporating PET in asphalt binder improved its adhesion to aggregates and its resistance to moisture-induced damage. Those findings also suggested challenges associated with the storage stability, thermal incompatibility of micronized PET with asphalt, and the inefficiency of the milling process used to produce micronized PET to be among the main obstacles to recycling particulate PET in HMA. Dos Santos Ferreira et al. (2022) investigated the mechanical properties of HMA containing recycled PET as an asphalt mix natural sand aggregate replacement. The thermogravimetric analysis demonstrated recycled PET can be incorporated into asphalt mixtures without experiencing thermal degradation up to 400 °C. The findings further indicated that replacing natural sand with 8% PET by volume did not impact the optimum asphalt binder content of the HMA because of the equivalence between binder consumption resulting from the rough surface of mineral aggregates forming agglomerations and the smooth surface of PET. Incorporating PET in the asphalt mix was found to lower maximum specific gravity and asphalt film thickness and increase the air void in the compacted mix. Replacing natural sand with PET was also found to improve the resistance to moisture-induced damage. Ma and Hesp (2022) investigated the effects of incorporating three types of commercially available PET fibers (with lengths of 6.5 mm and 18 mm) in an asphalt mix on its mechanical properties. It was found that the reinforcing effectiveness of the PET fibers and its effect on the cracking resistance of HMA depends on the length and diameter of the fibers. Specifically, longer fibers with larger diameters and rough surfaces were associated with increased cracking resistance

because of the higher interaction between asphalt binder and aggregates. Alternatively, in some studies (Merkel et al., 2020; Leng et al., 2018a,b), the chemical processing of PET for incorporating it into asphalt mixes has been investigated. It was reported that chemically processed PET-modified asphalt binders could enhance the resistance of asphalt binders to rutting, fatigue cracks, and low-temperature cracks compared to unmodified asphalt binders. Despite promising results, utilizing chemically processed PET in HMA can be energy-intensive, requires multiple chemicals, and may produce toxic byproducts (Merkel et al., 2020). These factors contribute to an increase in construction costs and environmental impact.

2.3 PET Plastic: A Strategic Choice for Recycling

PET can be synthesized by heating terephthalic acid and ethylene glycol, resulting in the formation of PET and a low-molecular-weight monomer polymer as a byproduct, which is characterized as a semicrystalline, thermoplastic polyester of high strength and transparency (Usman and Kunlin, 2024). The global PET market is projected to grow from $35.47 billion in 2021 to $39.23 billion in 2022 and further to $57.19 billion in 2026, with a compound annual growth rate (CAGR) of 10.6%. This indicates more PETs will be available in the global market soon. Additionally, a report published by the National Association for PET Container Resources (NAPCOR) revealed that in 2018, the U.S. market sold about 6,270 million pounds of PET bottles, but only 1,816 million pounds, or about 29.0%, were collected and resold through recycling programs. That means around 71% of PET bottles were left in the environment, waiting for recycling or landfilling. This amount is produced in only one year, increasing each year. In addition, the Association of Plastics Recyclers (APR) provided a detailed summary of the United States National Postconsumer Plastic Bottle Recycling Report (NAPCOR, 2019). It concluded that PET and high-density polyethylene (HDPE) bottles comprise 97.1% of the United States plastic bottle market. The rest of them are polypropylene (PP), low-density polyethylene (LDPE), and polyvinyl chloride (PVC). Although 98.9% of recycled plastics are either PET or HDPE, the last destinations for large amounts of plastic are landfills or the environment. Consequently, environmental pollution and toxicity of the waste PET have become a significant concern as debris has been found in groundwater, drinking water, soil, and the ocean (Smith et al., 2022). Furthermore, the infiltration of PET in the form of microplastics into food chains is a cause for concern due to the potential health risks it poses to humans, including the reduction in the migration and proliferation of human mesenchymal stem cells in the bone marrow and endothelial progenitor cells (Dhaka et al., 2022). Therefore, the widespread generation of waste PET needs a proper end-of-life management solution (Sulyman et al., 2016).

Waste PET bottles are primarily recycled by mechanical or chemical processes (Ben Zair et al., 2021; Khoonkari et al., 2015). This process involves grinding PET water bottles into flakes (NAPCOR, 2018). For instance, in 2019, 806 kilotons of recycled PET flakes were produced from 2,887 kilotons of post-consumer PET in the United States to manufacture recycled products such as fibers, sheets and films, strapping, and food and beverage bottles, among other products. These efforts accounted for 27.9% of total PET consumption (NAPCOR, 2019). Due to the technical challenges of reusing waste PET, its recycling rates are still low. Those challenges mainly consist of collection, sorting, reclaiming, and converting processes (Smith et al., 2022; Leng et al., 2018a). In addition, virgin PET's stable and low cost does not offer economic incentives for recycling (Vo et al., 2018). To generate value-added products from waste PET, it can be converted into nanofibers with high surface-to-volume ratio and porosity, which can replace virgin PET in highly valued applications such as batteries (Jung et al., 2016), sensors (Senthamizhan et al., 2014), tissue engineering (Santoro et al., 2016), pharmaceutical industry (Hu et al., 2014), and filter media (Bonfim et al., 2021). Many studies have been carried out to investigate the manufacturing of micro and nanofibers from PET plastics. For instance, Strain et al. (2015) synthesized nanofibrous isotropic membranes from recycled PET using a 30:70 weight ratio of DCM and TFA solutions, and then produced a PET mat for air filtration applications. Therefore, producing nano or microfibers from PET can be applied as a feasible technique for recycling.

2.4 Electrospun PET Fibers: Production and Characterization

Among fiber production techniques, electrospinning, one of the most rapidly growing commercial polymer processing methods, is widely used for manufacturing ultrathin nanofibers and nonwoven membranes. Electrospinning can be accomplished using two distinct approaches: (i) melt-spinning and (ii) solution-based electrospinning (Dasdemir et al., 2013). Heat is required to melt the material in melt-spinning, and repeated heating cycles degrade the material's mechanical properties (Beyler and Hirschler, 2002; Spinacé and De Paoli, 2001). Another drawback of this process is that the high viscosity of molten polymers makes it challenging to manufacture fragile, uniform fibers (Thompson et al., 2007). For this reason, solvent-based electrospinning is an alternative approach as it provides a high control over fiber morphology (Strain et al., 2015). In this approach, fibers are generated by applying an electric field to a polymer solution between two electrodes with opposite charges, one connected to the syringe containing the polymer solution and the other attached to a conductive collector. When electrostatic force overcomes the surface tension of a fiber-forming solution, electrospinning occurs, and a Taylor cone forms from solution droplets (Owida et al., 2022; Christiansen et al., 2021; Koenig et al., 2019**;** Xu et al., 2017; Zander et al., 2016; Doshi and Reneker, 1995). Also, in solution-based electrospinning, fiber morphology, geometry, and production rate are all influenced by various processing parameters, such as applied voltage, flow rate, nozzle diameter, collection distance, solution properties (including polymer molecular weight, concentration, electrical conductivity, surface tension, and solvent properties) and ambient conditions, like temperature and humidity (Cramariuc et al., 2013; Tan et al., 2005).

Tensile strength, elongation, Young's modulus, and Poisson's ratio are critical mechanical properties of EPM. Zhang et al. (2011) prepared fiber specimens of 7 mm width and 15 mm length and evaluated their mechanical properties in a tension test. On the other hand, Strain et al. (2015) employed a templated transfer approach (TTA) to determine the tensile strength of fibers. Tensile strength was calculated as the highest stress supported during the test, Young's modulus as the initial linear slope of the stress-strain curve, and toughness as the total area under the stress-strain curve. Vo et al. (2018) tested fiber samples with a universal tensile testing machine (gauge length: 20 mm, crosshead speed: 0.5 mm/s) at 20°C and 30% relative humidity (RH). Kim et al. (2011) determined tenacity, elongation at the failure point and Young's modulus of single fibers. FTIR spectroscopy was utilized by researchers to understand the chemical composition of different plastics. Using FTIR with a wavenumber range of 4,000 to 400 cm^{-1}, the functional groups of produced PET fiber mats can be determined (Abbas et al., 2018; Espíndola-González et al., 2011). Determining the morphological properties of a fiber mat, such as fiber diameter and orientation, is a complex process for which no well-established method exists. Scanning electron microscope (SEM) is widely used for the morphological analysis of the electrospun fibers (e.g**.,** Vo et al., 2018**;** Xu et al., 2017; He et al., 2015; Wang et al., 2013; Li et al., 2012; Ogata et al., 2007). Li et al. (2012) used energy dispersion spectroscopy for chemical analysis while conducting the SEM test. The SEM test does not directly provide the diameter of the fiber; instead, it will produce a scanned image of the fiber mat. Therefore, post-processing digital images generated by the SEM equipment can provide dimensions of the fibers (Xu et al., 2017; Vo et al., 2018; Li et al., 2012). Other techniques, such as using a micrometer and applying a digital magnifier, have been proposed to determine fibers' different dimensions (Zhang and Seeger, 2011).

Crystal orientation in the fiber bundle is also one of the essential parameters affecting their mechanical properties. Ogata et al. (2007**)** employed a spinning disk with a circumferential speed of approximately 1 mm/min to produce unidirectionally aligned PET fibers. He et al. (2015) utilized polarized FTIR spectroscopy to examine the crystal orientation of fibers in the amorphous regions. Other researchers used a differential scanning calorimeter (DSC) with a heating scan rate of 10°C/min in a temperature ranging from ambient temperature to 300°C in nitrogen to gain an understanding of the thermal properties of the fibers (Vo et al., 2018; He et al., 2015; Strain et al., 2015; Wang et al., 2013; Li et al., 2012; Ogata et al.,

2007). On the other hand, DSC thermograms were processed and obtained during the first heating of the fiber sample in the temperature range of 30 to 300°C at a rate of 20°C/min (Kim et al., 2011).

2.5 Asphalt Mixes Containing Fibers

Various additives are incorporated into asphalt mixes as modifiers to enhance pavement performance, prevent premature distress, and improve pavement longevity (Oruç et al., 2022). Fibers are added to enhance the mechanical properties of conventional dense-graded asphalt mixes (Kumbargeri and Biligiri, 2016; Großegger, 2016). Applying fiber-reinforced asphalt mixes in pavement construction improves resistance to rutting, fatigue cracking, and moisture-induced damage (Goel and Das, 2004). In fiber-reinforced asphalt, some portion of traffic-induced shear and tensile stresses in asphalt mix is transferred to the fiber, improving its resistance to rutting and cracking. This performance benefit depends on the type, mechanical properties, shape, length, thickness, and amount of the fibers incorporated in an asphalt mix (Ali et al., 2020; Park et al., 2015). However, the addition of fibers can result in an increase in binder stiffness, which may lead to dryness and brittleness of pavement and other problems (Chen and Lin, 2005). In some applications, fibers prevent bleeding in mixes with high binder content (Shukry et al., 2016). In addition, fibers in asphalt reduce water flow through interconnected voids (Marchioni and Becciu, 2015). There are numerous varieties of fibers, including polypropylene, polyester, asbestos, cellulose, carbon, steel, glass, and nylon fibers, each of which possesses its distinct material properties. These fibers have been utilized in asphalt mixes in various ways to improve their performance (Nelson et al., 2002; Ye et al., 2009; Abtahi et al., 2010). The efficacy of multiple types of fibers in pavement applications is summarized in the following sections.

2.5.1 Cellulose Fibers

Cellulose fibers produced from plants' bark, wood, or leaves have greater surface area than mineral or polyester fibers and a higher ability to bond with binder (Chen and Lin, 2005). According to a study conducted by Ye and Jian (2019), adding 0.3 to 0.5% cellulose fibers to an open-graded friction course (OGFC) better enhanced the binder's stability compared to polypropylene and polyester fibers. In addition, Afonso et al. (2017) discovered that, due to their high binder absorption capacity, cellulose fibers increase the rutting resistance of HMA but not the raveling resistance when combined with neat binders. In addition, incorporating cellulose fibers increased particle loss when tested using the Cantabro method in wet conditions. Andrés-Valeri et al. (2018) reported that cellulose fibers enhance raveling resistance up to a particular fiber content, beyond which raveling resistance begins to drop. As the fiber content exceeds the optimum binder content, the cohesiveness of the binder decreases, resulting in particle loss. However, when combined with modified binders, cellulose fibers can increase asphalt mixes' resistance to raveling.

2.5.2 Mineral and Glass Fibers

Mineral fibers are rigid and have the lowest softening point compared to polyester and cellulose fibers. Up to a specific optimal fiber concentration, the complex modulus of asphalt mixes containing mineral fibers increases, which results in increased stiffness and resistance to rutting. Beyond the optimum fiber content (OFC), the complex modulus of asphalt mixes decreases (Chen and Lin, 2005). Mineral fibers are effective at reducing binder bleeding (Ma et al., 2018; Tanzadeh et al., 2019), but in aged and unaged Cantabro tests, their efficacy is not found to be adequate. Glass fibers, on the other hand, can enhance indirect tensile strength (ITS) of asphalt mixes (Tanzadeh and Shahrezagamasaei, 2017; Chen and Lin, 2005). However, adding mineral fibers to an asphalt mix reduced its resistance to moisture-induced damage (Tanzadeh and Shahrezagamasaei, 2017). Adding glass fibers to asphalt mixes significantly increased their ITS value (Tanzadeh and Shahrezagamasaei, 2017; Tanzadeh et al., 2019; Enieb et al., 2021). In addition, it was found that incorporating glass fibers in a mix increased its binder absorption, resulting in an increase in air void and binder content without binder draining (Slebi-Acevedo et al., 2019). According to Wang et al. (2019), glass fibers also improve the cracking resistance of asphalt mixes, especially at low temperatures. Tanzadeh et al. (2019) reported that adding 12-millimeter-long glass fibers improved the mix's stiffness and tensile strength. This study also revealed the fibers reduced the permeability of the mix. In addition, glass fibers strengthened the asphalt mix's elastic properties by functioning as an elastic medium to improve the mix stiffness. Consequently, glass fibers are reported as a viable option for reducing permanent deformation in mixes (Enieb et al., 2019).

2.5.3 Steel Fibers

Steel fibers, when used as reinforcement, not only improve the mechanical properties of asphalt mixes but also can be used as a means to develop self-healing mixes (Karimi et al., 2018; Phan et al., 2018; Sun et al., 2016; Wang et al., 2016). When subjected to an electromagnetic field, the samples containing steel fibers can produce heat by generating currents in the conductive steel fibers. Consequently, the binder melts and heals the microfractures, preventing further crack propagation, a process known as self-healing (Liu et al., 2010). Additionally, incorporating steel fibers significantly enhances the resistance to particle loss (LastraGonzález et al., 2020). According to Lastra-Gonzalez et al. (2020), using steel wool and steel grit increases the ITS value, stiffness, and resistance to fatigue fracture of asphalt pavement. It is also reported that adding steel fibers to asphalt mixes does not impair workability, so they can be compacted with the same compaction effort required for asphalt mixes that do not contain fibers. In another study by Serin et al. (2012), fiber contents varying from 0 to 2.5% by the weight of binder content were evaluated. It was found that mixes containing 0.75% fiber showed the highest stability. The research also indicated high concentrations of very long steel fibers can contribute to the formation of clusters, resulting in lower stability values than fiber-free samples. This observation is consistent with those reported by Tabaković et al. (2019), who reported poor mixing and cluster formation may produce high-temperature zones that impair the specimen's structure.

2.5.4 Synthetic Fibers

Synthetic fibers commonly used in asphalt mixes are polypropylene, polyester, and aramid. The microstructure of those fibers helps them interlock with one another and improves the asphalt structure, resulting in a higher softening point. According to Tanzadeh et al. (2019), adding polypropylene fibers to asphalt reduces binder bleeding by up to 49% and increases strength by up to 50%. Adding glass fibers with polypropylene fibers produces even more promising results. These two combinations of fibers reduce drain by up to 80% and increase ITS by 65%. Notably, half of this improvement was solely attributable to polypropylene fibers, which function as a three-dimensional structure in the asphalt mix, enhancing binder stability and strength. On the other hand, adding polyester fibers enhanced resistance to raveling and overall stability. Ma et al. (2019) investigated using a modified binder with polyester, mineral, and cellulose fibers applied at a rate of 2.5% by aggregate weight. Polyester-containing mixes performed well in the wet Cantabro test, which indicated that adding fiber enhanced abrasion resistance and decreased susceptibility to moisture damage. The findings suggested mixes containing polyester fibers performed well under longer water immersion times and indicated the fibers substantially enhanced moisture resistance. Moreover, the thermal stress restrained specimen test demonstrated polyester fibers enhanced resistance to low-temperature cracking. However, using polyester fibers negatively affected the asphalt pavement's resilient modulus, strength, and permeability (Ma et al., 2018). The impact of incorporating polyolefin and aramid fibers into asphalt mixes depends on the binder type. For example, fibers used with unmodified binders are typically more effective than using them with SBS-modified binders (Kassem et al., 2018). Chen et al. (2008) investigated the functioning mechanism of mineral, cellulose, and polyester fibers in asphalt mixes. The findings revealed mineral fibers with smaller diameters are more durable than polyester fibers with larger diameters due to a greater interfacial area. In terms of tensile strength, however, polyester fibers outperformed mineral fibers.

This study was undertaken to address these environmental issues associated with recycling PET waste and to overcome the obstacles related to the existing recycling techniques used to incorporate PET into asphalt mixes. In addition, this study also covers the area of integrating PET into the load-bearing structure of asphalt mixes to capitalize on PET's superior mechanical properties. Lab-produced electrospun microfibers from waste PET bottles were used to accomplish these objectives. PET microfibers produced from waste PET by applying the solvent-based electrospinning technique were used. The PET fibers for this study were selected based on their superior mechanical properties and the significant environmental advantages that their recycling will result in. Several factors contributing to the use of PET for producing EPM are summarized as follows.

3. MATERIALS AND METHODS

3.1 Materials

3.1.1 Ground PET

The PET plastic used in this study was obtained from post-consumer water bottles. The stickers, caps, and bottle cap rings were removed and separated from the PET plastic to prepare the material for milling. Sorted PET was then cut into pieces no larger than 5 mm by 5 mm and dried at 45°C for 2 hours. According to a study by Ghabchi et al. (2021b), treating PET plastic pieces at low temperatures increases their fragility, resulting in greater milling efficiency. Hence, small fragments of PET were refrigerated at -18 °C for 4 hours before grinding. Next, a commercially available grinder with a double-blade rotor rotating at 15,000 rpm was utilized to grind approximately 10g of PET particles in each batch. After grinding, the PET particles were passed through a No. 4 sieve (4.75 mm) and collected for further evaluation (Figure 3.1). Any residual particles on the 4.75 mm sieve were added to the following grinding batch. This process was repeated several times until a sufficient amount of ground PET was obtained. The particle size distribution of the ground PET is presented in Figure 3.2.

Figure 3.1 A photographic view of ground PET

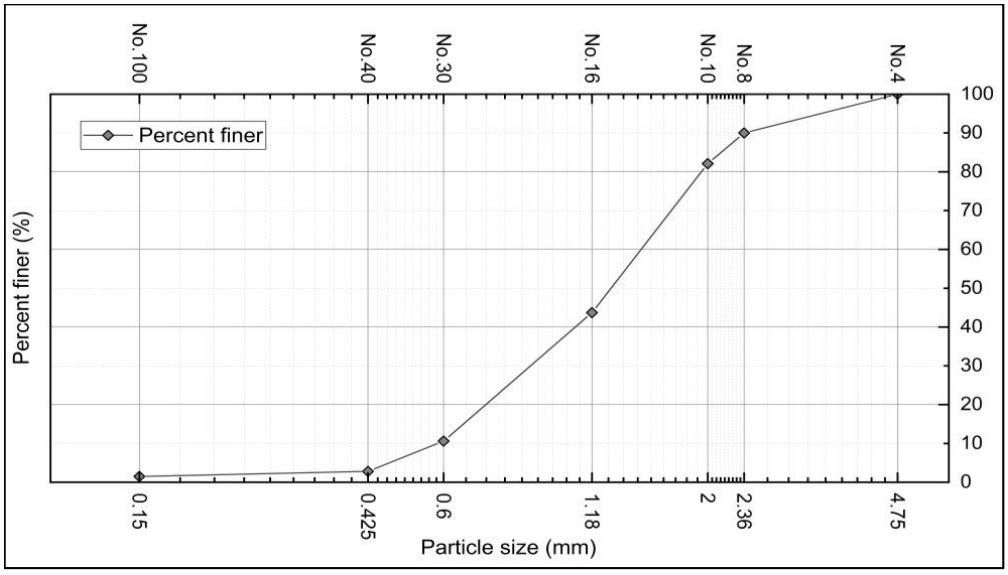

Figure 3.2 Particle size distribution of ground PET

3.1.2 Electrospun PET Microfiber (EPM)

An electrospinning setup consists of three main components, namely (i) a high-voltage power supply (HVPS), (ii) a syringe pump with a conductive needle, and (iii) a conductive collector (Owida et al., 2022). This study used an in-house-fabricated electrospinning apparatus to produce EPM in the laboratory (Figure 3.3). It is important to note the two electrodes (nozzle and collector) were enclosed entirely within a 600 mm by 600 mm by 450 mm in-house fabricated plexiglass box. A syringe pump was placed on an adjustable platform outside the plexiglass box. This setup also included a 10 mL glass syringe containing electrospinning solution. A steel needle with an internal diameter of 1.26 mm was used at the tip of the syringe. The needle was then passed horizontally through a hole (Equivalent to a #10- or 3.0-mm needle diameter) created on the wall of the plexiglass box. A collector plate (28 cm by 14 cm) attached to a wooden board was placed inside the plexiglass box 20 cm from the tip of the syringe needle. Figure 3.3 depicts the in-house fabricated electrospinning setup and its components.

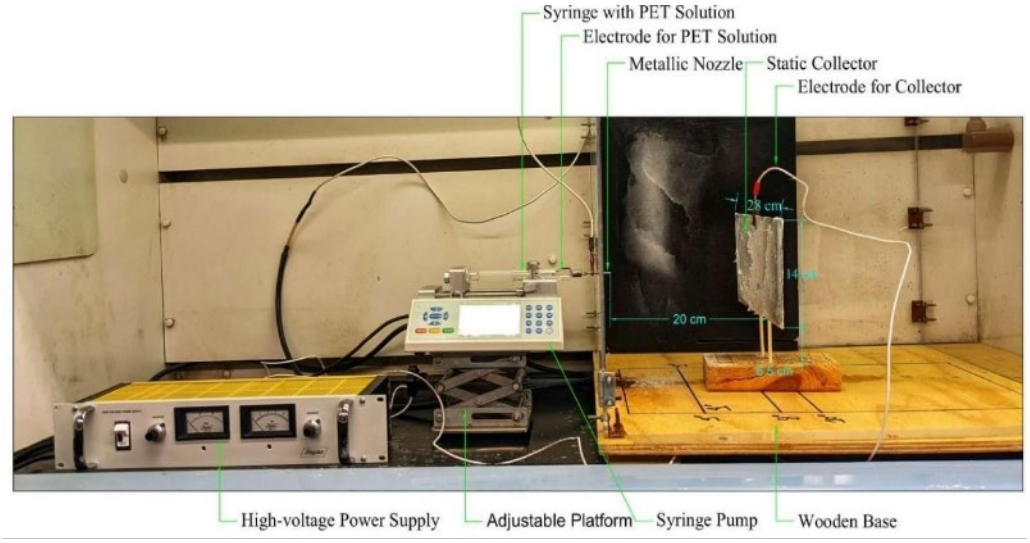

Figure 3.3 A photographic view of the in-house fabricated electrospinning setup

The electrospinning solution was prepared in a fume hood by mixing dichloromethane (DCM) and trifluoroacetic acid (TFA) at a volumetric ratio of 30 to 70, respectively. Then, the solution's weight was measured. According to Veleirinho et al. (2008), TFA and DCM are volatile solvents that can quickly evaporate at room temperature and pressure. Therefore, to prevent loss of solvents, the solution container was tightly sealed and kept in a well-ventilated area at the time of mixing. Two different polymer solutions comprising 15% and 20% of ground PET by the solution weight were prepared. To facilitate the process, the blend of the ground PET and the solution was stirred in an air-tight container using a magnetic stirrer at room temperature for 24 hours before electrospinning. The workflow of preparing PET electrospinning solution is depicted in Figure 3.4.

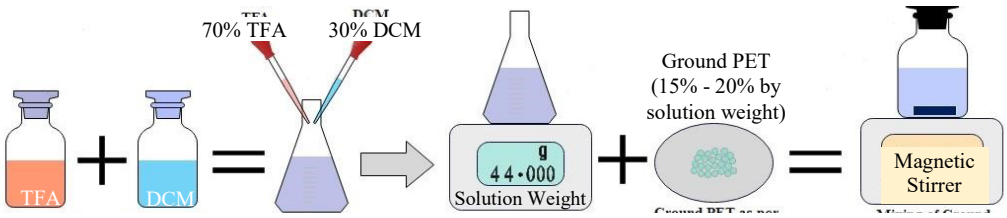

Figure 3.4 Workflow followed for preparing electrospinning solution

The prepared electrospinning solution was transferred into a 10 mL glass syringe, placed in the syringe pump, and the flow rate was set on the pump. The pump and the loaded syringe were placed on an adjustable platform. The height of the platform was adjusted to allow the needle to pass through a hole created in the plexiglass with its axis perpendicular and opposing the center of the metallic collector. Then, the HVPS (set to supply 20 kV) was connected to the nozzle (metallic needle), and the conductive collector and the syringe pump were initiated. For each solution type, EPMs were synthesized at flow rates of 250, 120, 60, 50, and 40 μL/min (Table 3.1). After depositing an adequate amount of PET fibers on the collector, the EPM mat was carefully collected, labeled, and set aside for further testing.

Table 3.1 Electrospinning parameters

Electrospinning Parameters	Solution Types	Ground PET Amount (% by the wt. of solution)	Flow Rate (μL/min)	EPM Label
Tip-to-Collector Distance: 20 cm Electrospinning Voltage: 20kV TFA and DCM 70/30 by Volume	S_1	15%	250	F250_15%
			120	F120_15%
			60	F60_15%
			50	F50_15%
			40	F40_15%
	S_2	20%	250	F250_20%
			120	F120_20%
			60	F60_20%
			50	F50_20%
			40	F40_20%

3.1.3 Asphalt Binders

Three types of asphalt binders, PG 58-28, PG 58-34, and PG 64-28, were collected from Jebro Co. in Sioux City, IA. The PG 58-28 asphalt binder was modified by adding 0.2, 0.5, 0.7, and 1.0 % of EPM (by binder's weight). The PG 58-34 and PG 64-28 were not modified with EPM — they were used as comparison baselines representing polymer-modified asphalt binders. Table 3.2 provides a summary of the binder blends prepared for testing in the laboratory.

Table 3.2 Asphalt binder blends prepared for testing

Asphalt Binder	EPM (% binder wt.)	Asphalt Binder Blend Label
PG 58-28	0	PG58-28 (Neat)
	0.2	PG58-28+0.2%EPM
	0.5	PG58-28+0.5%EPM
	0.7	PG58-28+0.7%EPM
	1	PG58-28+1.0%EPM
PG 58-34	0	PG58-34(Neat)
PG 64-28	0	PG64-28(Neat)

3.1.4 Aggregates

Aggregates with mostly quartzite mineralogy were collected from a local asphalt plant and selected from five different stockpiles. The size distributions of each stockpile (bins) are depicted in Figure 3.4. The nominal maximum aggregate sizes (NMAS) for Bin-1, Bin-2, Bin-3, Bin-4, and Bin-5 were 19.0, 12.5, 4.76, 9.5, and 2.36 mm, respectively. The samples were transported to the asphalt laboratory and stored. The aggregates collected from the stockpiles were then used to establish a mix design and produce asphalt mixes in the laboratory.

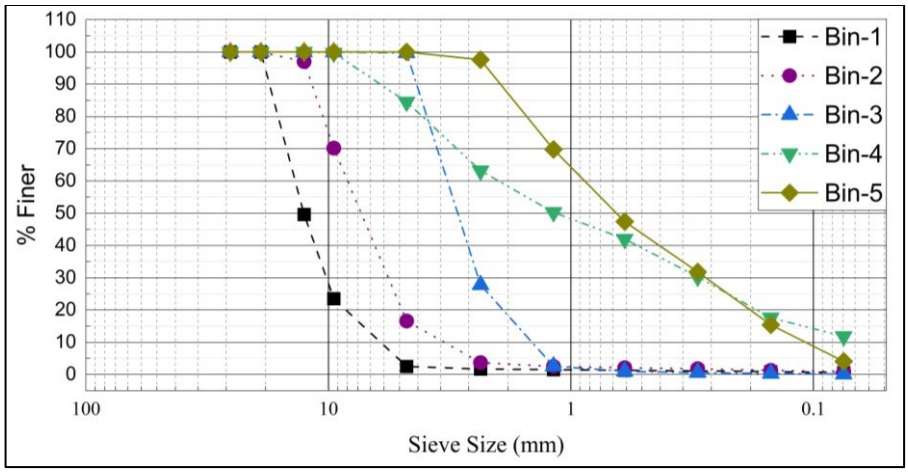

Figure 3.5 Particle size distribution of collected aggregate stockpiles

3.1.5 Asphalt Mix

The asphalt mix tested in this study was designed following Superpave requirements per AASHTO M 323 (AASHTO, 2017a) standard specification and AASHTO R 35 (AASHTO, 2017b) standard practice. The aggregate structure of the collected aggregates from stockpiles (Bin-1 to Bin-5), shown in Figure 3.3, was selected to be blended at 15, 20, 15, 30, and 20% (total weight of blended aggregate), respectively. The combined gradation of the aggregate structure has a nominal maximum aggregate size (NMAS) of 12.5 mm, as shown in Figure 3.6.

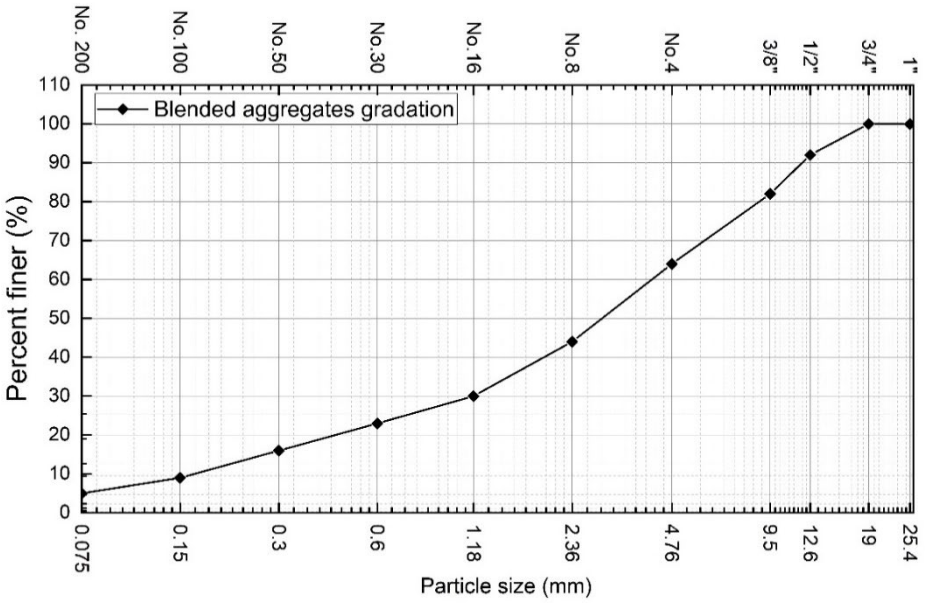

Figure 3.6 Asphalt mix combined aggregate particle size distribution

To determine the optimum asphalt binder content, two identical specimens of loose asphalt mix were prepared to determine the mix's maximum theoretical specific gravity (G_{mm}). For this purpose, 1500 g of aggregate was batched according to the aggregate structure for each sample (Figure 3.7a). The batched aggregates and PG 58-28 asphalt binder were then heated and mixed at 160°C in the oven (Figure 3.7b). The loose mixes were aged for two hours at 135°C in the oven (Figure 3.8c). After 24 hours of cooling the sample at room temperature, the Gmm of the trial blend mixes prepared at each binder content was determined according to the AASHTO T 209 (AASHTO, 2011) standard method. To prepare a trial batch

for preparing SGC-compacted samples, the aggregates were batched to produce a mix specimen of approximately 4800 g following the specified aggregate batch proportions. The heated binder and aggregates were mixed using a bucket mixer. The mix was placed in a flat pan, heated for two hours at 135°C in an oven, and stirred every 30 minutes for short-term aging (Figure 3.8a). For each trial binder content, two specimens were compacted at the design number of gyrations (N_{Design} = 75 gyrations) using an SGC according to AASHTO R 35 (AASTHO, 2017b) (Figure 3.8b). The gyratory samples of 150 mm diameter (Figure 3.9c) were compacted according to AASHTO T 312 (AASHTO, 2011). Then, the bulk specific gravity (G_{mb}) of the compacted specimens was determined according to AASHTO T 166 (AASHTO, 2011) standard test procedure (Figures 3.8d and 3.8e).

Figure 3.7 Photographic views of (a) batching, (b) mixing aggregates and asphalt binder, and (c) G_{mm} test

Three trial binder contents of 4.5%, 5.0%, and 5.5% were used to prepare and compact mixes to determine the optimum binder content. For mixes and cylindrical samples prepared with each binder content, G_{mm} and G_{mb} values were determined, important volumetric properties of each mix were determined, and binder content corresponding to 4.0% air void was selected as the optimum binder content (5.4%). Table 3.3 presents important volumetric properties of the asphalt mix prepared at the mix design optimum asphalt binder content of 5.4% and compared to the requirements set by AASHTO M323 standard specifications (AASHTO, 2017a).

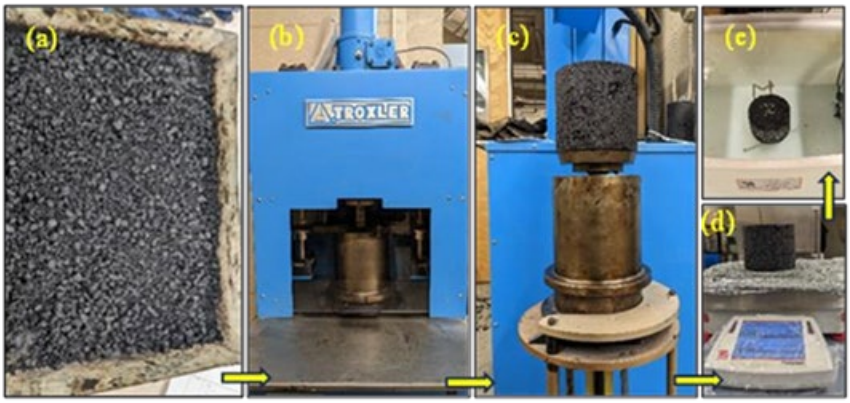

Figure 3.8 Photographic views of (a) loose asphalt mix; (b) SGC compactor; (c) compacted cylindrical sample; (d) determination of bulk specific gravity of cylindrical samples

Table 3.3 Volumetric properties of the designed asphalt mix

Properties	Value	AASHTO M323 Requirements
Asphalt Binder Type	PG 58-28	
Optimum Asphalt Binder Content (%)	5.4%	
Voids in Mineral Aggregates (%)	15.1%	>14
Voids Filled with Asphalt (%)	74.7%	65-78
Effective Binder Content (%)	4.8%	
Dust Proportion	0.9	0.6-1.2
Density @ N_{ini} (%)	88.9%	<90.5

The asphalt mix samples required for laboratory tests, namely Hamburg wheel tracker, tensile strength ratio, and semicircular bend tests, were batched and prepared in the laboratory using the established mix design. More specifically, asphalt mixes containing 0, 0.5, 1.0, and 1.5% EPM (by weight of asphalt binder) were prepared and used for compacting the samples as per geometries indicated by the corresponding standards for each test. The size of the EPM fibers used in mix preparation was 3 mm by 35 mm (Figure 3.9). EPM was added to the mix using a method utilized by Alfalah et al. (2020).

Figure 3.9 A photographic view of the EPM used for the preparation of asphalt mixes

For this purpose, the EPM was first split into three equal-weight portions. Then, the preheated aggregates were blended with the asphalt binder in a bucket mixer (Figure 3.10a) and mixed to consistency. Then, the first portion of the EPM was gradually added while mixing progressed until a consistent mix was produced and no fibers were visible (Figure 3.10b). This process was repeated until all EPMs were added. The produced asphalt mix was kept for further laboratory aging and HMA sample preparation (Figure 3.10c). Table 3.4 presents the different asphalt mix blends produced in the lab.

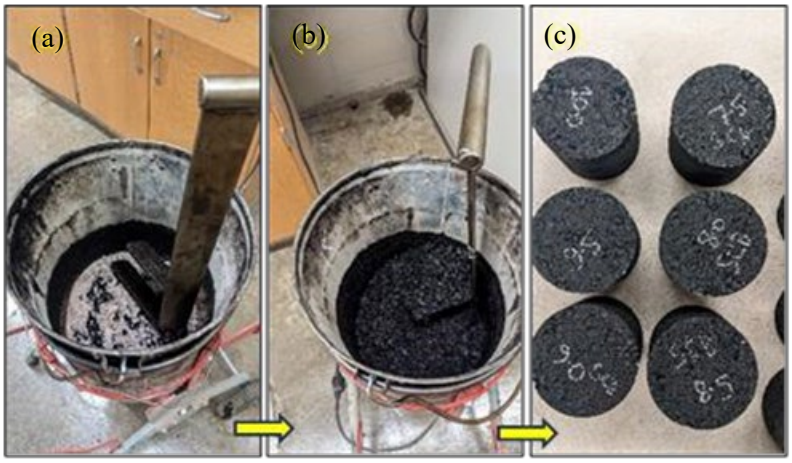

Figure 3.10 Photographic views of (a) aggregates and binder batch in a bucket mixer, (b) mixing EPM with the asphalt mix in a bucket mixer, and (c) compacted cylindrical samples

Table 3.4 Asphalt mixes prepared for testing

Asphalt Binder Type	EPM (% binder wt.)	Asphalt Mix Label
PG 58-28	0	HMA-C
	0.5	HMA+0.5%EPM
	1.0	HMA+1.0%EPM
	1.5	HMA+1.5%EPM

3.2 Test Methods

3.2.1 Chemical Structure of EPM – Fourier-Transform Infrared Spectroscopy

The Fourier-transform infrared spectroscopy (FTIR) technique was employed to investigate chemical structure of the EPM. Additionally, this test provided information about any chemical changes in the EPM compared to PET. The FTIR spectroscopy was performed using a PerkinElmer Universal ATR (Perkin–Elmer Corporation, Norwalk, Connecticut, USA). EPM samples were placed in contact with the ATR element (ZnSe crystal, 45° ends) at room temperature. For this purpose, desiccated samples were tested at a wavenumber range of between 4000 and 350 cm^{-1}. The spectra obtained from testing were further analyzed to detect functional groups present in the tested specimens.

3.2.2 Morphology of EPM - Scanning Electron Microscopy (SEM) Test

Morphology of the produced EPM was determined using a scanning electron microscope (SEM). The EPM mats cut into small pieces (Figure 3.11a) were first coated with a layer of gold-palladium using a CrC-150 sputtering machine (Figure 3.11b). Then, a conductive adhesive was used to attach the EPM to

the SEM sample base (Figure 3.11c). The thickness of the coating layer was 0.15 kÅ. The SEM test was carried out using a 20 kV accelerating voltage to ensure good resolution (Figure 3.11d). From the SEM micrographs, the diameter of the EPM was measured using an image processing software (ImageJ) developed by the National Institutes of Health of the United States.

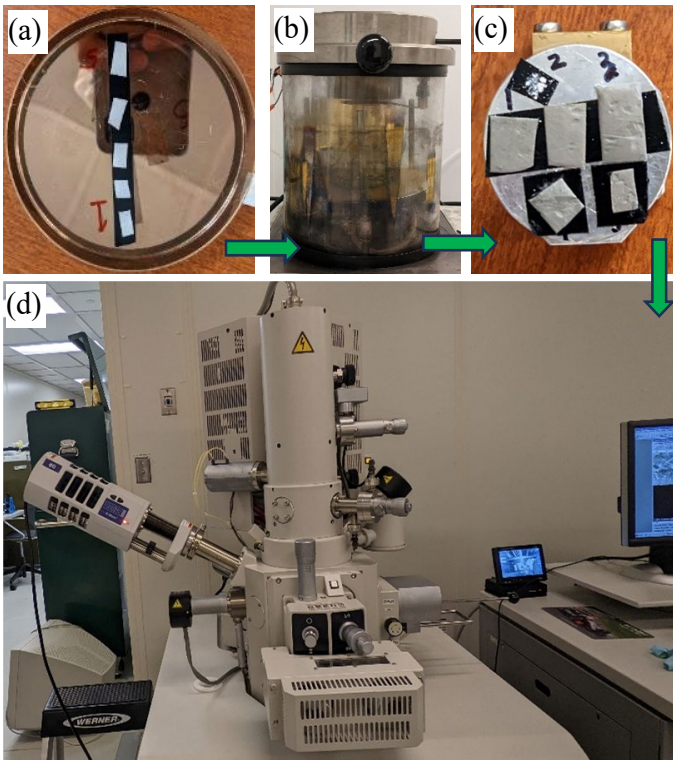

Figure 3.11 Photographic images of (a) EPM mats cut to small pieces, (b) coating of the EPM specimens, (c) coated EPM specimens in SEM sample base, and (d) SEM imaging

3.2.3 Tensile Strength of EPM

The presence of lateral instability and different travel distances from the nozzle to the collection plate in the electrospinning process causes nonuniform fiber deposition. Consequently, the fiber thickness, closer to the axis of the nozzle, is higher and gradually decreases toward the edges of the collector. In addition, it is not feasible to test individual fibers because the resulting single fiber is small, and the produced fiber mat has a nonwoven structure (Ghabchi and Castro, 2021). Hence, to determine the tensile strength of EPM, the method proposed by Ghabchi and Castro (2021) was applied. This method maintained constant weight and approximately the same cross-sectional area in every sample. Therefore, to prepare the identical specimens for the tensile strength test, the EPM mat deposited in the center of the plate was carefully collected from the static collector and allowed to dry for a minimum of 24 hours in a ventilated chamber at room temperature. Later, the loose mat was placed on aluminum foil (Figure 3.12a) and folded in multiple directions (Figure 3.12b). The EPM mat and aluminum foil were cut into an approximate size of 115 mm by 140 mm, and then the weight of the resized EPM mat was determined on a scale up to 0.001g accuracy (Figure 3.12c). If the weight of the strip exceeded the designated amount, it was readjusted by removing a thin layer from the strip utilizing a sharp utility knife (Figure 3.12e**)**. After achieving the specified weight (Figure 3.12f) and dimensions, pieces of sandpaper on both ends of the fiber strip were glued (Figure 3.11g). The glue strip was kept aside for at least two hours before testing to allow the glue to dry. Based on observations, the glued sandpaper served two purposes. First, it kept the

two or more layers of EPM strips together and assisted them to perform like a single-layered mat. Second, it provided additional grip to the jaws of the loading frame. During the transfer of the EPM strip to the loading frame, care was taken to ensure the outer edge of the jaws clamped the EPM mat and applied tensile force to the mat (Figure 3.12h). Finally, the tensile strength test was conducted using a loading frame provided by Texture Technologies Corp., USA (Figure 3.12i). The sample was subjected to tensile force at 2 millimeters per minute. Four identical specimens were tested for each EPM type, and the specimens' tensile strength was determined by analyzing the collected load and displacement data.

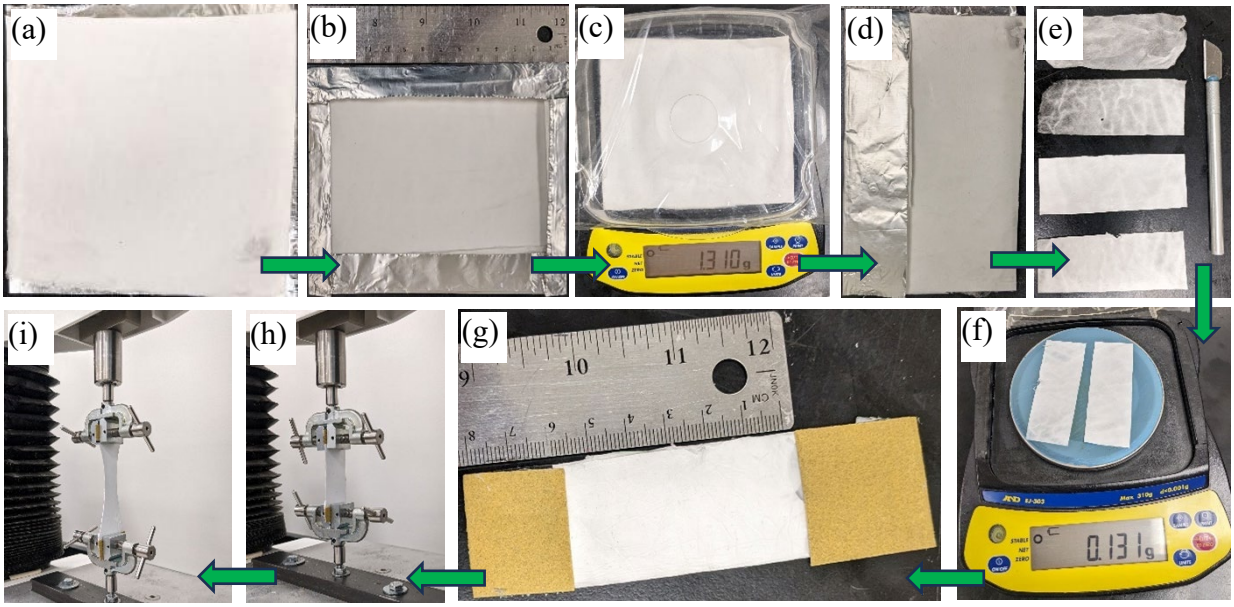

Figure 3.12 Photographic views of conducting tensile strength tests of EPM (a) An EPM mat on aluminum foil; (b) folding along EPM mat's edge; (c) weighting the EPM specimen; (d) folding the EPM mat along its long edge for strip preparation; (e) adjusting the weight of the 50 mm by 27 mm EPM strip to 0.130 g; (f) controlling the EPM strip weight; (g) attaching the ends of the EPM strip to sandpaper; (h) clamping the EPM strip on to the loading frame; and (i) tensile strength test in progress

3.2.4 Laboratory Aging of Asphalt Binders

Asphalt binders must be aged in the laboratory to replicate oxidative aging during the production, transportation, and construction of the asphalt mix (short-term aging) and the pavement's service life (long-term aging). Hence, a rolling thin-film oven (RTFO) was employed to conduct short-term aging of the asphalt binder in the laboratory by following the AASHTO T 240 (AASHTO, 2011) standard method. In addition, a pressure-aging vessel (PAV) was utilized to conduct long-term aging of asphalt binders following the AASHTO R 28 (AASHTO, 2011) standard procedure.

3.2.5 Asphalt Binder Rheology – Dynamic Shear Rheometer (DSR) Test

A dynamic shear rheometer (DSR) was employed to characterize the viscous and elastic properties of the asphalt binder blends at high and intermediate temperatures by following the AASHTO T 315 (AASHTO, 2020) standard method. The DSR test was conducted at different temperatures to measure the asphalt binder's complex shear modulus (G*) and phase angle (δ). G* and δ were further used to determine the rutting factor (G*/sinδ) at high temperature (H-T) and the fatigue parameter (G*sinδ) at intermediate temperature (I-T) (AASHTO, 2020). A 25-mm diameter parallel plate setup and a 1-mm gap were used to test unaged and RTFO-aged binders. On the other hand, for the PAV-aged binders, an 8 mm diameter

parallel-plate setup and a 2 mm gap were used to measure G* and δ values. The measured values were used to determine the asphalt binder's continuous H-T grade and the H-T PG grade.

3.2.6 Asphalt Binder Rheology – Multiple Stress Creep and Recovery Test

The multiple stress creep and recovery (MSCR) test was conducted on the RTFO-aged asphalt binder blends using DSR equipment following the AASHTO T350 (AASHTO, 2019) standard method. Tests were conducted at 58°C and selected based on the climatic zone of the specific area where the asphalt binder is used for construction. The test was carried out at stress levels of 0.1 and 3.2 kPa, and nonrecoverable creep compliance (J_{nr}) and recovery (R) values were subsequently determined.

3.2.7 Asphalt Binder Rheology – Bending Beam Rheometer (BBR) Test

To evaluate the low-temperature (L-T) cracking potential of asphalt binders, a bending beam rheometer (BBR) was utilized to test PAV-aged asphalt binder samples according to the AASHTO T 313 standard method (AASHTO, 2019). The results of the BBR tests conducted at low temperatures were further analyzed to determine the creep stiffness (S) and creep rate (m-value) by applying a 980 ± 50mN load over 240 seconds. The values of S and m, measured 60 seconds after load application (S_{60} and m_{60}), were used to determine the continuous L-T grade and the L-T Superpave PG of asphalt binders. In addition, S and m-values determined from conducting the BBR test at two temperatures were used to calculate critical temperature (T_c) values. The T_c is the temperature at which the specified stiffness and stress relaxation limits correspond precisely. $T_{c,S}$ (equation 3.1) is the critical stiffness temperature, which is determined where the stiffness after 60 seconds of loading (S_{60}) equals 300 MPa. On the other hand, $T_{c,m}$ (equation 3.2) represents the critical stress relaxation temperature, which is determined where the m-value after 60 seconds of loading (m60) equals 0.300 (Anderson et al., 2011). The variation in critical temperature, shown as ΔT_c, is calculated from equation 3.3 and represents non-load-related thermal cracking potential.

$$T_{c,S} = T_1 + \left(\frac{(T_1 - T_2) * (log300 - logS_1)}{logS_1 - logS_2}\right) - 10 \quad \text{(Equation 3.1)}$$

$$T_{c,m} = T_1 + \left(\frac{(T_1 - T_2) * (0.300 - m_1)}{m_1 - m_2}\right) - 10 \quad \text{(Equation 3.2)}$$

$$\Delta T_c = T_{c,S} - T_{c,m} \quad \text{(Equation 3.3)}$$

where,

S_1 = creep stiffness (MPa) measured at T_1 (°C);
S_2 = creep stiffness (MPa) measured at T_2 (°C);
m_1 = creep rate (mm/s) measured at T_1 (°C);
m_2 = creep rate (mm/s) measured at T_2 (°C);
T_1 = temperature (°C) at which S and m pass; and
T_2 = temperature (°C) at which S and m fail to pass.

3.2.8 Asphalt Binder Adhesion – Binder Bond Strength (BBS) Test

The adhesion quality and susceptibility of the asphalt binder-aggregate to moisture-induced damage were evaluated by conducting the binder bond strength (BBS) tests (Figure 3.14). This was achieved by measuring the pull-off tensile strength (POTS) of the asphalt binder placed on an aggregate substratum using a pull-off device (DeFlesko PosiTest AT-A) following the AASHTO T 361 standard method (AASHTO, 2022). The BBS tests were conducted on dry and moisture-conditioned specimens. To prepare the samples, the pull stubs were attached to the aggregate substrate (Figure 3.13a). After keeping

the samples at room temperature for about one hour, the dry samples were placed in an environmental chamber at 20°C and kept there for 24 hours before testing. To conduct the BBS tests on moisture-conditioned specimens, a separate set of samples was immersed in a water bath at 40°C for 24 hours (Figure 3.13b). Then, the samples were removed and left to reach the testing temperature in an environmental chamber at 20°C for one hour. At least eight samples were tested for each asphalt binder-aggregate composition (Figure 3.13c). After conducting the tests, the failure mechanism (adhesive or cohesive) was determined (Figure 3.13d). The pull-off tensile strength (POTS) values were recorded, and their average values were presented as $POTS_{dry}$ for dry samples and $POTS_{wet}$ for moisture-conditioned samples. The pull-off strength ratio (PSR) was then determined by dividing $POTS_{wet}$ by $POTS_{dry}$.

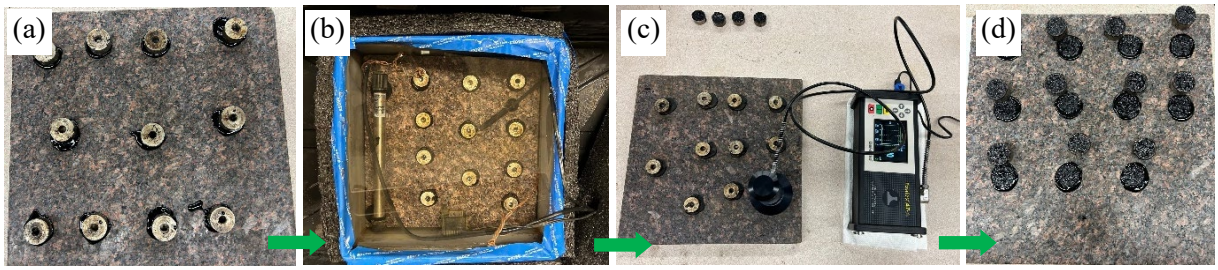

Figure 3.13 Photographic views of (a) prepared BBS sample, (b) moisture conditioning sample in a temperature-controlled water bath, (c) testing BBS samples, and (d) failure mechanisms

3.2.9 Resistance of Asphalt Mix to Rutting – Hamburg Wheel Tracker (HWT) Test

To assess the resistance of asphalt mixes to rutting and their potential for moisture-induced damage, the Hamburg wheel tracker (HWT) tests were carried out following the AASHTO T 324 (AASHTO, 2011) standard method. Samples were compacted in an SGC to a diameter and height of 150 mm and 60 mm, respectively, to achieve 7.0 ± 0.5% air voids. Edges of two pairs of cylindrical samples were saw-cut to meet the geometry requirements of the standard method. Then, the samples were placed in molds provided with the HWT equipment (Figure 3.14). The testing procedure involved steel wheels of 705 N weight moving back and forth on the surface of the HMA specimens while submerged in a water bath at 50 ± 1 °C, as specified by the standard method. The machine's steel wheels have a diameter of 203 mm, a width of 47 mm, and oscillate at a rate of 52 ± 2 passes per minute. Linear variable differential transformers (LVDT) determine the relative vertical deformation of the samples being tested, and data are recorded in a computer. The test was programmed to end autonomously after reaching 20,000 passes or 12.5 mm of maximum vertical deformation, whichever occured first.

Figure 3.14 A photographic view of the HMA samples in the HWT device

3.2.10 Resistance of Asphalt Mix to Stripping – Tensile Strength Ratio (TSR) Test

The moisture-induced damage (stripping) potential of the asphalt mixes was determined by conducting a tensile strength ratio (TSR) test by following the AASHTO T 283 (AASHTO, 2011) standard method. An SGC operated at height mode was used to compact cylindrical HMA specimens with a diameter of 150 mm, a height of 95 ± 5 mm, and air voids of 7.0 ± 0.5%. Three specimens from each HMA type were kept under dry conditions (dry specimens), while the remaining three specimens were conditioned (wet specimens). The conditioning of specimens consisted of vacuum saturating them by applying 28 kPa absolute pressure. Then, the mass of the vacuum-saturated surface dry sample was measured to determine the degree of saturation achieved. If the saturation percentage was less than 70%, the specimens were subjected to more vacuum saturation. If the saturation level was above 80%, the specimen was discarded. Following saturation, the specimens were wrapped in cling wrap, placed in plastic airtight bags with 10 mL of water, and kept at -18 °C for 16 hours. Next, they were transferred to a water bath at 60°C and kept for 24 hours. The specimens were then kept submerged in water at 25°C for two hours before being tested in a testing jig loaded in a loading frame (Figure 3.15a) to determine their indirectly measured tensile strength (ITS). Samples were loaded at 5.08 cm vertical per minute until failure (Figure 3.15b). Equations 3.4 and 3.5 were used to determine the ITS and TSR values of the tested specimens, respectively.

$$\mathrm{ITS} = \frac{2\mathrm{F}}{\pi \mathrm{tD}} \qquad \text{(Equation 3.4)}$$

$$\mathrm{TSR} = \frac{\mathrm{ITS}_{wet}}{\mathrm{ITS}_{dry}} \qquad \text{(Equation 3.5)}$$

where,

ITS = indirectly measured tensile strength (kPa);
F = peak force (kN);
t = cylindrical specimen's thickness (m);
D = cylindrical specimen's diameter (m);
TSR = tensile strength ratio;
ITS_{dry} = indirectly measured tensile strength of the dry asphalt specimen (kPa); and
ITS_{wet} = indirectly measured tensile strength of the moisture-conditioned asphalt specimen (kPa).

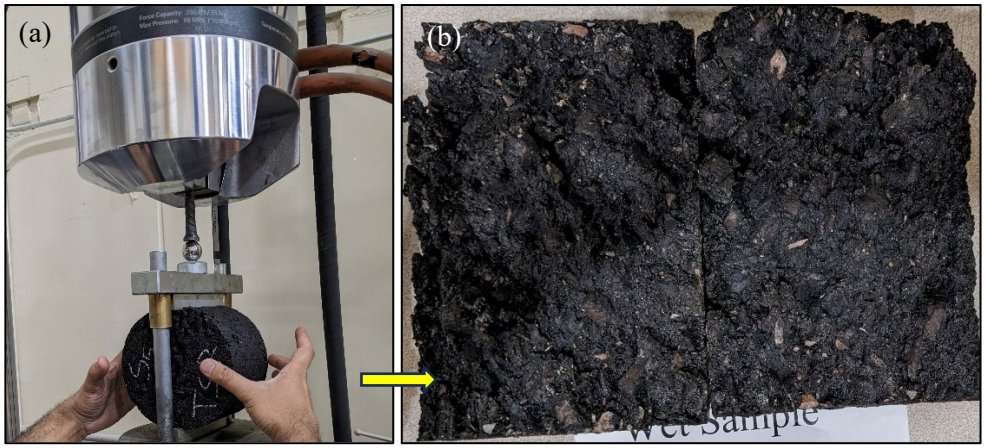

Figure 3.15 Photographic views of (a) TSR test setup and (b) failure surface

3.2.11 Resistance of Asphalt Mix to Stripping – Tensile Strength Ratio (TSR) Test

The semicircular bend (SCB) test on asphalt mixes was conducted following the ASTM D8044 (ASTM, 2017) standard method to determine their resistance to cracking. For this purpose, an SGC was used to compact asphalt mix samples with a diameter of 150 mm and a height of 135 mm. Then, subsequently, specimens with a thickness of 57 ±1 mm were saw-cut from the compacted samples by discarding the top and bottom sections of the 135 mm tall specimen, which measured 15 ± 5 mm in length. After preparing the saw-cut cylindrical specimens, they were further cut along their diameter to obtain two semicircular half-cylinders. The weight of the compacted loose mix was adjusted to obtain half-cylinder samples with a semicircular cross-section with 7.0 ± 0.5% air voids. Samples were aged in a forced-air convection oven at 85°C for 120 hours. Then, a precision saw was used to cut notches in the midspan of the samples with depths of 25, 32, and 38 mm. Four SCB specimens were evaluated for every notch depth. Before performing the SCB test, all specimens were conditioned for two hours at 19°C, which is the intermediate temperature prescribed by the ASTM D8044 (ASTM, 2017). Finally, the specimens were tested in an asphalt mix performance tester (AMPT) by subjecting them to a monotonic load applied at a constant rate of 0.5 mm/min in a three-point bending load configuration until fracture (Figure 3.16). The force and displacement data were recorded in a computer and were used to determine the critical strain energy release rate (J_c) using equation 3.6.

$$J_c = -\left(\frac{1}{b}\right)\frac{dU}{da} \qquad \text{(Equation 3.6)}$$

where,

b = sample's thickness (m);
a = notch depth (m);
U = strain energy at failure (kJ); and
dU/da = change of strain energy with the notch depth (kJ/m);

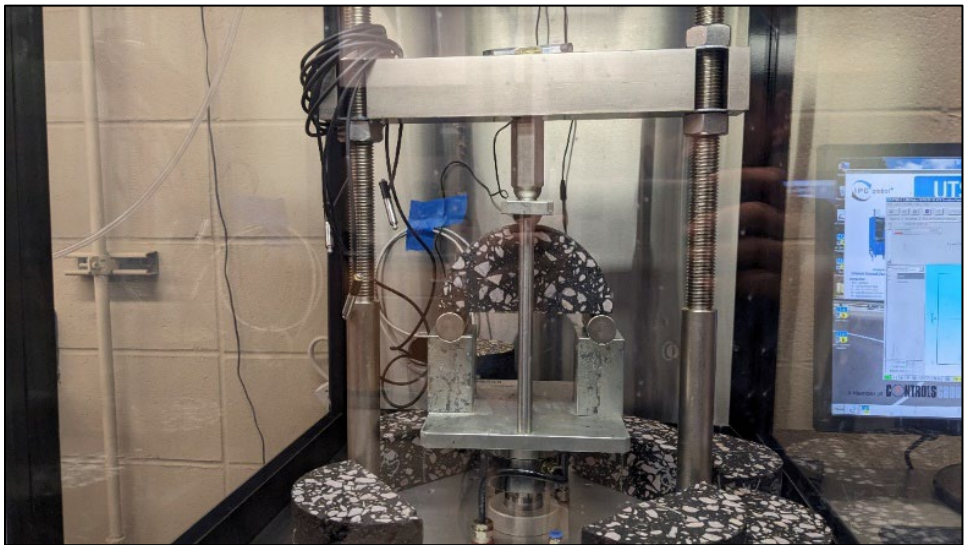

Figure 3.16 A photographic view of a SCB specimen subjected to loading in an AMPT

4. RESULTS AND DISCUSSION

4.1 Characteristics of the Electrospun PET Microfiber (EPM)

4.1.1 Chemical Structure of EPM – FTIR Test

Figures 4.1a and 4.1b depict the infra-red (IR) spectra of the EPM produced by using 15 and 20% PET concentrations in the electrospinning solutions and various flow rates, respectively. These spectra illustrated the sample's absorbance as a function of wavenumber. In FTIR spectra, the plot of absorbance versus wavenumber showed peaks related to specific vibrational modes of molecules in the sample. Four distinct major spectral peaks were observed in Figures 4.1a and 4.1b, which complied with the inherent structure of PET and EPM. One of these peaks was located in the diagnostic region at 1715cm^{-1}, while the remaining three were in the fingerprint region at 1245, 1095, and 715cm^{-1} wavenumbers. Using the known IR spectrum table by frequency range from Chemistry LibreTexts (Infrared Spectroscopy Absorption Table, 2020), it was determined that the peaks match the following functional groups: ester carbonyl (C=O) at 1715cm^{-1}, C–O asymmetric and symmetric stretching at 1245 and 1095cm^{-1}, and C–H wagging vibrations from aromatic structures at 725cm^{-1}. In addition, minor peaks at 1410, 1015, and 875cm^{-1} were observed in each sample. However, these minor peaks did not demonstrate a significant difference between the spectra of PET samples from the waste and EPM mat produced in the lab. The EPM samples, including those made from different concentrations of PET, exhibited identical spectra compared to the micronized PET sample. Therefore, it can be concluded the electrospinning process and the use of TFA and DCM reagents in preparing different PET solutions did not cause any chemical alterations to the PET's chemical structure. Also, it was concluded that the drying process applied for the produced fiber efficiently removed all traces of solvents in the produced fibers. For example, if TFA was present in the fiber mat after air-drying the samples for 24 hours, it should have been visible within the 1400-1000cm^{-1} region of IR spectra due to the presence of trifluoromethyl (-CF_3) functional group. Similarly, if any trace of the DCM were present in the fibers, the dichloromethane (C-Cl) symmetric and asymmetric stretching should have appeared in the 850-550cm^{-1} range. As no distinguished peaks correlating with the trifluoromethyl (-CF_3) group or the dichloromethane (C-Cl) symmetric and asymmetric stretching were observed in the IR spectra of desiccated fiber mats compared to that of PET, it can be concluded that the air drying process allowed for the complete evaporation of all solvents used in the production of the EPM mat.

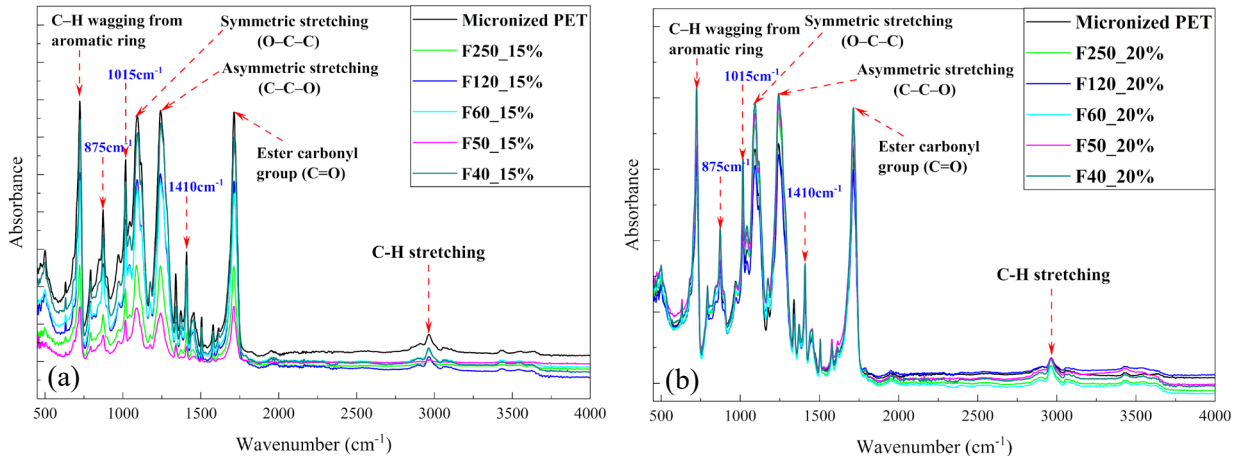

Figure 4.1 IR-spectra of ground PET and produced EPM produced at various solutions' flow rates with (a) 15% PET concentration and (b) 20% PET concentration

4.1.2 Size and Morphology of EPM Fibers– SEM Test

Figures 4.2 and 4.3 show the SEM micrographs of produced EPM using two different PET concentrations, 15% and 20% (by solution weight), respectively, and various flow rates. For the production of EPM using each PET concentration, five different flow rates, namely 40, 50, 60, 120, and 250µL/min, were applied. From the SEM micrographs, the size distribution of fibers was determined by analyzing them in ImageJ software with the help of the DiameterJ plugin. A histogram obtained from ImageJ data was generated to determine the average diameter of the fibers produced at each flow rate. It can be observed that the average fiber diameter increased with increasing flow rate for both types of fibers produced by PET concentrations of 15% and 20%. Notably, when 15% PET concentration was used in the solution, the mean fiber diameter increased from 673nm (Figure 4.2a) for 40µL/min flow rate to 706, 743, 778, and 799nm (Figures 4.2b, c, d, and e) when flow rates of 50, 60, 120, and 250µL/min were applied, respectively. Similarly, when a concentration of 20% PET was used in the solution, the average fiber diameter increased from 735nm at 40µL/min (Figure 4.3a) flow rate to 746, 770, 778, and 792 nm (Figure 4.3b, c, d, and e) at 50, 60, 120, and 250 µL/min flow rate, respectively. It can be concluded that when PET concentration was kept at 15%, the effect of the solution flow rate on the average fiber diameter was significantly higher than those observed in EPMs produced at 20% PET concentration. This observation was due to a change in the solution's viscosity due to increasing PET concentration, which affected the electrospinning jet shape and geometry (Bonfim et al., 2021). The polymer concentration significantly affects viscosity of the solution, which, in turn, influences the surface tension, flow, and fiber elongation during electrospinning. Elongation of the jet impacts the diameter of the resulting fibers, with thinner fibers forming from elongated jets and thicker fibers forming from jets with less elongation (Bonfim et al., 2021). Therefore, the higher concentration of PET (20%) in TFA and DCM solution increased the viscosity of the solution compared to experiments conducted using 15% PET concentration. An increase in the solution's viscosity made it more difficult for the electrospinning jet to elongate, leading to larger fiber diameters, as observed in the samples with a 20% PET concentration. In addition, and consistent with the findings of Strain et al. (2015), changing the flow rate by a factor of six (at a given concentration) had a marginal effect on the thickness of the fibers at higher concentrations. This suggests the impact of the flow rate on the fiber diameter was less significant at higher PET concentrations, possibly because of the viscosity of the solution. In contrast, solutions with low concentrations and flow rates demonstrated less resistance to the fiber deformation caused by the applied electric field, resulting in thinner fiber formation (Cho et al., 2020; Lasprilla-Botero et al., 2018).

Figures 4.4 and 4.5 depict SEM micrographs of EPM produced from two concentrations of PET, namely 15% and 20%, respectively, in a solution consisting of 70 volumetric parts of TFA and 30 volumetric parts of DCM. As shown in the SEM micrographs, reducing the electrospinning flow rate eliminated beaded structures and formed thinner, more cylindrical fibers. When the flow rate is excessively high, the electrostatic field may not completely stretch the solution jet, resulting in larger droplets and, ultimately, the production of thicker and defective fibers. The solution's flow rate through the needle significantly affects the droplets' size (Zong et al., 2002). Decreasing the flow rate can produce fibers with a reduced diameter and smoother surface (Mercante et al., 2017). Different electrospinning parameters were changed to achieve smooth and continuous fibers, and their effect on the EPM's quality was investigated. Specifically, PET concentrations of 15% and 20% and flow rates ranging from 250 to 40µL/min were examined in this study. In contrast, increasing the concentration of PET in the solution produced fibers with a more uniform morphology. Multiple studies have demonstrated that the characteristics of electrospun fibers are determined mainly by polymer type, solution properties (such as concentration), and various parameters such as applied voltage and flow rate (Chen et al., 2008).

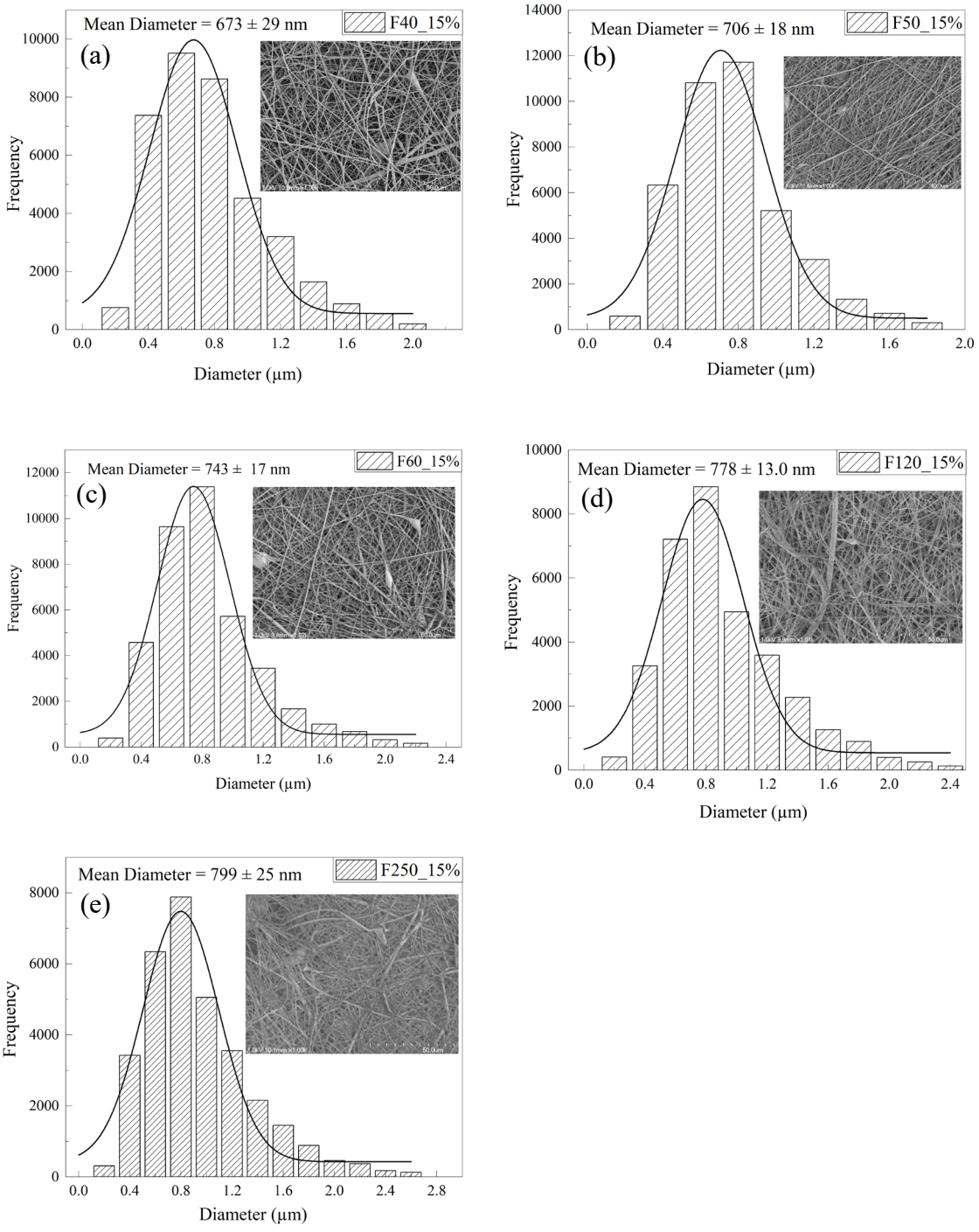

Figure 4.2 Diameter distribution of EPM formed by electrospinning a solution containing 15% PET concentration and flow rates of (a) 40µL/min, (b) 50µL/min, (c) 60µL/min, (d) 120µL/min and (e) 250µL/min

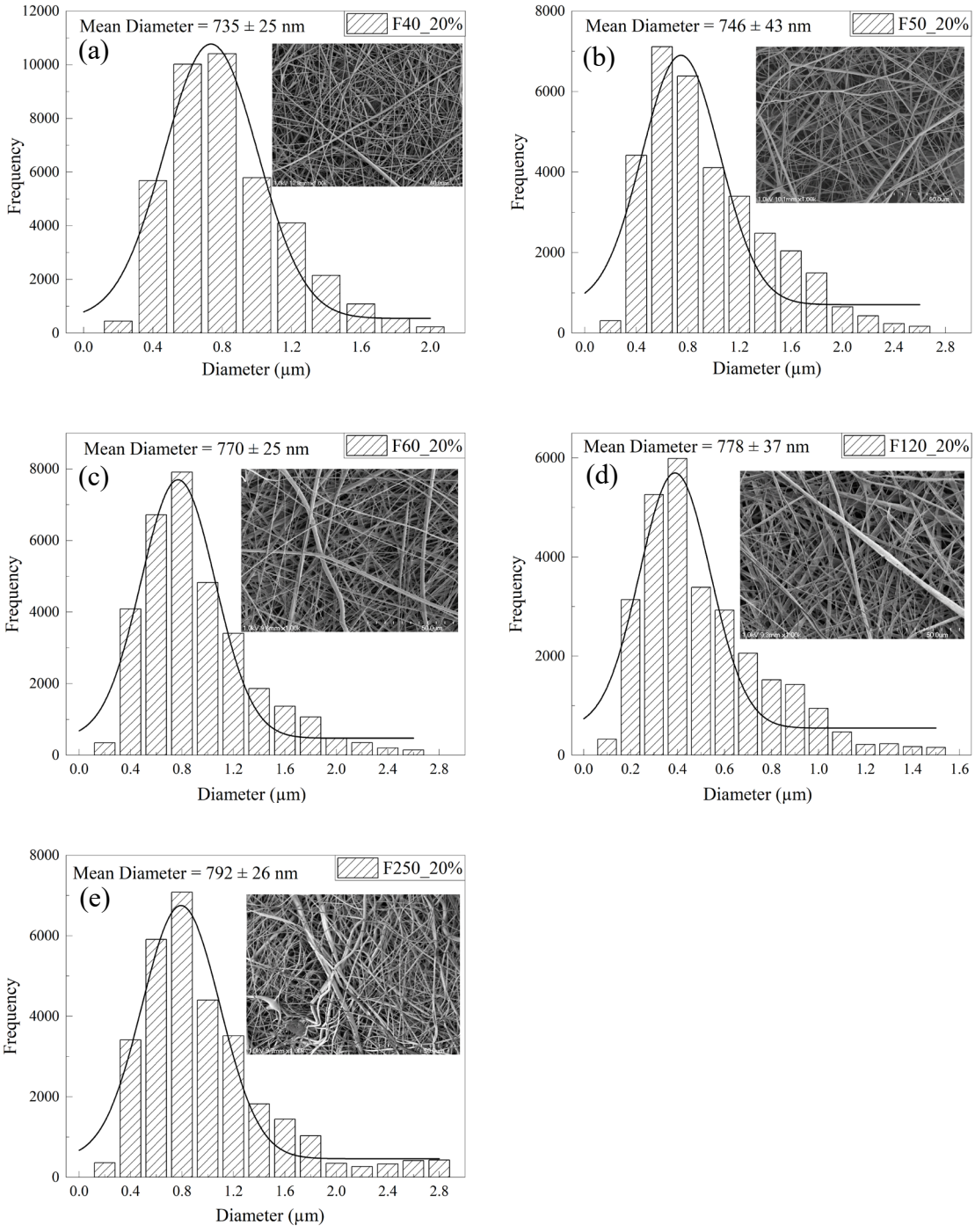

Figure 4.3 Diameter distribution of EPM formed by electrospinning a solution containing 20% PET concentration and flow rates of (a) 40μL/min, (b) 50μL/min, (c) 60μL/min, (d) 120μL/min and (e) 250μL/min

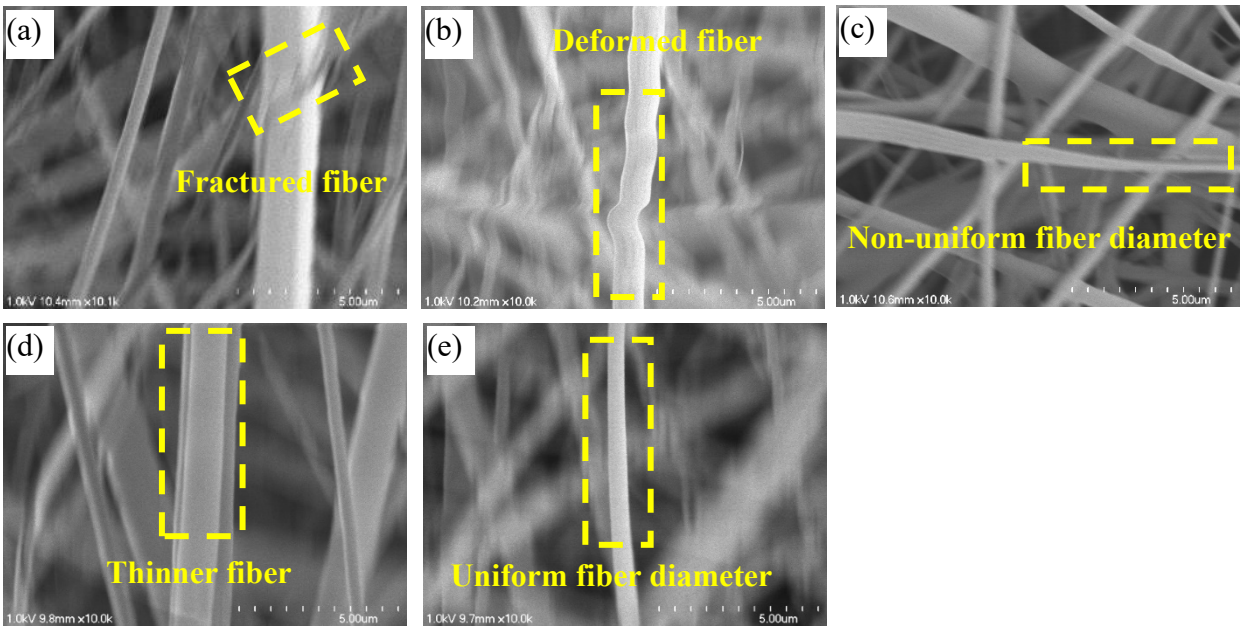

Figure 4.4 SEM micrographs of EPMs produced by electrospinning of a solution containing 15% PET concentration and flow rates of (a) 250µL/min, (b) 120µL/min, (c) 60µL/min, (d) 50µL/min and (e) 40µL/min showing the morphology of EPM

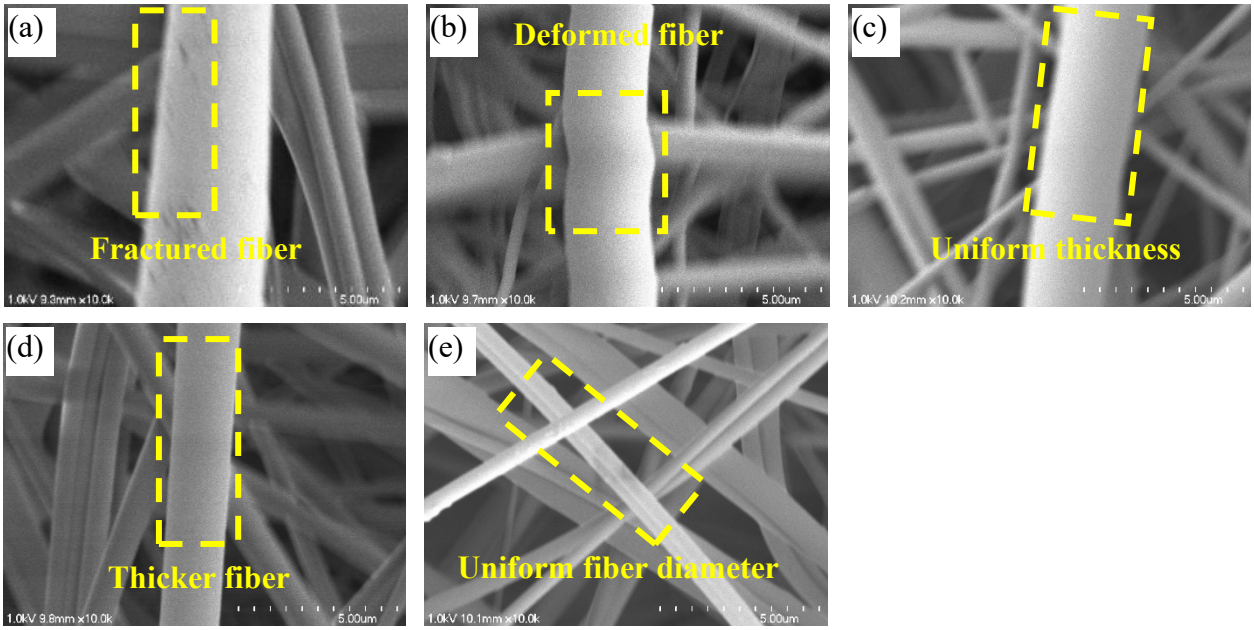

Figure 4.5 SEM micrographs of EPMs produced by electrospinning of a solution containing 20% PET concentration and flow rates of (a) 250µL/min, (b) 120µL/min, (c) 60µL/min, (d) 50µL/min and (e) 40µL/min showing the morphology of EPM

The SEM micrographs in Figures 4.4 and 4.5 obtained at a flow rate of 250µL/min reveal that fibers showed some surface fractures. In contrast, when the flow rate was reduced to 120µL/min, the produced fibers did not exhibit fractures on their surfaces; instead, they displayed deformations along their axis, as shown in Figures 4.4b and 4.5b for both PET concentrations. When the flow rate was further decreased to 60µL/min, the resulting fibers showed a non-uniform thickness at a concentration of 15% PET (Figure 4.4c), whereas fibers with a uniform thickness were observed at a concentration of 20% PET (Figure

4.5c) produced using the same flow rate. The flow rates of 50 (Figures 4.4d and 4.5d) and 40μL/min for both 15% and 20% PET concentrations resulted in even more uniform fibers than their respective higher flow rates, as shown in Figures 4.4e and 4.5e. However, the thickness of the fibers at various concentrations and flow rates varied. This phenomenon is predominantly attributable to the inverse effects of surface tension and increase in solution viscosity and flow rate, which cause the solution-air interface to expand (Aydemir and Demiryürek, 2022). An increased flow rate resulted in an unstable jet, producing more considerable variations in the fibers' diameters. In addition, it has been observed that at an optimal viscosity and flow rate, which produces a stable and continuous flow, defect-free fibers can be produced (Haider et al., 2018). In this study, when the flow rates of less than 120 μL/min were used, uniform and defect-free fibers began to form for both 15% and 20% PET concentrations. In summary, the fibers with the highest uniformity were consistently generated at the lowest spinnable flow rates, regardless of the viscosity and PET concentrations. Generally, fibers produced at low flow rates exhibited a smooth and cylindrical shape, and their surface was free of structural defects.

4.1.3 Mechanical Properties of EPM Fibers

The mechanical characteristics of EPM were evaluated by conducting uniaxial tensile tests on EPM mats. Variations of different mechanical properties of the EPMs with fiber diameters (from SEM images) are depicted in Figure 4.6. Figures 4.6a and 4.6 show the force and strain corresponded to the ultimate strength and strain, respectively, as fiber diameters increased. In other words, an increase in EPM's diameter resulted in a reduction in the strength and ductility of the produced fibers. Specifically, the force corresponding to the ultimate strength was found to decline from 6.54 N to 1.14 N for a PET concentration of 15% as the fiber diameter increased from 673 nm to 799 nm.

Similar trends were observed for:

- EPM prepared by solutions having 20% PET concentration. In this case, the force corresponding to ultimate strength dropped from 16.02 N to 4.72 N as the fiber diameter changed from 735 nm to 792 nm. In addition, the ultimate strain was found to drop from 28.6 % to 6.2% for a PET concentration of 15% as the fiber diameter increased from 673 nm to 799 nm.
- EPM prepared by solutions having 20% PET concentration. In this case, the strain corresponding to ultimate strength dropped from 48.36 % to 14.86 % as the fiber diameter changed from 735nm to 792 nm. It was observed that the force corresponding to the ultimate strength and strain for the same flow rates were higher when a concentration of 20% PET was used compared to EPMs produced using solutions having 15% PET concentration. The modulus of EPM was found to increase from 13.02 N to 245.48 N for a PET concentration of 15% as the fiber diameter decreased from 799 to 706 nm (Figure 4.6c). However, upon further reduction in diameter to 673 nm, the EPM's modulus dropped to 141.46 N.
- EPM prepared by solutions having 20% PET concentration. In this case, the modulus increased from 100.54 N to 370.88 N as the fiber diameter changed from 792 nm to 746 nm. Nevertheless, a subsequent reduction in diameter to 735nm led to a decline in modulus to 361.94 N. The modulus and force values corresponding to the yield strength measured for the fibers produced with the PET concentration of 15% increased by 74 and 4 %, respectively, due to increasing the fiber diameter from 673 to 706 nm. Raising the diameter of the fiber from 706 to 799 nm reduced both modulus and yield force values by 95 and 86%, respectively (Figure 4.6c and 4.6d).

For EPMs produced using solutions of 20% PET concentration, an increase in fiber diameters from 735 nm to 748 nm was associated with an increase in modulus and yield force. However, modulus and ultimate strain values decreased as the diameter further changed from 746 nm to 792 nm. Despite showing similar variation patterns of modulus and ultimate strain values with fiber diameters in both PET concentrations, fibers produced using 20% PET concentration showed higher modulus and ultimate strain values than those produced with solutions of 15% PET concentration.

Overall, the changes observed in the mechanical properties of EPM were attributed to the ultrafine nanofibers' interconnected chain orientation network and uniform distribution of the fibers' internal structure as fibers get finer (Papkov et al., 2013). Reviewing the presented mechanical properties of the EPMs produced in the laboratory revealed the highest modulus and strength values were achieved when the fibers were produced by electrospinning a solution of 20% PET concentration at a flow rate of 50 µL/min. While smoother and more uniform fibers were achieved by electrospinning PET solutions flow rates below 50µL/min, a significant drop in their diameter decreased substantially, resulting in a reduction in the force corresponding to yield point and a more pronounced plastic behavior. However, as the flow rate decreased, the produced fibers became finer and more cylindrical, resulting in enhanced mechanical properties. Consequently, at reduced flow rates, the ultimate strength and toughness increased.

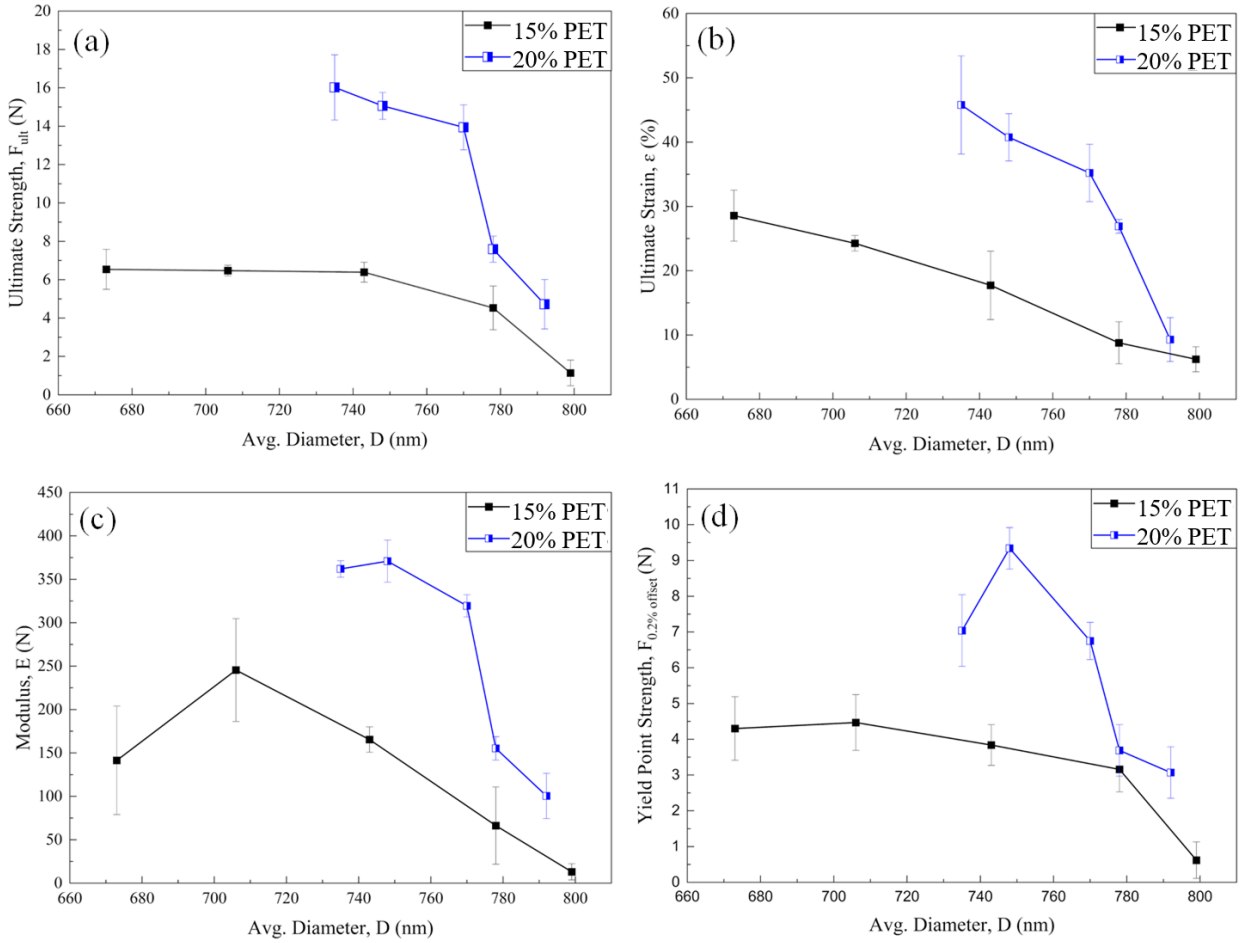

Figure 4.6 Mechanical properties of EPM produced using 15% and 20% PET concentrations and different flow rates with fiber diameters (a) ultimate strength, (b) strain at ultimate strength, (c) modulus, (d) yield strength at 0.2% offset

4.1.4 Selection of the EPM Type as an Asphalt Binder Additive

From the EPM production experience and after the characterization of EPM, as discussed in sections 4.1.1, 4.1.2, and 4.1.3, it was found using high flow rates and low PET concentrations in the electrospinning process produced fibers that were defective, beaded, and had inconsistent geometries. In addition, their mechanical characteristics were less desirable when compared to other tested EPMs. On the other hand, using high PET concentration and very low flow rates in the electrospinning process slowed the fiber production rate and caused frequent clogging of the electrospinning needle and frequent interruption in the process. Notably, the fiber production rate is essential to enhance feasibility of the

asphalt industry's large-scale use of EPM. Considering the overall challenges associated with the mass production of EPM through electrospinning and after reviewing the fibers' characteristics presented in the preceding sections, a 20% PET concentration and 60µL/min flow rate were considered electrospinning parameters for further mass production of EPM. This type of EPM was utilized to modify PG 58-28 asphalt binder and asphalt mixes. Table 4.1 summarizes the morphology and mechanical properties of this specific type of EPM fiber. In the upcoming sections of this document, this type of fiber will be referred to as EPM.

Table 4.1 Characteristics of the EPM selected for asphalt binder and mix modification

EPM Properties	Unit	Measured Value	Standard Deviation
PET concentration	%	20	-
Electrospinning flow rate	µL/min	60	-
Fiber diameter	nm	770	25
Ultimate strength	N	13.94	1.17
Ultimate strain	%	31.98	4.46
Modulus	N	319.43	12.83
Yield strength	N	6.75	0.52
Fiber toughness	N/m^2	3.47	2.69

4.2 Effect of EPM as an Additive on Asphalt Binders' Characteristics

4.2.1 Rutting Factor

The rutting factor of asphalt binder is a parameter used to express its ability to resist shear deformation at elevated temperatures. The rutting factor depends on complex modulus (|G*|) and phase angle (δ) values measured for an asphalt binder, defined as |G*|/sin δ. The higher the rutting factor values, the higher the resistance to shear flow and rutting. Figure 4.7 summarizes the rutting factors of unaged and RTFO-aged asphalt binders (PG 58-28 binder containing 0, 0.2, 0.5, 0.7, and 1.0% EPM and neat PG 58-34 and PG 64-28 binders) calculated based on the |G*| and δ values measured through testing them using a DSR equipment at different temperatures. The results indicated that at the same temperature and aging conditions, the rutting factor of PG 58-28 binder blends containing EPM was higher than that of neat PG 58-28 asphalt binder. Specifically, the rutting factors measured for the unaged PG 58-28 asphalt binder containing 0.2, 0.5, 0.7, and 1.0% EPM at 64°C were 34, 56, 115, and 125% higher than that of the neat PG 58-28 binder, respectively. A similar trend of variation in the rutting factor with incorporating EPM in PG 58-28 was also observed after RTFO-aging of the binder blends. Therefore, it can be concluded that incorporating EPM into neat PG 58-28 increased the asphalt binder's stiffness and elasticity and, hence, its resistance to rutting. However, at given temperatures and aging conditions, the |G*|/sin δ value of EPM-modified PG 58-28 asphalt binders is higher than PG 58-28 and PG 58-34 but lower than PG 64-28. The efficient load transfer from the asphalt matrix to the EPM fibers contributes to an improvement in the asphalt binder's resistance to rutting. On the other hand, according to Arabani and Shabani (2019) and Chen and Xu (2010), fibers tend to absorb the asphalt molecules, which consequently increases the asphalt binder viscosity and an improved resistance to rutting. In addition, it can be concluded that incorporating EPM up to 1.0% in the asphalt binder enhanced its resistance to rutting at all test temperatures. However, the direct addition of EPM into the asphalt binder in quantities more than 1.0% by asphalt binder's weight resulted in difficulties associated with uniform dispersion due to fiber concentration and agglomerations. Notably, the rutting parameter, |G*|/sin δ, does not consider the asphalt binder's recovery after loading and its sensitivity to different vehicular load levels. An asphalt

binder's elastic recovery and non-recoverable creep play a crucial role in explaining its resistance to permanent deformation during and after loading.

The Superpave binder specifications specify minimum |G*|/sin δ values for rutting resistance at temperature. According to the specifications, the minimum rutting factor for unaged and RTFO-aged asphalt binders must be above 1.0 and 2.2 kPa, respectively, to meet the critical H-T requirement. Incorporating 0.2, 0.5, 0.7, and 1.0% EPM in PG 58-28 asphalt binder bumped up the H-T PG of the binder to 64, 64, 70, and 70°C, respectively. Although an increase in EPM content from 0.2 to 0.5% and 0.7 to 1.0% resulted in an increase in the G*/sin δ value for the RTFO-aged binder, the overall PG grade remained unchanged in both instances.

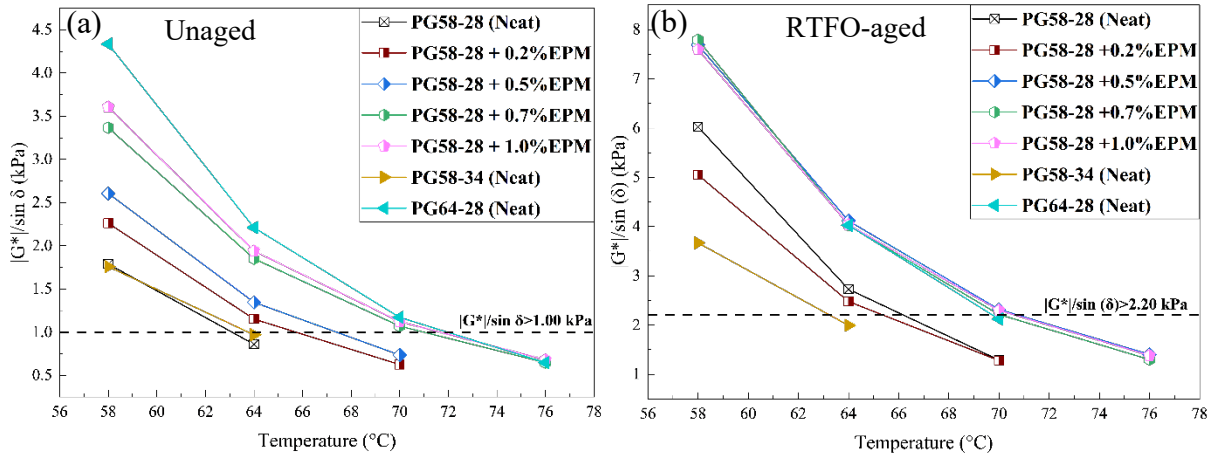

Figure 4.7 Variation of |G*|/sin δ with test temperatures of (a) unaged and (b) RTFO-aged asphalt binders

While the rutting factor is necessary for the H-T PG grading of asphalt binder, conducting an MSCR test and interpreting its results will provide more insight into the rutting potential of asphalt binders containing EPM subjected to vehicular loads.

4.2.2 Fatigue Parameter

A high value of the fatigue parameter (|G*| sin δ) measured at intermediate temperature (I-T) indicates a poor resistance to fatigue cracking. Therefore, to understand the fatigue performance of different asphalt binders and the effect of incorporating EPM in the binder blends on their resistance to fatigue cracking in the asphalt binders, DSR tests were performed on PAV-aged asphalt binders at temperatures ranging from 9 to 25°C with 3°C intervals. Their fatigue parameters were determined and summarized in Figure 4.8. Incorporating EPM in PG 58-28 asphalt binder resulted in a reduction in its fatigue parameter compared to neat PG 58-28 binders. Specifically, the |G*| sin δ value measured for the PAV-aged PG 58-28 containing 0.2, 0.5, 0.7, and 1.0% EPM at 12°C was 31, 40, 31, and 29% lower than that of the neat PG 58-28 binder, respectively. The results show incorporating 0.5% EPM in asphalt binder was the most effective in improving resistance of the binder to fatigue cracking. The peak improvement in the resistance to fatigue cracking at 0.5% EPM concentration can be attributed to the fact that at higher EPM content, the rheological properties of asphalt binders were dominated by fiber properties rather than asphalt binders. The reduction in the fatigue parameter due to incorporating EPM in the PG 58-28 asphalt binder suggests that asphalt binder containing EPM fibers is more resistant to fatigue when compared with the neat binder. This observation is also confirmed by the findings of Zhang et al. (2019). Another noteworthy observation was adding EPM to the neat PG 58-28 asphalt binder resulted in a lower fatigue parameter when compared to the neat PG 64-28 binder at temperatures of 12 and 15°C. This suggests the

fatigue performance of an EPM-modified PG 58-28 binder was superior to that of a neat polymer-modified PG 64-28 binder. The PG critical intermediate temperatures were calculated based on G*sinδ ≤ 5000 kPa for each PAV-aged binder (AASHTO, 2017). It was found that the critical intermediate temperature of PAV-aged neat PG 58-28 binder (18.4°C) dropped to 14.4, 13.3, 14.3, and 14.6°C when 0.2, 0.5, 0.7, and 1.0% EPM were incorporated, respectively. This finding indicates the addition of EPM to neat asphalt binder resulted in an enhancement of their fatigue resistance. However, the I-T failure temperature of EPM-incorporated asphalt binder was lower than PG 64-28 but higher than PG 58-34. Comparing the I-T value of the PG 64-28 (PMB) binder to the I-T values of the EPM-modified binder revealed that the PG 58-28 containing EPM had significantly lower I-T values than the neat PG 64-28. The preceding discussion demonstrates adding EPM to asphalt binder can improve its resistance to fatigue cracking while preserving its performance at intermediate temperatures.

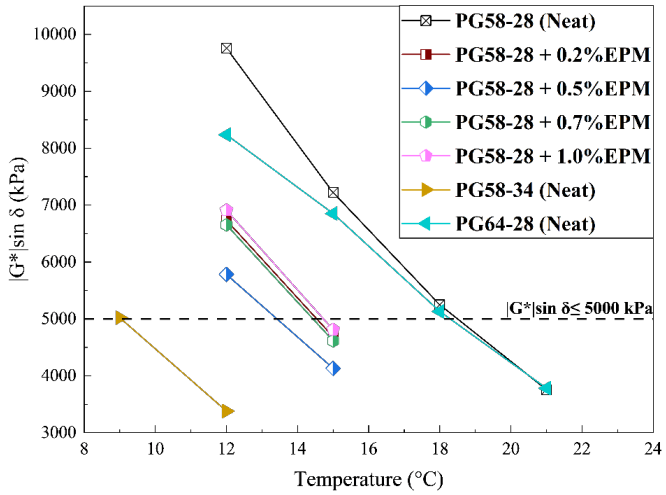

Figure 4.8 Fatigue parameters of asphalt binder blends measured at different temperatures

4.2.3 Resistance to Thermal Cracking

Measuring the low temperature (L-T) stiffness modulus (S) and creep rate (m) allows for determination of the resistance of the asphalt binders to L-T cracking. Therefore, a BBR was used to evaluate the resistance of asphalt blends containing EPM to L-T cracking based on measuring the S and m-values. Figure 4.9 shows the variation of the S and m-values of different neat and EPM-incorporated asphalt binders. It is evident that as the temperature increased from -30 to -12°C, asphalt binder stiffness values decreased. Under the same test temperature conditions, stiffness of the asphalt binders gradually increased with the increase in the EPM content, up to 0.7%. Specifically, at -18°C, incorporating 0.7% EPM in PG 58-28 binder increased the creep stiffness from 221.9 to 498.7 MPa, a 125% increase. Also, incorporating 1.0% EPM in the PG 58-28 binder further reduced stiffness of the binder at the same temperature compared to the PG 58-28 containing 0.7% EPM. Therefore, it can be concluded that incorporating EPM fibers in the binder helped bear some of the stress during the loading process, thereby increasing its stiffness. Increasing the EPM content of the binder further increased the creep stiffness. Apart from stiffness, the m-value is an essential parameter that describes the asphalt binder's capability for stress relaxation. A greater m-value indicates a higher stress relaxation, implying superior low-temperature performance during rapid temperature drops. According to the Superpave specification, the minimum m-value of asphalt binder should be 0.300. Figure 4.9 demonstrates the m-values measured for various asphalt binder types and temperatures. Under identical temperature conditions, the m-value decreases as the EPM fiber content increases. For example, at -24°C, the m-values of asphalt blends with various EPM fiber contents were less than 0.3, which did not satisfy the Superpave specification's requirements. This

suggests that adding EPM fibers to asphalt has a slight adverse effect on the asphalt binder's resistance to low-temperature cracking. When the EPM content in the neat binder exceeded 0.5%, the properties of the binder were presumed to be influenced more by the properties of the EPM fibers than by the asphalt binder itself. This can be observed when the temperature abruptly drops from -12°C to -24°C as the EPM fibers approach their glass transition temperature, causing the binder to stiffen. Adding EPM fibers effectively increased the asphalt's viscosity, increasing its stiffness. Incorporating EPM could also increase the binder's glass transition temperature, decreasing its L-T performance. Notably, the BBR test evaluates the L-T performance of the binder using parameters, such as creep stiffness and creep rate. As a result, it might not adequately represent the elongation properties of EPM-modified binders. Therefore, it is difficult to evaluate the toughening effects of EPM in asphalt using only the limited data provided by the BBR test.

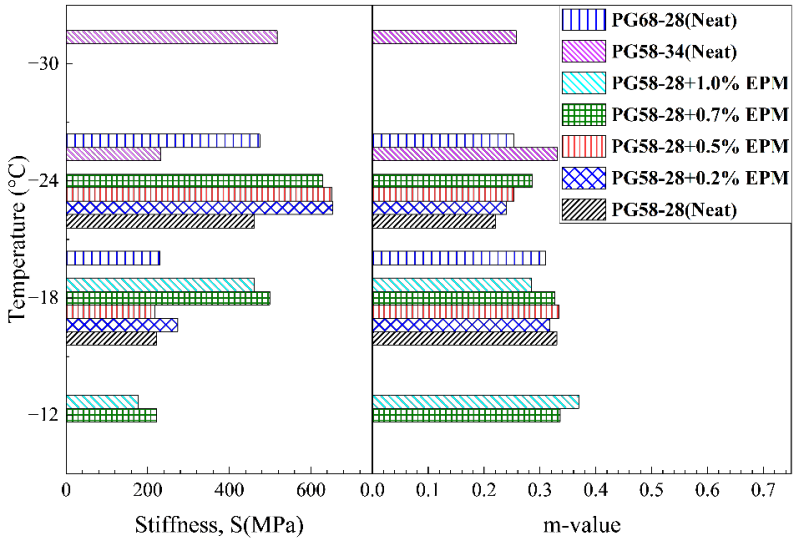

Figure 4.9 A summary of the S and m values of different blends of neat and EPM-containing binders

As discussed earlier, ΔTc (Delta Tc) is another parameter used to evaluate the aging and non-load-related cracking potential of asphalt binders. In a given asphalt binder, the $\Delta Tc > 0$ or $\Delta Tc < 0$ indicates whether the L-T PG of the asphalt binder is controlled by its creep stiffness (S) or creep rate (m), respectively. Recently, it has been perceived that if $\Delta Tc \geq -2.5$°C, the asphalt binder is considered to have good resistance to low-temperature cracking. Otherwise, the asphalt binder is more susceptible to low-temperature cracking, indicating potential aging issues. Figure 4.10 provides a summary of the ΔT_c values for neat PG 58-34, neat PG 64-28, and PG 58-28 asphalt binder containing 0.0, 0.2, 0.5, 0.7, and 1.0% EPM (by asphalt binder's weight). The ΔT_c values of the neat PG 58-28, PG 64-28, and PG 58-34 asphalt binders were found to be -0.8, -1.1, and 0.6°C, respectively, indicating an excellent resistance to long-term L-T cracking. When EPM fibers were added to the m-controlled neat PG 58-28 binder, the ΔT_c value shifted from negative to positive, indicating a transition to S-controlled behavior. Specifically, the ΔT_c values of PG 58-28 asphalt binder containing 0.2, 0.5, 0.7, and 1.0%EPM were +0.7, +0.8, +7.7, and +1.6°C, respectively, an improved resistance to long-term L-T aging-related cracking.

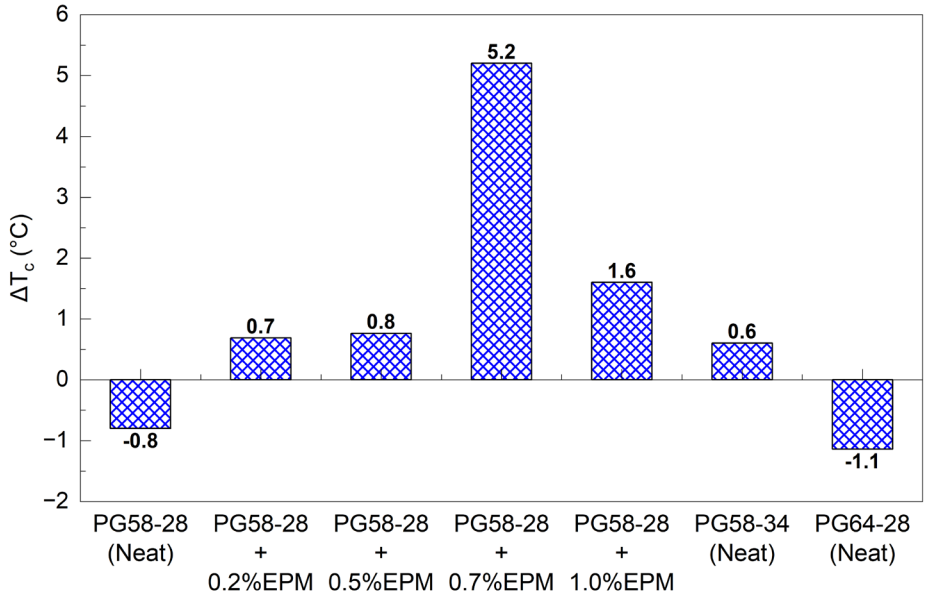

Figure 4.10 ΔT_c values measured for different blends of neat and EPM-containing binders

4.2.4 Superpave PG Grade of Asphalt Binder Blends

A summary of the continuous H-T and L-T grades of neat PG 58-28, neat PG 58-34, and PG 64-28 binder blends containing 0.2, 0.5, 0.7, and 1.0% EPM determined by AASHTO M 320 (AASHTO, 2017) is provided in Figure 4.11. It was found that adding 0.2% EPM to PG 58-28 asphalt binder resulted in a 2.6°C increase in the H-T grade and a 1.0°C increase in the L-T grade compared to the neat binder. Notably, the positive impact on the H-T grade was over 2.5 times greater than the negative impact on the L-T grade. In addition, the inclusion of 0.2% EPM bumped the H-T grade up to a PG 64-28, whereas the L-T grade remained unchanged. Furthermore, adding 0.5% EPM to the PG 58-28 asphalt binder increased the H-T grade of the neat binder by 4.2°C and decreased the L-T grade by 0.2°C. In other words, the H-T grade of PG 58-28+0.5%EPM was comparable to that of neat PG 64-28, while the L-T grade was marginally lower than that of neat PG 58-28. This demonstrates that 0.5% EPM fibers can supplant PG 64-28 while maintaining comparable performance. Figure 4.11 also indicates the H-T grade continued to rise as the amount of EPM in the neat PG 58-28 binder increased. For instance, adding 1.0% EPM to PG 58-28 enhanced the H-T grade by two PG grades, resulting in a performance grade of PG 70-22. However, incorporating 0.5% EPM in the PG 58-28 asphalt binder raised its L-T by 4.3°C, resulting in a PG 70-22 performance grade. Figure 4.11 also suggested that PG 58-28+ 0.5% EPM exhibited the highest similarity to neat PG 64-28, a polymer-modified binder. This shows that PG 58-28 could be engineered with the right amount of EPM to obtain an asphalt binder with a PG grade similar to that of a polymer-modified binder (PMB) — PG 64-28 in this case. This discovery is significant because it demonstrates the viability of augmenting the PG grade of the neat binder while substituting a non-PMB binder with a hybrid asphalt binder containing waste PET plastic. This study has provided valuable insights into the potential of incorporating EPM to improve the performance of asphalt binders, especially regarding rutting resistance, and opened the door to tailoring binder properties to satisfy specific requirements.

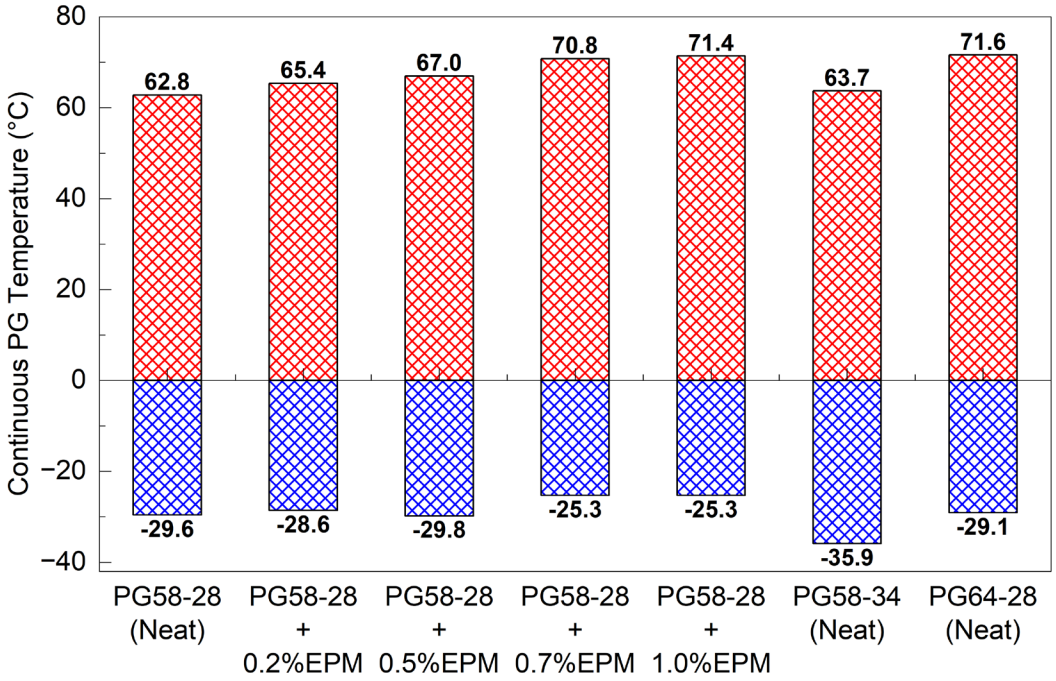

Figure 4.11 Continuous grades of different asphalt binder blends

4.2.5 Vehicular Load-Related Rutting Potential

The results of the MSCR test conducted on the asphalt binder blends were utilized to determine the effect of incorporating EPM in asphalt binder on its elastic recovery (R), non-recoverable creep compliance (J_{nr}), and stress sensitivity. In addition, the MSCR grades of the asphalt binder blends under different vehicular loading conditions at 58°C were determined.

The residual deformation at repeated loading reflects the delayed elastic properties of the asphalt binder, and the non-recoverable creep compliance (J_{nr}) serves as an indicator for evaluating the permanent deformation. The J_{nr} value quantifies the irreversible creep and represents the asphalt binder's delayed elasticity. As the value of J_{nr} approaches zero, it indicates an increased resistance to rutting (Ghanoon et al., 2020). Figure 4.12 presents J_{nr} values determined for the neat PG 58-28, neat PG 58-34, and PG 64-28 binder and blends containing 0.2, 0.5, 0.7, and 1.0% EPM, measured at 0.1 kPa and 3.2 kPa stress levels. The addition of EPM to PG 58-28 binder resulted in a reduction in J_{nr} values. When 0.2% EPM was added to the PG 58-28 binder, the J_{nr} values measured at 0.1 kPa and 3.2 kPa stress levels showed a reduction by approximately 30 and 2.5%, respectively, when compared with neat PG 58-28. Similarly, the addition of 0.5% EPM to PG 58-28 reduced the J_{nr} values of the neat binder by 82 and 49% at 0.1 and 3.2 kPa stress levels, respectively. As the amount of the incorporated EPM increased to 0.7 and 1.0%, the J_{nr} values also decreased by 85 and 53% and 89 and 55%, respectively. It is notable that by incorporating 0.5% EPM into PG 58-28, the J_{nr} values for the EPM-modified binder were even lower than those for neat PG 58-34 (0.81 and 1.36 kPa^{-1} at 0.1 and 3.2 kPa, respectively). Nonetheless, the J_{nr} values for neat PG 64-28 binders were lower than those of all other binders (0.35 and 0.51 kPa^{-1} at 0.1 and 3.2 kPa, respectively). This indicates that adding EPM to the neat PG 58-28 binder enhanced its resistance to permanent deformation (non-recoverable creep). In addition, the results also indicated the incorporation of EPM stiffens the binder, thereby increasing its resistance to rutting. Notably, as the stress level increased to 3.2 kPa, the J_{nr} values also increased. This implies a higher traffic load would result in a higher permanent deformation of the EPM-modified binder. According to Zhang et al. (2016), the higher

the non-recoverable creep compliance, the larger the permanent deformation under the repeated load. The J_{nr} values in Figure 4.12 show that even the PG 64-28 (PMB) had J_{nr} values substantially higher than the PG 58-28 asphalt binder, containing 0.5, 0.7, and 1.0% EPM at different stress levels.

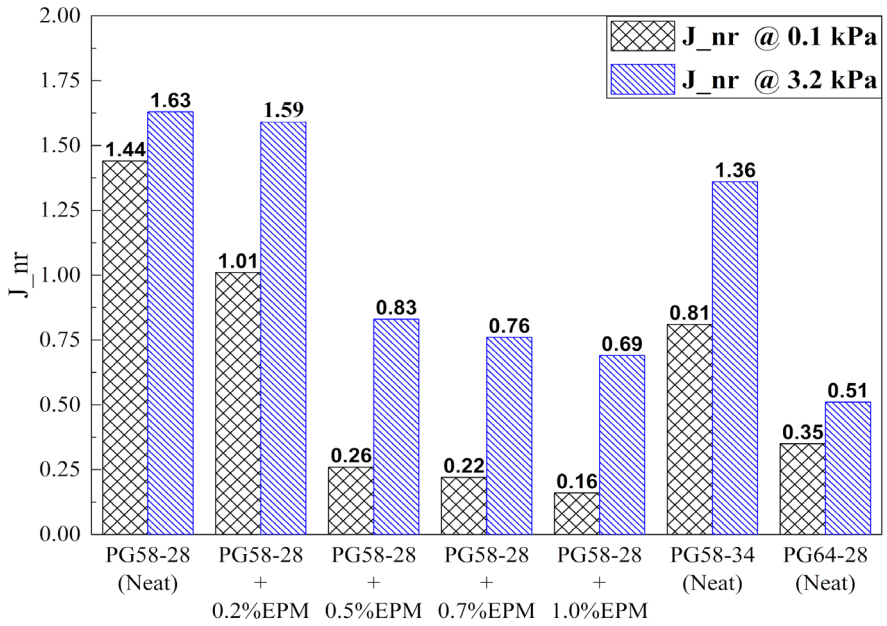

Figure 4.12 Non-recoverable creep compliance (J_{nr}) for the tested asphalt binder blends

The elastic recovery (R) is a parameter obtained from the MSCR test used to characterize the elastic behavior of a binder subjected to traffic loading, which defines the ability of a binder to recover its original shape after deformation (Al-Sabaeei et al., 2022). A higher recovery percentage means the asphalt binder is more elastic since more strain returns to its original state within nine seconds of each resting cycle (Ghansoon and Tanzadeh, 2019). Figure 4.13 summarizes the elastic recovery values for the neat PG 58-34, neat PG 64-28, and PG 58-28 asphalt binder containing different amounts of EPM. It was observed that adding EPM to neat PG 58-28 improved its elastic recovery value. Figure 4.13 also reveals the elastic recovery of the neat PG 58-28 binder was 6.03 and 1.05%, respectively, at 0.1 and 3.2 kPa stress levels, indicating its limited resistance to rutting. However, as EPM was added to PG 58-28 asphalt binder, its elastic recovery increased. This observation suggests incorporating EPM increased the asphalt binder's potential to regain its original shape after being subjected to vehicular loads and a higher resistance to rutting. For example, adding 0.2% EPM to PG 58-28 binder increased the R values measured at 0.1 and 3.2 kPa stress levels by approximately 405 and 273%, respectively. Additionally, as the EPM amounts added to PG 58-28 asphalt binder were increased, the elastic recovery continued to rise. The maximum elastic recovery was observed when 1.0% EPM was incorporated in the PG 58-28 asphalt binder, with R values of 75.33 and 21.39% at 0.1 and 3.2 kPa, respectively.

Furthermore, from Figure 4.13, the incorporation of EPM in PG 58-28 binder was more effective in improving the elastic recovery of asphalt binder at both low and high stress levels (0.1 and 3.2 kPa), which indicates improved resistance to rutting under high traffic loads. It is noteworthy that the PG 58-28 asphalt binder containing 0.5, 0.7, and 1.0% EPM exhibited elastic recovery values at 0.1 kPa stress levels, which were higher than the polymer-modified asphalt binders, PG 58-34 and PG 64-28. However, at a high stress level (3.2 kPa), the EPM-modified binder exhibited elastic recovery values lower than those of the PG 64-28 and PG 58-34 asphalt binders. This phenomenon can be explained by the interfacial bond strength proposed by Ashish and Singh (2018), which plays a vital role in the transmission of load from the asphalt matrix to the fibers. The significant difference observed in elastic recovery values at 0.1 kPa and 3.2 kPa stress levels suggests that at the low stress level (0.1 kPa), the interfacial bond strength

was sufficiently strong to transmit the applied shear load from the asphalt matrix phase to the EPMs, which means applied stress was distributed on both the EPM and the asphalt matrix. However, the interfacial bond strength might not be as strong and efficient in transferring the stress to the EPM at a higher stress level (3.2 kPa) than a lower one. Consequently, the asphalt binder matrix carried a significant fraction of the load at higher stress levels than EPM. Therefore, the elastic recovery of the asphalt binder at a high stress level was to an extended part controlled by a non-PMB asphalt binder (PG 58-28) rather than the EPM.

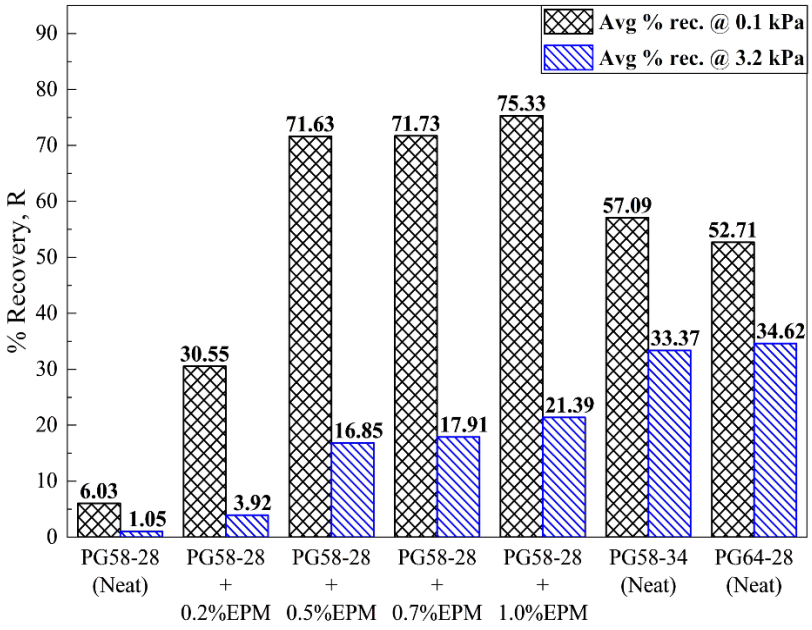

Figure 4.13 Elastic recovery of different tested asphalt binder blends

While the J_{nr} and R values are essential parameters concerning an asphalt binder's rutting potential, the asphalt binder's stress sensitivity should also be limited. A high level of stress sensitivity is undesirable in an asphalt binder as it reduces resistance of the pavement to rutting. A parameter, known as the J_{nr} difference value (J_{nr_diff}), is used to evaluate the stress sensitivity of an asphalt binder, according to AASHTO M 332 (AASHTO, 2017). A relatively low stress sensitivity is advantageous because it allows the pavement to withstand the deformations induced by dynamic vehicle loads, extending its service life (Yang et al., 2019).

Figure 4.14 summarizes the values of J_{nr_diff} determined for neat PG 58-34, neat PG 64-28, and PG 58-28 containing different quantities of EPM. The neat PG 58-28 had the lowest J_{nr_diff} value compared to all tested binders and higher stability under variable axle loading conditions. On the other hand, PG 58-28+0.2% EPM exhibited the lowest stress sensitivity among all EPM-modified binders, which is 57.68%. Besides, the J_{nr_diff} values for the neat PG 58-28, PG 58-34, and PG 64-28 binders were 13.66, 68.43, and 44.66%, respectively. In addition, the J_{nr_diff} values for PG 58-28+0.5%EPM, PG 58-28+0.7%EPM, and PG 58-28+1.0%EPM binders were 220, 252, and 324%, respectively. Therefore, Figure 4.16 demonstrates that, except for the PG 58-28+0.2% EPM, none of the EPM-modified PG 58-28 binders met the AASHTO MP 19 requirement.

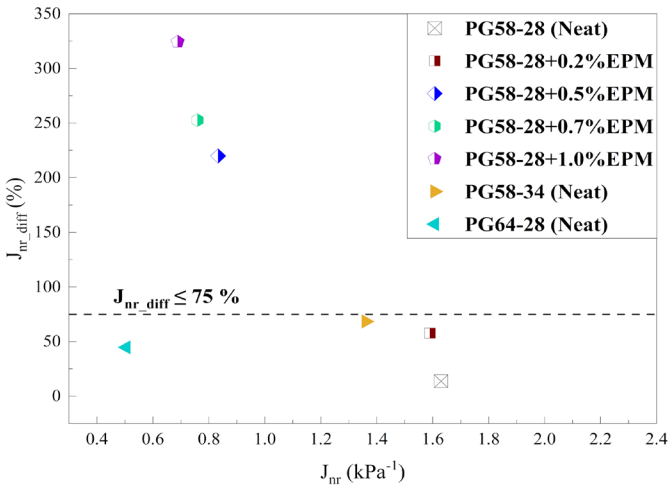

Figure 4.14 Stress sensitivity of different tested asphalt binder blends

In conclusion, an increase in the EPM content resulted in an increase in the J_{nr_diff} value, which implied a rise in the asphalt binder's stress sensitivity under varying axle-loading conditions. Adding EPM fiber at concentrations from 0.2 to 1.0% increased the J_{nr_diff} value significantly from 57.7 to 324.4%. The observed increase in stress sensitivity with increasing EPM content can be attributed to factors, such as the interfacial bond strength between the EPM and asphalt binder matrix and the dispersion of the EPM fibers discussed earlier.

4.2.6 MSCR Grade of Asphalt Binder Blends

As per the vehicular traffic requirements specified in AASHTO M 332 (AASHTO, 2017), various loading categories classify asphalt binders. Figure 4.15 depicts the variations in J_{nr} and R values for various binder blends measured at 3.2 kPa of stress. Also, the AASHTO recovery curve and zones corresponding to various traffic categories, namely standard (S), high (H), very high (V), and extremely high (E), are shown in Figure 4.15. It was observed that the R-J_{nr} pairs corresponding to the neat PG 64-28 and neat PG 58-34 were positioned on or above the AASHTO recovery curve, indicating polymer-modified binders (PMB). However, R-J_{nr} pairs corresponding to the neat PG 58-28 and its blends with various amounts of EPM fell below the AASHTO recovery curve, failing to meet the PMB binder requirements. It was also observed PG 64-28 (PMB) and PG 58-28 containing 0.5, 0.7, and 1.0% EPM were classified as PG 58V. This demonstrates their resistance to very heavy vehicular loads, such as traffic volumes exceeding 30 million equivalent single axle loads (ESALs) or stationary traffic with speeds below 20 kilometers per hour. This indicates that PG 58-28 binder blends containing more than 0.2% EPM were on par with PG 64-28 regarding their MSCR grade. In addition, neat PG 58-34, neat PG 58-28, and its blend with 0.2% EPM met the PG 58H requirements. This indicates their capacity to withstand heavy vehicular loads, equivalent to 10 to 30 million ESALs or slow-moving traffic with speeds between 20 and 70 km/h.

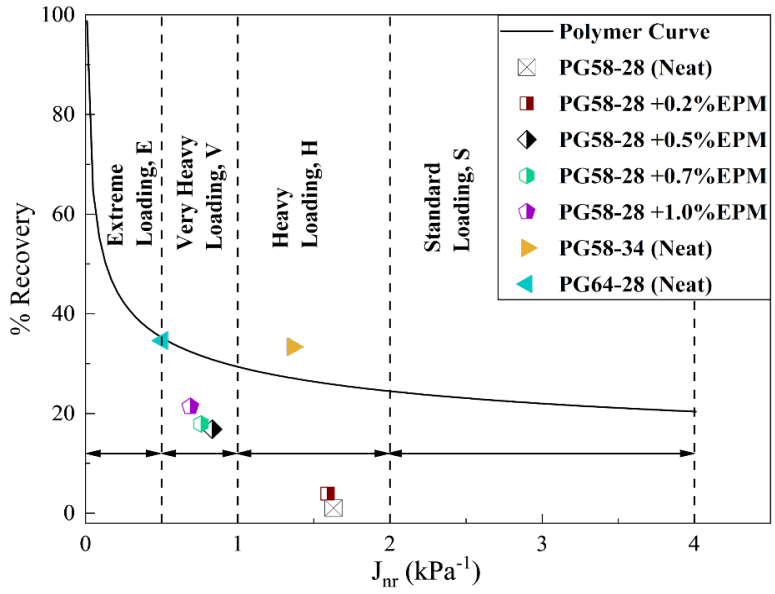

Figure 4.15 The Jnr and R values of asphalt binders measured at 58°C and 3.2 kPa stress level

4.2.7 Asphalt Binder-Aggregate Adhesion

Figure 4.16 summarizes the POS_{dry}, POS_{wet}, and PSR values obtained from the BBS tests on asphalt binder blends with granite aggregate. The POS_{dry} value measured in the neat PG 58-28 asphalt binder and granite aggregate (940.8 kPa) was found to decrease by 33.6, 32.0, 35.0, and 35.8% as a result of incorporating 0.2, 0.5, 0.7, and 1.0% EPM in the binder, respectively. These findings indicate adding EPM to the neat PG 58-28 binder reduced adhesion to granite aggregate. The decrease in the pull-off strength at the binder-aggregate interface could be attributed to the increased surface area present in the asphalt binder, resulting in less asphalt binder available to adhere to the aggregates and an overall reduction of adhesion. As the EPM content increased, the pull-off strength continued to decrease accordingly.

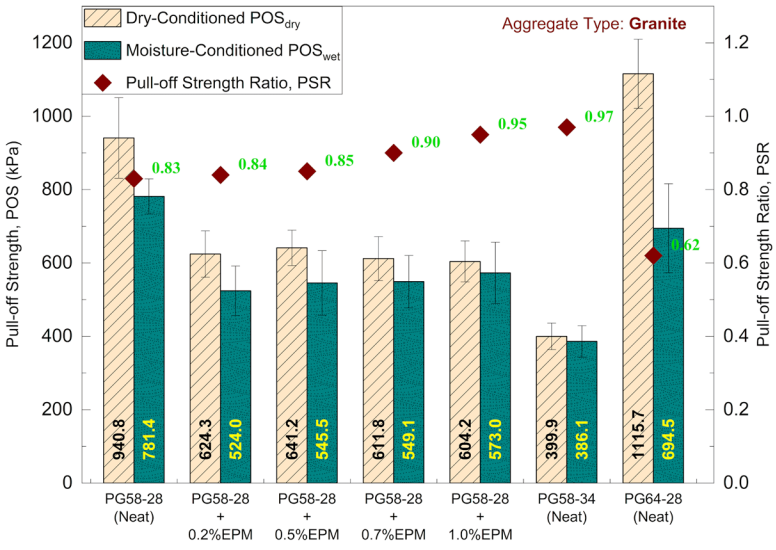

Figure 4.16 POS_{dry}, POS_{wet}, and PSR values of asphalt binder blends with granite aggregate

From Figure 4.16, the PSR value of PG 58-28 with granite (0.83) increased to 0.84, 0.85, 0.90, and 0.95 due to incorporating 0.2, 0.5, 0.7, and 1.0% EPM, respectively. This shows incorporating EPM into the PG 58-28 binder enhanced its resistance to moisture-induced damage. It appears that EPMs in the asphalt binder might have restricted the mobility of the ions and polar molecules, limiting the debonding effect of water. Overall, it was observed that the asphalt binders containing EPM exhibited resistance to moisture-induced damage, which was similar to or better than the polymer-modified binders. In summary, incorporating various amounts of EPM into the PG 58-28 asphalt binder with granite notably enhanced its resistance to moisture-induced damage despite reducing overall bond strength in dry conditions.

4.3 Effect of EPM as an Additive on Asphalt Mix Characteristics

4.3.1 Hamburg Wheel Tracker (HWT) Test

The resistance of asphalt mixes to rutting and stripping was evaluated by conducting an HWT test per the AASHTO T 324 standard test method (AASHTO, 2019). The HWT device automatically records permanent deformation at 11 equally spaced locations on the wheel path during each wheel pass. Two sets of identical specimens (four cylindrical samples) were prepared for each mix and tested in water at 50ºC. Three distinct phases are observed in HWT results: (i) the post-compaction phase corresponds to consolidation of the specimen as the asphalt mix is compacted under the wheel load. The principal deformation mechanism is the compaction of the mix caused by the applied load; (ii) The creep phase is identified predominantly by the viscous flow of asphalt mixes. This phase is characterized by a creep slope, representing a constant rut depth rate per load cycle. The viscous behavior of asphalt mixes is responsible for permanent deformation during the creep phase; (iii) In some cases, the stripping begins when the bond between the asphalt binder and aggregate weakens, which results in visible damage to the asphalt mix structure manifested by a dramatic increase in creep slope. The stripping inflection point (SIP) corresponds to the number of wheel passes at which stripping onsets and the slope of the permanent deformation shows a significant change rapidly.

Figure 4.17 shows the variations of rut depths with wheel passes obtained from conducting HWT tests on asphalt mixes containing no EPM (HMA-C) that containing 0.5% EPM, (HMA + 0.5% EPM), that containing 1.0% EPM (HMA + 1.0% EPM), and that containing 1.5% EPM (HMA + 1.5% EPM). All the HMA mixes exhibited only post-compaction consolidation and creep, and none showed a SIP, indicating an adequate resistance to moisture-induced damage. The post-compaction consolidation ended when the number of wheel passes reached approximately 3,500, 3,000, 2,500, and 4,000 loading cycles for HMA-C, HMA + 0.5% EPM, HMA + 1.0% EPM, and HMA + 1.5% EPM mixes, respectively. It is worth noting that the addition of EPM to the mix shortened the post-compaction phase, meaning fewer loading cycles are required to transition into the creep phase. This observation indicates EPM fibers can reduce the post-compaction consolidation of the HMA, delaying early deformations. Following the post-compaction phase, an extended and distinct creep phase was observed, which continued for the remaining loading cycles until the end of the test (20,000 passes). As a significant stripping phase was not evident, it was concluded that adding the EPM did not compromise the asphalt-binder aggregate bonding and effectively resisted the stripping. Throughout the entire 20,000 loading cycles, the rutting depths of all HMA samples remained well below 12.5 mm, the maximum allowable rut depths for many DOTs. It was observednasphalt mixes containing 0.5% and 1.0% EPM effectively reduced the maximum rut depths compared to the HMA-C. However, when the EPM content was increased to 1.5%, the maximum recorded rut depth increased and became similar to those observed in HMA-C. Table 4.2 summarizes the creep slope values and rut depths measured at 5,000-wheel pass intervals for the tested mixes. It was observed that the rut depths for HMA-C, which does not contain any EPM, were 4.6, 6.0, 7.0, and 7.9 mm at 5000, 10,000, 15,000, and 20,000 wheel passes, respectively. The results indicated that HMA-C had a creep slope of 5,196 passes/mm.

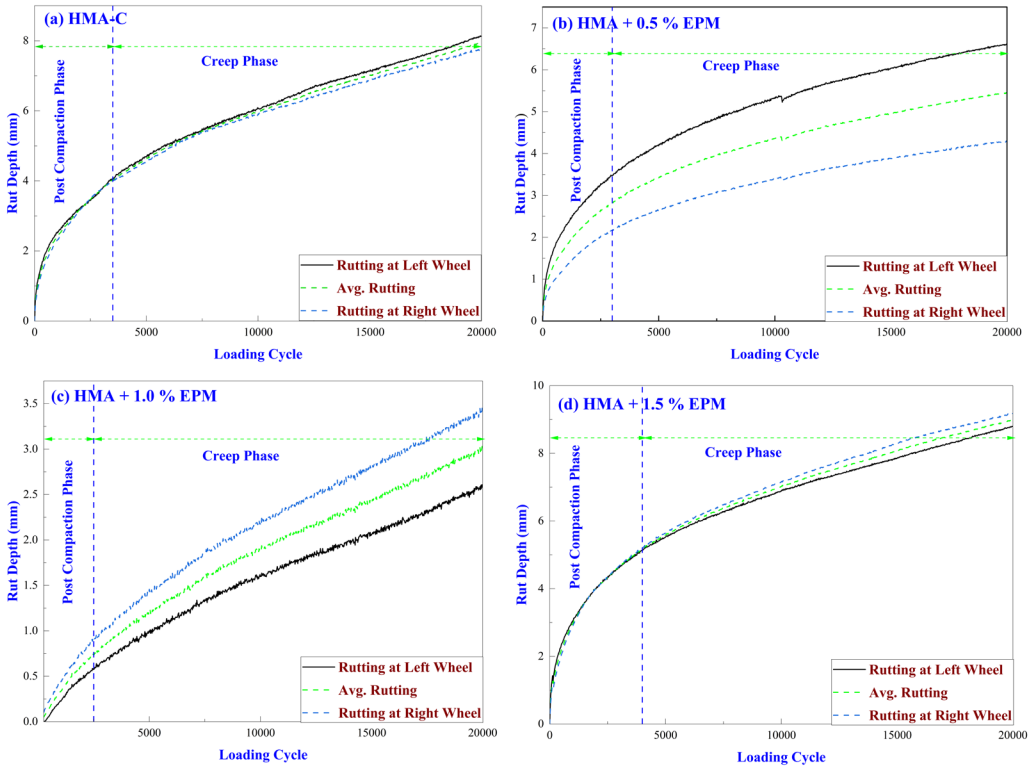

Figure 4.17 Permanent deformation development in asphalt mixes with wheel passes in the HWT test

Table 4.2 Summary of measured permanent deformation and creep slope for different mixes in the HWT test

Mix Type	Permanent Deformation	Number of Wheel Passes				Inverse Creep Slope (Passes/mm)
		5,000	10,000	15,000	20,000	
HMA-C	Deformation Under the Left Wheel (mm)	4.7	6.1	7.1	8.1	5,390
	Deformation Under the Right Wheel (mm)	4.6	5.9	6.9	7.8	5,002
	Average Deformation (mm)	4.6	6.0	7.0	7.9	5,196
HMA +0.5%EPM	Deformation Under the Left Wheel (mm)	2.6	3.4	-3.9	4.3	10,904
	Deformation Under the Right Wheel (mm)	4.2	5.3	-6.0	6.6	7,622
	Average Deformation (mm)	3.4	4.4	-5.0	5.5	9,263
HMA +1.0%EPM	Deformation Under the Left Wheel (mm)	1.0	1.6	2.1	2.6	10,362
	Deformation Under the Right Wheel (mm)	1.5	2.2	2.8	3.4	8,172
	Average Deformation (mm)	1.2	1.9	2.4	3.0	9,267
HMA +1.5%EPM	Deformation Under the Left Wheel (mm)	5.5	6.9	7.9	8.8	5,273
	Deformation Under the Right Wheel (mm)	5.6	7.2	8.3	9.2	4,935
	Average Deformation (mm)	5.6	7.0	8.1	9.0	5,104

In contrast, the measured rut depths for HMA+0.5% EPM at 5000, 10,000, 15,000, and 20,000 loading cycles were 3.4, 4.4, 5.0, and 5.5 mm, respectively. This indicates adding 0.5% EPM to the asphalt mix significantly enhanced its resistance to rutting compared to HMA-C. The creep slope of 9,263 passes/mm recorded for HMA+0.5% EPM indicates a more than 78% reduction in rutting rate due to using 0.5% EPM compared to HMA-C. Furthermore, the rut depths recorded for HMA+1.0% EPM mix after 5,000, 10,000, 15,000, and 20,000 wheel passes were 1.2, 1.9, 2.4, and 3.0 mm, respectively. The creep slope measured for the same mix was 9,267 passes/mm. This indicates the HMA containing 1.0% EPM, by weight of the asphalt binder, experienced a progression in rutting, which was approximately 78% slower

than that in HMA-C. This improvement in rutting resistance can be attributed to the critical role played by EPM and the aggregate skeleton in the mix, including effective load distribution, particle interlock, reduced binder viscosity, reduced tensile and shear deformation due to the fibers and increased binder stiffness, as well as an enhanced shear strength due to the presence of the EPM. The HMA+1.5% EPM mix exhibited rut depths of 5.6, 7.0, 8.1, and 9.0 mm at 5,000, 10,000, 15,000, and 20,000 wheel passes, respectively. The creep slope measured for HMA+1.5% EPM was 5,104 passes/mm. These observations indicated that the mix containing 1.5% EPM experienced permanent deformation at a rate similar to that in HMA-C. This change in creep slope is attributed to the asphalt binder film thickness on aggregates and EPM. Since the binder content in all batches of asphalt mixes remained unchanged, adding EPM increased the available surface to be coated by asphalt, reducing asphalt film thickness. On the other hand, adding EPM increased the mixture's overall stiffness by reducing the ductility of the mastic. Finally, more EPM means more binder absorption and less effective binder content (P_{be}), which means less binder to coat the aggregates. As a result, asphalt mixes exhibited higher rutting resistance at low EPM contents (0.5 and 1.0%) than the HMA-C. However, when the EPM content was increased to 1.5%, the asphalt mix showed a resistance to rutting approximately equal to that of the HMA-C.

Figure 4.18 summarizes the maximum average rut depths observed in different HMA mixes. Consistent with the previously discussed observations, the results indicated for EPM contents less than 1.5%, an increase in the EPM contents resulted in a reduction in average rut depths compared to HMA-C. This shows a 30% and 62% reduction in the maximum rut depths when 0.5% and 1.0% EPM were incorporated in the mix, respectively, compared to the HMA-C. As the EPM content reached 1.5%, observed ruth depth increased by 14% compared to HMA-C. Overall, one may conclude that adding EPM to the asphalt mix improved its resistance to tutting, but this improvement was not observed beyond a certain amount of EPM. Therefore, determining an optimum EPM content to gain the maximum benefits from incorporating fibers in the mix is necessary.

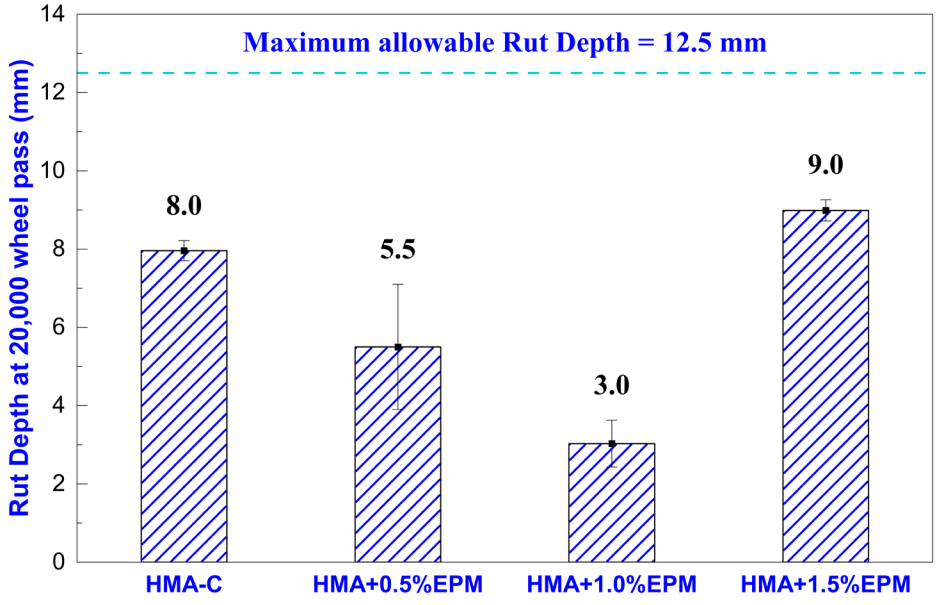

Figure 4.18 Maximum rut depths measured for different mixes in the HWT test

4.3.2 Tensile Strength Ratio (HWT) Test

The indirect tensile strength (ITS) tests were conducted, using the AASHTO T 283 standard method, on dry and moisture-conditioned samples to determine the moisture-induced damage potential in asphalt mixes. Figure 4.19 shows the average tensile strength values for the dry set and moisture-conditioned sample sets for each type of tested asphalt mix. The TSR values calculated for each mix type are also shown in Figure 4.20. The average tensile strength of dry-conditioned and moisture-conditioned HMA-C samples was 786.1 and 643.0 kPa, respectively, with a TSR value of 81.8%. After adding 0.5% EPM to the asphalt mixes, the average tensile strength of the dry and moisture-conditioned samples rose to 1004.8 and 867.0 kPa, respectively, with a TSR value of 86.3%. This indicates incorporating 0.5% EPM in asphalt mixes resulted in a 28% and 44% increase in the tensile strength of mixes in dry and wet conditions compared to those in the HMA-C mix, respectively. The EPM with a tensile strength higher than that of asphalt binder at 25ºC improved the tensile strength of asphalt mastic as a reinforced composite compared to that of the HMA-C. It was observed that a further increase in the EPM content in the asphalt mixes (HMA + 1.0% EPM and HMA + 1.5% EPM) resulted in a reduction in the tensile strengths of both dry and moisture-conditioned samples compared to HMA-C. More specifically, incorporating 1.0% and 1.5% EPM in the mix resulted in a 9 %and 14% reduction in the tensile strength of dry specimens, respectively, compared to HMA-C. However, the tensile strength of the moisture-conditioned samples containing 1.0% and 1.5% EPM remained unchanged compared to that of the HMA-C.

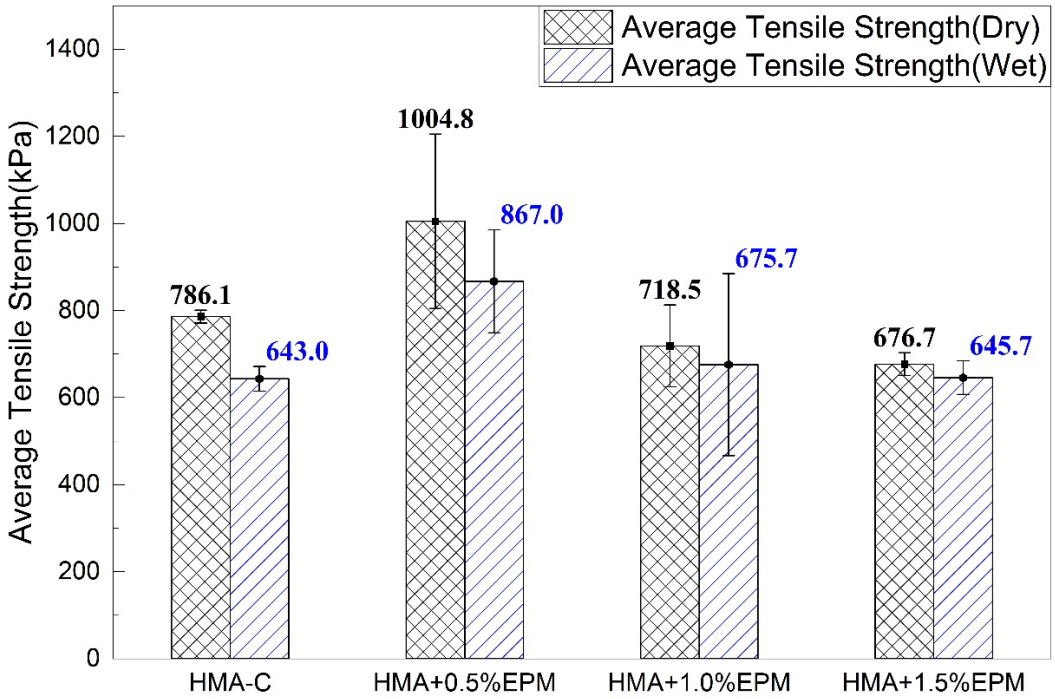

Figure 4.19 Tensile strength values measured for dry and moisture-conditioned mixes

According to Zhu et al. (2020), the optimum asphalt binder content of the asphalt mix increases after adding fibers, which is directly related to the asphalt film thickness. Consequently, further addition of EPM reduced the film thickness surrounding the aggregates and fibers. This occurred because more binder was required to coat the fibers, while binder content was kept constant in all mixes. Therefore, while adding EPM fibers beyond 0.5% hurt the tensile strength of samples tested in dry conditions, their presence was advantageous in reducing moisture damage to the mixture. This was observed because the tensile strength of the moisture-conditioned samples of the HMA containing 1.0% and 1,5% EPM

remained unchanged compared to that of the HMA-C. Figure 4.20 shows that the TSR values measured for HMA-C, HMA + 0.5% EPM, HMA + 1.0% EPM, and HMA + 1.5% EPM were 81.8, 86.3, 94.0, and 95.4%, respectively. It can be concluded that incorporating EPM into the HMA mix increased its resistance to moisture-induced damage. Interestingly, the continuous incorporation of EPM into asphalt mixes resulted in a constant rise in TSR values compared to HMA-C. Therefore, one may conclude incorporating the EPM in asphalt mixes can improve their resistance to moisture-induced damage. It should be noted that while the TSR test is used as a screening tool in the mix design process, some studies have assessed the moisture-induced damage potential based on the fracture energy parameters of asphalt mix and thermodynamic approaches (e.g., Ghabchi et al., 2016; Ghabchi and Acharya, 2022).

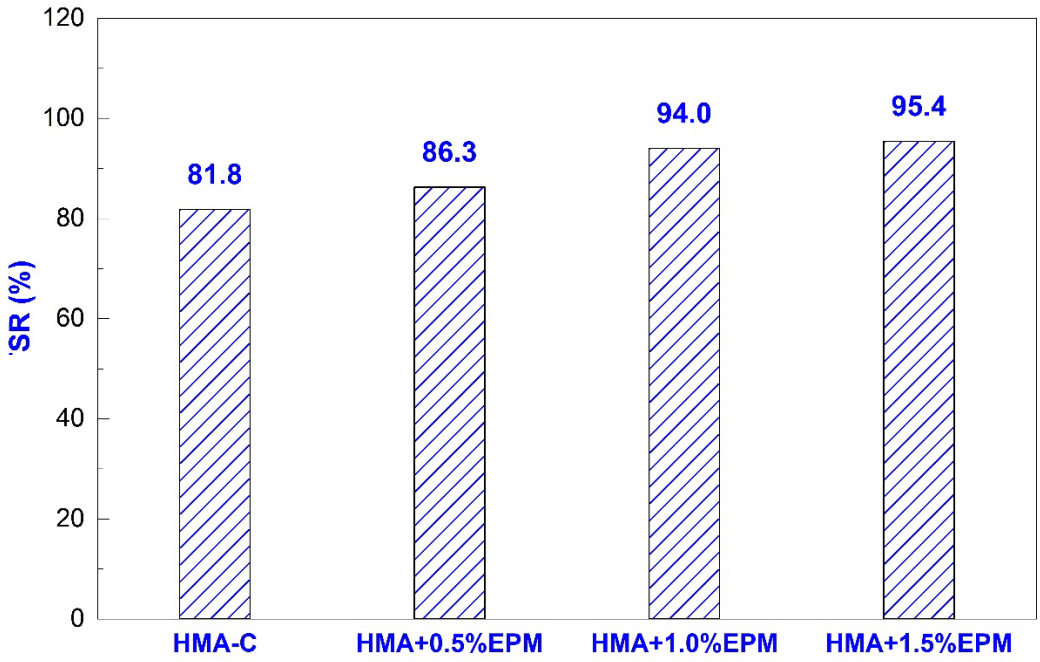

Figure 4.20 Tensile strength ratio (TSR) values for the tested asphalt mixes

4.3.3 Semicircular Bend (SCB) Test

Cracking at intermediate temperatures is a frequently observed distress in asphalt pavements. The SCB test was utilized to determine the resistance of the mixes to cracking. Fracture energy parameters obtained from conducting the SCB test are found to have an excellent correlation with asphalt pavements' resistance to cracking under traffic loads (Mohammad et al., 2012). Load-deformation curves developed by the SCB test are analyzed to determine the critical strain energy release rate (J_c). By conducting an SCB test on samples of different notch depths, the sensitivity of the crack initiation energy to notch depth is calculated for the unit thickness of the sample, providing insight into the asphalt material's resistance to cracking. To evaluate the resistance to cracking at intermediate temperature, fracture tests were conducted on SCB specimens having 25, 32, and 38 mm notch depths at 19°C. In each notch depth, at least four samples were tested. Figure 4.21 presents the critical strain energy release rate (J_c) values for asphalt mixes containing 0%, 0.5%, 1.0%, and 1.5% EPM. It can be observed the J_c value measured for an HMA-C (0.40 kJ/m^2) increased by 10% after incorporating 0.5% EPM in it, a J_c value of 0.44 kJ/m^2. Similarly, the J_c value for the HMA+1.0% EPM mix (0.58 kJ/m^2) was 45% higher than that of the HMA-C. Furthermore, incorporating 1.5% EPM in the mix resulted in a 66% increase in J_c value (0.66 kJ/m2) compared to the HMA-C mix. This observation indicates incorporating EPM in asphalt mixes substantially improved their resistance to cracking. This enhancement in resistance to cracking due to incorporating EPMs in the mix was attributed to the fibers' capacity to absorb and distribute the

concentrated tension generated by loading, which can result in flexure-induced tension zones in an asphalt mix layer. Due to their tensile strength, fibers in an asphalt mix result in an extended crack path, resulting in a higher fracture energy absorption capacity than asphalt mixes without any fibers. Therefore, the presence of EPM contributes to delaying the initiation of the microcracks (Ye et al., 2009). Notably, ASTM D8044 (ASTM, 2017) recommends a minimum J_c value of 0.50 kJ/m^2 for an acceptable resistance to cracking. Figure 4.21 demonstrates that the measured J_c values for HMA-C (0.40 kJ/m^2) and HMA+0.5% EPM (0.44 kJ/m^2) were below this recommended threshold. However, adding 1.0% and 1.5% EPM effectively increased the J_c values, exceeding the minimum recommended threshold. This indicates that adding 1.0% and 1.5 % EPM can be considered an effective method for improving asphalt mixes' resistance to cracking to meet the requirements of ASTM D8044 (ASTM, 2017).

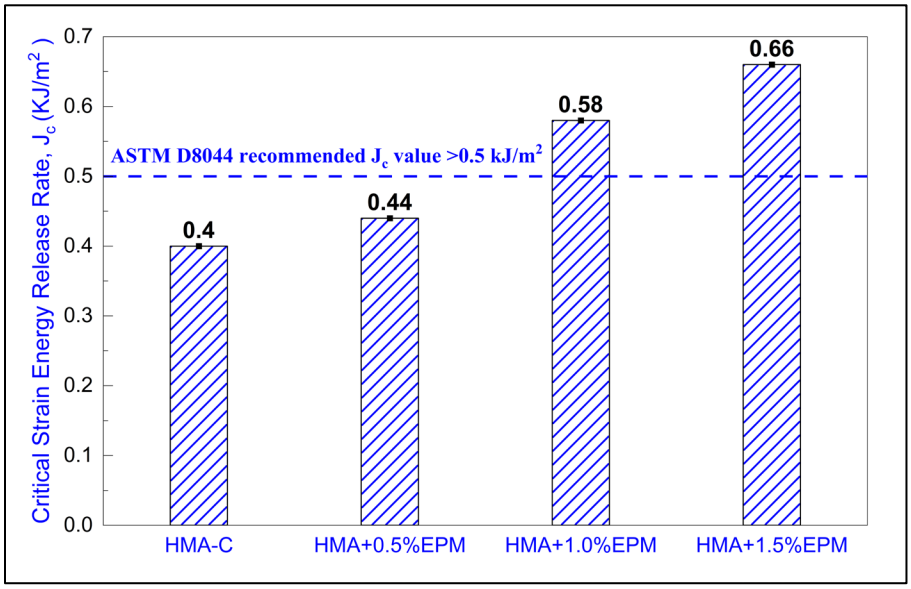

Figure 4.21 Critical strain energy release rate (J_c) measured for different HMA mixes

5. CONCLUSIONS AND RECOMMENDATIONS

The following conclusions are based on the findings, observations, and analysis from the tests conducted in this study.

1. The chemical analysis of EPMs using FTIR spectroscopy indicated no significant alterations in the molecular structure of PET due to using the DCM and TFA solution and the electrospinning process. Also, no traces of DCM of TFA or additional functional groups were found in any of the tested EPMs. It was further concluded drying fibers in a ventilated environment at room temperature for 24 hours is adequate for complete evaporation of the solvent.
2. After processing the SEM micrographs, it was found reducing the solution flow rate decreased the fiber diameter. Higher PET concentrations in the electrospinning solution resulted in fibers with larger diameters while causing some inconsistencies.
3. A qualitative study of the SEM micrographs revealed that regardless of the PET concentration in the solution, the fibers with the highest degree of uniformity were consistently generated at the lowest spinnable flow rate. Increasing the flow rates resulted in rough, non-uniform, and fractured fibers. For 15% PET concentration, uniform, smooth surface and cylindrical EPMs were produced at flow rates less than 60 µL/min. For PET concentration of 20%, uniform, smooth surface and cylindrical EPMs were produced at flow rates less than 120 µL/min.
4. Tensile strength tests on EPMs revealed reducing the diameter of the produced EPM improved the strength, force corresponding to the yield point, and elastic modulus of the fibers.
5. The chemical aging and dissolution of the asphalt binder's polar chemical groups were linked to the asphalt binder's increased stiffness and reduced cohesive bond.
6. Based on the chemical, morphological, and mechanical characteristics, and the requirements for mass production of EPMs, it was determined utilizing a solution with a PET concentration of 20% and a flow rate of 60 µL/min led to the production of EPMs exhibiting optimal mechanical properties. These attributes included high tensile strength, strain, yield strength, and toughness.
7. The total SFE of $MgCl_2$ solutions increased as the concentration increased, in contrast to NaCl, where an increase in concentration led to a decrease in the total SFE component.
8. An increase in the EPM content incorporated into the neat PG 58-28 asphalt binder increased the G* value of the neat binder. In both the unaged and RTFO-aged asphalt binders, the G* values decreased with increasing temperature but increased with increasing EPM content and the aging of asphalt binders.
9. Incorporating EPM in the PG 58-28 asphalt binder resulted in a significant increase in the rutting factor of the blend compared to the neat binder. The rutting factors of EPM-modified binders were also higher than those of the PG 58-34 binder (PMB). Nonetheless, at higher percentages of EPM and under RTFO-aged conditions, the rutting factor of the PG 58-28 containing 0.7% EPM was close to that of the neat PG 64-28 binder. The neat PG 58-28 had a Superpave PG of PG 58-XX. The H-T grade of PG 70-XX was achievable by adding EPM to the neat PG 58-28 asphalt binder.

10. Incorporating EPM in PG 58-28 asphalt binder improved its resistance to fatigue cracking compared to neat PG 58-28 binder. This was reflected in the PAV-aged asphalt binder's intermediate temperature (I-T) after testing it in a DSR. Asphalt binder containing EPM had an I-T value lower than the neat PG 58-28 and PG 64-28 binders but higher than the PG 58-34 binder.
11. The BBR test results suggested that adding EPM fiber to the neat PG 58-28 binder increased the stiffness and m-value at -24°C. Therefore, EPM in the neat PG 58-28 binder harmed thermal cracking resistance. The positive ΔTc value of the modified binder suggested all the binders were S-controlled and acted like polymer-modified binders PG 58-34.
12. At 58°C, adding EPM to the neat PG 58-28 binder resulted in a reduction in its J_{nr} value, lower than the neat PG 58-34. However, it was higher than the neat PG 64-28. It was found only PG 58-28 containing 0.2% EPM among all the EPM-modified binders had a stress sensitivity lower than 75%, and the rest had a higher stress sensitivity. The addition of EPM to the neat PG 58-28 binder did not make it meet the requirements for a polymer-modified binder.
13. From BBS tests, it was found adding EPM to the PG 58-28 asphalt binder enhanced its resistance to moisture-induced damage at the binder-aggregate interface. Including EPM in PG 58-28 (a non-PMB) asphalt binder improved its ability to resist moisture damage at levels comparable with PG 64-28 (a PMB).
14. Based on the results of HWT tests, increasing the EPM content in the asphalt mix up to 1.0% resulted in continuous improvement in the resistance to rutting and moisture-induced damage compared to the mix without any fibers. However, a further increase in EPM content in the mix to 1.5% was found to have a negative effect on the resistance of the mix to rutting compared to the mix without any fibers.
15. Adding EPM to the asphalt mix increased its TSR value compared to the mix containing no fibers, improving resistance to moisture-induced damage.
16. The SCB tests indicated an increase in the EPM content in the asphalt mixes tested in this study continuously improved their resistance to cracking compared to the control mix.

Based on this study's limitations and observations, the following recommendations are suggested for future studies.

1. It is recommended different methods of electrospinning EPM be explored and evaluated, focusing on techniques such as melting electrospinning. This alternative method can eliminate the need for chemicals. Additionally, investigating different techniques for enhancing fiber production, such as experimenting with various solvents and their ratios, is suggested to be considered. These efforts would contribute to advancing the production process and expanding the range of applications for EPM fibers.

2. Optimizing several production factors is recommended for improved control over the morphology of EPM fibers. The flow rate must be carefully regulated at the beginning of the electrospinning. The diameter and uniformity of the produced fibers can be substantially altered by adjusting the flow rate. Secondly, it is essential to maintain a controlled humidity level in the laboratory. Fluctuations in humidity can influence the electrospinning procedure and result in morphological variations in the fibers. During the electrospinning procedure, it is essential to maintain a stable and regulated humidity level. Dispersing the solution horizontally onto the collection plate was studied in this work. For future studies, exploring vertical flow is suggested. When the solution is flowing horizontally, it may take different travel trajectories. Consequently, the morphology of electrospun fibers may vary along the collection plate. Electrospinning the solution vertically makes achieving a more consistent and controlled travel path possible, enhancing fiber morphology.

3. Using highly polar solvents to produce EPM fibers makes the fibers' surfaces highly charged. To mitigate this issue, alternative electrospinning techniques that can lower the surface charge of EPM fibers should be investigated. By employing these alternative techniques, achieving a more balanced surface charge distribution may be possible, resulting in enhanced dispersion in asphalt.

4. Before the proposed modified asphalt can be adopted as a construction material in pavements, additional field-scale construction, long-term pavement performance monitoring, and life cycle cost analysis (LCCA) should be conducted. The conclusions regarding mix performance were derived from tests performed on a specific mix design that included local aggregates, a particular grading, and other site-specific variables. These results may not be directly applicable to other mixes or material varieties. To expand the applicability of the findings further, research should be carried out to include a variety of materials. This would entail testing the asphalt binders and different aggregate sources, aggregate gradations, and other mix variables.

6. REFERENCES

[1] AASHTO M 320, 2017. Standard Specification for Performance-Graded Asphalt Binder. Standard Specifications for Transportation Materials and Methods of Sampling and Testing, American Association of State Highway and Transportation Officials (AASHTO), Washington, D.C.

[2] AASHTO M 323, 2017a. Standard Specification for Superpave Volumetric Mix Design. Standard Specifications for Transportation Materials and Methods of Sampling and Testing, American Association of State Highway and Transportation Officials (AASHTO), Washington, D.C.

[3] AASHTO M 332, 2017. Standard Specification for Performance-Graded Asphalt Binder Using Multiple Stress Creep Recovery (MSCR) Test. Standard Specifications for Transportation Materials and Methods of Sampling and Testing, American Association of State Highway and Transportation Officials (AASHTO), Washington, D.C.

[4] AASHTO R 28, 2011. Standard Practice for Accelerated Aging of Asphalt Binder Using a Pressurized Aging Vessel (PAV). Standard Specifications for Transportation Materials and Methods of Sampling and Testing, American Association of State Highway and Transportation Officials (AASHTO), Washington, D.C.

[5] AASHTO R 35, 2017b. Standard Practice for Superpave Volumetric Design for Asphalt Mixtures. Standard Specifications for Transportation Materials and Methods of Sampling and Testing, American Association of State Highway and Transportation Officials (AASHTO), Washington, D.C.

[6] AASHTO T 166, 2011. Standard Method of Test for Bulk Specific Gravity (G mb) of Compacted Asphalt Mixtures Using Saturated Surface-Dry Specimens. Standard Specifications for Transportation Materials and Methods of Sampling and Testing, American Association of State Highway and Transportation Officials (AASHTO), Washington, D.C.

[7] AASHTO T 209, 2011. Standard Method of Test for Theoretical Maximum Specific Gravity (G mm) and Density of Asphalt Mixtures. Standard Specifications for Transportation Materials and Methods of Sampling and Testing, American Association of State Highway and Transportation Officials (AASHTO), Washington, D.C.

[8] AASHTO T 240, 2011. Standard Method of Test for Effect of Heat and Air on a Moving Film of Asphalt (Rolling Thin-Film Oven Test). Standard Specifications for Transportation Materials and Methods of Sampling and Testing, American Association of State Highway and Transportation Officials (AASHTO), Washington, D.C.

[9] AASHTO T 283, 2011. Standard Method of Test for Resistance of Compacted Asphalt Mixtures to Moisture-Induced Damage. Standard Specifications for Transportation Materials and Methods of Sampling and Testing, American Association of State Highway and Transportation Officials (AASHTO), Washington, D.C.

[10] AASHTO T 312, 2011. Standard Method of Test for Preparing and Determining the Density of Asphalt Mixture Specimens by Means of the Superpave Gyratory Compactor. Standard Specifications for Transportation Materials and Methods of Sampling and Testing, American Association of State Highway and Transportation Officials (AASHTO), Washington, D.C.

[11] AASHTO T 313, 2019. Standard Method of Test for Determining the Flexural Creep Stiffness of Asphalt Binder Using the Bending Beam Rheometer (BBR). Standard Specifications for Transportation Materials and Methods of Sampling and Testing, American Association of State Highway and Transportation Officials (AASHTO), Washington, D.C.

[12] AASHTO T 315, 2020. Standard Method of Test for Determining the Rheological Properties of Asphalt Binder Using a Dynamic Shear Rheometer (DSR). Standard Specifications for Transportation Materials and Methods of Sampling and Testing, American Association of State Highway and Transportation Officials (AASHTO), Washington, D.C.

[13] AASHTO T 324, 2011. Standard Method of Test for Hamburg Wheel-Track Testing of Compacted Hot Mix Asphalt (HMA). Standard Specifications for Transportation Materials and Methods of Sampling and Testing, American Association of State Highway and Transportation Officials (AASHTO), Washington, D.C.

[14] AASHTO T 324, 2019. Standard Method of Test for Hamburg Wheel-Track Testing of Compacted Hot Mix Asphalt (HMA). Standard Specifications for Transportation Materials and Methods of Sampling and Testing, American Association of State Highway and Transportation Officials (AASHTO), Washington, D.C.

[15] AASHTO T 350, 2019. Standard Method of Test for Multiple Stress Creep Recovery (MSCR) Test of Asphalt Binder Using a Dynamic Shear Rheometer (DSR). Standard Specifications for Transportation Materials and Methods of Sampling and Testing, American Association of State Highway and Transportation Officials (AASHTO), Washington, D.C.

[16] AASHTO T 361, 2022. Standard Method of Test for Determining Asphalt Binder Bond Strength by Means of the Binder Bond Strength (BBS) Test. Standard Specifications for Transportation Materials and Methods of Sampling and Testing, American Association of State Highway and Transportation Officials (AASHTO), Washington, D.C.

[17] Abbas, J. A., Said, I. A., Mohamed, M. A., Yasin, S. A., Ali, Z. A., and Ahmed, I. H., 2018. Electrospinning of polyethylene terephthalate (PET) nanofibers: Optimization study using taguchi design of experiment. *In IOP conference series: materials science and engineering (Vol. 454, No. 1, p. 012130). IOP Publishing*.

[18] Abtahi, S. M., Sheikhzadeh, M., and Hejazi, S. M., 2010. Fiber-reinforced asphalt-concrete–a review. *Construction and Building Materials*, 24(6), 871-877.

[19] Afonso, M. L., Dinis-Almeida, M., and Fael, C. S., 2017. Study of the porous asphalt performance with cellulosic fibres. Construction and Building Materials, 135, 104-111.

[20] Ahmadinia, E., Zargar, M., Karim, M.R., Abdelaziz, M. and Ahmadinia, E., 2012. Performance evaluation of utilization of waste Polyethylene Terephthalate (PET) in stone mastic asphalt. Construction and Building Materials, 36, pp.984-989.

[21] Alfalah, A., Offenbacker, D., Ali, A., Decarlo, C., Lein, W., Mehta, Y., and Elshaer, M., 2020. Assessment of the impact of fiber types on the performance of fiber-reinforced hot mix asphalt. Transportation Research Record, 2674(4), 337-347.

[22] Ali, B., Qureshi, L. A., and Khan, S. U., 2020. Flexural behavior of glass fiber-reinforced recycled aggregate concrete and its impact on the cost and carbon footprint of concrete pavement. Construction and Building Materials, 262, 120820.

[23] Almeida e Silva, J. de A., Guedes Rodrigues, J. K., Carvalho, M. W., Lopes Lucena, L. C. de F., and Cavalcante, E.H., 2018. Mechanical performance of asphalt mixtures using polymer-micronized PET-modified binder. *Road Materials and Pavement Design*, *19*(4), pp.1001-1009.

[24] Almeida e Silva, J. de A., Lopes Lucena, L. C. de F., Guedes Rodrigues, J. K., Carvalho, M. W., and Beserra Costa, D., 2015. Use of micronized polyethylene terephthalate (PET) waste in asphalt binder. *Petroleum Science and Technology*, *33*(15-16), pp.1508-1515.

[25] Al-Sabaeei, A. M., Napiah, M. B., Sutanto, M. H., Alaloul, W. S., Zoorob, S. E., and Usman, A., 2022. Influence of nanosilica particles on the high-temperature performance of waste denim fibre-modified bitumen. *International Journal of Pavement Engineering, 23(2), 207-220*.

[26] Andrés-Valeri, V.C., Rodriguez-Torres, J., Calzada-Perez, M.A. and Rodriguez-Hernandez, J., 2018. Exploratory study of porous asphalt mixtures with additions of reclaimed tetra pak material. *Construction and Building Materials*, *160*, pp.233-239.

[27] Arabani, M., and Shabani, A., 2019. Evaluation of the ceramic fiber modified asphalt binder. *Construction and Building Materials, 205, 377-386*.

[28] Ashish, P. K., and Singh, D., 2018. High-and intermediate-temperature performance of asphalt binder containing carbon nanotube using different rheological approaches. *Journal of Materials in Civil Engineering, 30(1), 04017254*.

[29] ASTM D8044, 2017. Standard Test Method for Evaluation of Asphalt Mixture Cracking Resistance using the Semi-Circular Bend Test (SCB) at Intermediate Temperatures. 2016 Annual Book of ASTM Standards, ASTM International, West Conshohocken, PA.

[30] Aydemir, H., and Demiryürek, O., 2022. The effect of electrospinning parameters on morphology and diameter of polyethylene terephthalate (PET) and recycled polyethylene terephthalate (r-PET) nanofibers. *The Journal of The Textile Institute, 1-12*.

[31] Ben Zair, M. M., Jakarni, F. M., Muniandy, R., and Hassim, S., 2021. A brief review: application of recycled polyethylene terephthalate in asphalt pavement reinforcement. *Sustainability, 13(3), 1303*.

[32] Beyler, C. L., and Hirschler, M. M., 2002. Thermal decomposition of polymers. *SFPE handbook of fire protection engineering, 2(7)*.

[33] Bonfim, D. P., Cruz, F. G., Bretas, R. E., Guerra, V. G., and Aguiar, M. L., 2021. A sustainable recycling alternative: Electrospun PET-membranes for air nanofiltration. *Polymers, 13(7), 1166*.

[34] Chavan, S., and Rao, P., 2016. Utilization of Waste PET Bottle Fibers in Concrete as an Innovation in Building Materials— [A Review Paper]. *Int. J. Eng. Res, 5(1), 304-307.*

[35] Chen, H. X., Li, N. L., Hu, C., and Zhang, Z., 2004. Mechanical performance of fibers-reinforced asphalt mixture. J *Chan Univ (Nat Sci Ed), 24(2), 1-5.*

[36] Chen, H., and Xu, Q., 2010. Experimental study of fibers in stabilizing and reinforcing asphalt binder. *Fuel, 89(7), 1616-1622.*

[37] Chen, J. S., and Lin, K. Y., 2005. Mechanism and behavior of bitumen strength reinforcement using fibers. *Journal of materials science, 40, 87-95.*

[38] Chen, M. J., and Wong, Y. D., 2013. Porous asphalt mixture with 100% recycled concrete aggregate. *Road Materials and Pavement Design, 14(4), 921-932*.

[39] Chen, M. J., and Wong, Y. D., 2015. Porous asphalt mixture with a combination of solid waste aggregates. *Journal of Materials in Civil Engineering, 27(6), 04014194*.

[40] Chen, Z., Wu, S. P., Zhu, Z. H., and Liu, J. S., 2008. Experimental evaluation on high temperature rheological properties of various fiber modified asphalt binders. *Journal of Central South University of Technology, 15, 135-139*.

[41] Cho, C. J., Chang, Y. S., Lin, Y. Z., Jiang, D. H., Chen, W. H., Lin, W. Y., Chen, C.W., Rwei, S.P. and Kuo, C. C., 2020. Green electrospun nanofiber membranes filter prepared from novel biomass thermoplastic copolyester: Morphologies and filtration properties. *Journal of the Taiwan Institute of Chemical Engineers, 106, 206-214*.

[42] Christiansen, L., Gurevich, L., Wang, D., and Fojan, P., 2021. Melt Electrospinning of PET and Composite PET-Aerogel Fibers: An Experimental and Modeling Study. *Materials, 14(16), 4699*.

[43] Copeland, A., 2005. Moisture in asphalt pavements in the United States: A financial perspective. *In First international workshop on moisture damage.*

[44] Copeland, A., 2011. Reclaimed asphalt pavement in asphalt mixtures: State of the practice (No. FHWA-HRT-11-021). United States. Federal Highway Administration. *Office of Research, Development, and Technology.*

[45] Cramariuc, B., Cramariuc, R., Scarlet, R., Manea, L. R., Lupu, I. G., and Cramariuc, O., 2013. Fiber diameter in electrospinning process. *Journal of Electrostatics, 71(3), 189-198*.

[46] Dasdemir, M., Topalbekiroglu, M., and Demir, A., 2013. Electrospinning of thermoplastic polyurethane microfibers and nanofibers from polymer solution and melt. *Journal of Applied Polymer Science, 127(3), 1901-1908*.

[47] Dhaka, V., Singh, S., Anil, A. G., Sunil Kumar Naik, T. S., Garg, S., Samuel, J., Kumar, M., Ramamurthy, P.C., and Singh, J., 2022. Occurrence, toxicity and remediation of polyethylene terephthalate plastics. A review. *Environmental Chemistry Letters, 1-24*.

[48] dos Santos Ferreira, J. W., Marroquin, J. F. R., Felix, J. F., Farias, M. M., and Casagrande, M. D. T., 2022. The feasibility of recycled micro polyethylene terephthalate (PET) replacing natural sand in hot-mix asphalt. *Construction and Building Materials, 330, 127276*.

[49] Doshi, J., and Reneker, D. H., 1995. Electrospinning process and applications of electrospun fibers. *Journal of electrostatics, 35(2-3), 151-160*.

[50] Enieb, M., Diab, A., and Yang, X., 2021. Short-and long-term properties of glass fiber reinforced asphalt mixtures. *International Journal of Pavement Engineering, 22(1), 64-76.*

[51] Espíndola-González, A., Martínez-Hernández, A. L., Fernández-Escobar, F., Castaño, V. M., Brostow, W., Datashvili, T., and Velasco-Santos, C., 2011. Natural-synthetic hybrid polymers developed via electrospinning: the effect of PET in chitosan/starch system. *International journal of molecular sciences, 12(3), 1908-1920*.

[52] Freeman, R. D., Burati, J. L., Amirkhanian, S. N., and Bridges, W. C., 1989. Polyester fibers in asphalt paving mixtures*. In Association of Asphalt Paving Technologists Proc (Vol. 58).*

[53] Ghabchi, R. and Acharya, R., 2022. Evaluation of Fracture Energy Parameters for Predicting Moisture-Induced Damage in Asphalt Mixes. *Transportation Infrastructure Geotechnology*, *9*(3), pp.356-384.

[54] Ghabchi, R. and Castro, M.P.P., 2021a. Evaluation of a biofuel residue-derived recycling agent with a low carbon footprint. *Transportation Engineering*, *5*, p.100085.

[55] Ghabchi, R. and Castro, M.P.P., 2021b. Effect of laboratory-produced cellulose nanofiber as an additive on performance of asphalt binders and mixes. *Construction and Building Materials*, *286*, p.122922.

[56] Ghabchi, R. and Pereira Castro, M.P., 2022. Characterisation of a hybrid plant-based asphalt binder replacement with high reactive phenolic monomer content. *International Journal of Pavement Engineering*, *23*(13), pp.4675-4696.

[57] Ghabchi, R., 2022. Effect of Lignin Type as an Additive on Rheology and Adhesion Properties of Asphalt Binder. *Solids*, *3*(4), pp.603-619.

[58] Ghabchi, R., Arshadi, A., Zaman, M. and March, F., 2021a. Technical challenges of utilizing ground tire rubber in asphalt pavements in the united states. *Materials*, *14*(16), p.4482.

[59] Ghabchi, R., Dharmarathna, C.P. and Mihandoust, M., 2021b. Feasibility of Using Micronized Recycled Polyethylene Terephthalate (PET) as an Asphalt Binder Additive: A Laboratory Study. *Construction and Building Materials.* 292, p.123377.

[60] Ghabchi, R., Singh, D., Zaman, M. and Hossain, Z., 2016. Micro-structural analysis of moisture-induced damage potential of asphalt mixes containing RAP. *Journal of Testing and Evaluation*, *44*(1), pp.194-205.

[61] Ghanoon, S. A., and Tanzadeh, J., 2019. Laboratory evaluation of nano-silica modification on rutting resistance of asphalt Binder. *Construction and Building Materials, 223, 1074-1082*.

[62] Ghanoon, S. A., Tanzadeh, J., and Mirsepahi, M., 2020. Laboratory evaluation of the composition of nano-clay, nano-lime and SBS modifiers on rutting resistance of asphalt binder. *Construction and Building Materials, 238, 117592*.

[63] Haider, A., Haider, S., and Kang, I. K., 2018. A comprehensive review summarizing the effect of electrospinning parameters and potential applications of nanofibers in biomedical and biotechnology. *Arabian Journal of Chemistry, 11(8), 1165-1188*.

[64] Hassan, H. F., Al-Oraimi, S., and Taha, R., 2005. Evaluation of open-graded friction course mixtures containing cellulose fibers and styrene butadiene rubber polymer. *Journal of materials in civil engineering, 17(4), 416-422.*

[65] Hassani, A., Ganjidoust, H. and Maghanaki, A.A., 2005. Use of plastic waste (poly-ethylene terephthalate) in asphalt concrete mixture as aggregate replacement. Waste Management and Research, 23(4), pp.322-327.

[66] He, S. S., Wei, M. Y., Liu, M. H., and Xue, W. L., 2015. Characterization of virgin and recycled poly (ethylene terephthalate) (PET) fibers. *The Journal of the Textile Institute, 106(8), 800-806*.

[67] Hu, X., Liu, S., Zhou, G., Huang, Y., Xie, Z., and Jing, X., 2014. Electrospinning of polymeric nanofibers for drug delivery applications. *Journal of controlled release, 185, 12-21*.

[68] Huang, B., Li, G., and Mohammad, L. N., 2003. Analytical modeling and experimental study of tensile strength of asphalt concrete composite at low temperatures. *Composites Part B: Engineering, 34(8), 705-714*.

[69] Huang, H., and White, T. D., 1996. Dynamic properties of fiber-modified overlay mixture. *Transportation Research Record, 1545(1), 98-104.*

[70] Huang, Y. H., 2004. Pavement analysis and design (Vol. 2, pp. 401-409). *Upper Saddle River, NJ: Pearson Prentice Hall.*

[71] Jung, J. W., Lee, C. L., Yu, S., and Kim, I. D., 2016. Electrospun nanofibers as a platform for advanced secondary batteries: a comprehensive review. *Journal of materials chemistry A, 4(3), 703-750.*

[72] Karimi, M. M., Jahanbakhsh, H., Jahangiri, B., and Nejad, F. M., 2018. Induced heating-healing characterization of activated carbon modified asphalt concrete under microwave radiation. *Construction and Building Materials, 178, 254-271.*

[73] Kassem, H. A., Saleh, N. F., Zalghout, A. A., and Chehab, G. R., 2018. Advanced characterization of asphalt concrete mixtures reinforced with synthetic fibers. *Journal of Materials in Civil Engineering, 30(11), 04018307.*

[74] Khoonkari, M., Haghighi, A. H., Sefidbakht, Y., Shekoohi, K., and Ghaderian, A., 2015. Chemical recycling of PET wastes with different catalysts. *International Journal of Polymer Science, 2015*.

[75] Kim, J. H., Yang, S. S., and Hudson, S. M., 2011. Comparison of the structure-property relationships for PTT and PET fibers spun at various take-up speeds. *Fibers and Polymers, 12(6), 771-777*.

[76] Koenig, K., Beukenberg, K., Langensiepen, F., and Seide, G., 2019. A new prototype melt-electrospinning device for the production of biobased thermoplastic sub-microfibers and nanofibers. *Biomaterials Research, 23(1), 1-12*.

[77] Koo, B. M., Kim, J. H. J., Kim, S. B., and Mun, S., 2014. Material and structural performance evaluations of Hwangtoh admixtures and recycled PET fiber-added eco-friendly concrete for CO2 emission reduction. *Materials, 7(8), 5959-5981*.

[78] Kumbargeri, Y. S., and Biligiri, K. P., 2016. Understanding aging behaviour of conventional asphalt binders used in India. *Transportation Research Procedia, 17, 282-290*.

[79] Lasprilla-Botero, J., Alvarez-Lainez, M., and Lagaron, J. M., 2018. The influence of electrospinning parameters and solvent selection on the morphology and diameter of polyimide nanofibers. *Materials Today Communications, 14, 1-9*.

[80] Lastra-González, P., Indacoechea-Vega, I., Calzada-Pérez, M. A., Vega-Zamanillo, Á., and Castro-Fresno, D., 2020. Assessment of induction heating in the performance of porous asphalt mixtures. Road *Materials and Pavement Design, 21(8), 2302-2320*.

[81] Lee, S. J., Rust, J. P., Hamouda, H., Kim, Y. R., and Borden, R. H., 2005. Fatigue cracking resistance of fiber-reinforced asphalt concrete. *Textile Research Journal, 75(2), 123-128*.

[82] Leng, Z., Padhan, R. K., and Sreeram, A., 2018a. Production of a sustainable paving material through chemical recycling of waste PET into crumb rubber modified asphalt. *Journal of cleaner production, 180, 682-688.*

[83] Leng, Z., Padhan, R.K. and Sreeram, A., 2018a. Production of a sustainable paving material through chemical recycling of waste PET into crumb rubber modified asphalt. *Journal of cleaner production*, *180*, pp.682-688.

[84] Leng, Z., Sreeram, A., Padhan, R.K. and Tan, Z., 2018b. Value-added application of waste PET based additives in bituminous mixtures containing high percentage of reclaimed asphalt pavement (RAP). *Journal of cleaner production*, *196*, pp.615-625.

[85] Li, X., Liu, H., Wang, J., and Li, C., 2012. Preparation and properties of PET/SiO_2 composite micro/nanofibers by a laser melt-electrospinning system. *Journal of applied polymer science, 125(3), 2050-2055*.

[86] Liu, Q., Schlangen, E., van de Ven, M., and García, Á., 2010. Healing of porous asphalt concrete via induction heating. *Road Materials and Pavement Design, 11(sup1), 527-542*.

[87] Ma, J., and Hesp, S. A., 2022. Effect of recycled polyethylene terephthalate (PET) fiber on the fracture resistance of asphalt mixtures. *Construction and Building Materials, 342, 127944*.

[88] Ma, J., Yu, L., Chen, S., Chen, W., Wang, Y., Guang, S., Zhang, X., Lu, W., Wang, Y., and Bao, J., 2018. Structure–property evolution of poly (ethylene terephthalate) fibers in industrialized process under complex coupling of stress and temperature field. *Macromolecules, 52(2), 565-574.*

[89] Marchioni, M., and Becciu, G., 2015. Experimental results on permeable pavements in urban areas: A synthetic review. *International Journal of Sustainable Development and Planning, 10(6), 806-817*.

[90] Maurer, D. A., and Malasheskie, G. J., 1989. Field performance of fabrics and fibers to retard reflective cracking. *Geotextiles and Geomembranes, 8(3), 239-267*.

[91] Mercante, L. A., Scagion, V. P., Migliorini, F. L., Mattoso, L. H., and Correa, D. S., 2017. Electrospinning-based (bio) sensors for food and agricultural applications: A review. *TrAC Trends in Analytical Chemistry, 91, 91-103*.

[92] Merkel, D.R., Kuang, W., Malhotra, D., Petrossian, G., Zhong, L., Simmons, K.L., Zhang, J. and Cosimbescu, L., 2020. Waste PET Chemical Processing to Terephthalic Amides and Their Effect on Asphalt Performance. *ACS Sustainable Chemistry and Engineering*, *8*(14), pp.5615-5625.

[93] Miao, Y., von Jouanne, A., and Yokochi, A., 2021. Current technologies in depolymerization process and the road ahead. *Polymers, 13(3), 449.*

[94] Modarres, A. and Hamedi, H., 2014a. Developing laboratory fatigue and resilient modulus models for modified asphalt mixes with waste plastic bottles (PET). *Construction and Building Materials*, *68*, pp.259-267.

[95] Modarres, A. and Hamedi, H., 2014b. Effect of waste plastic bottles on the stiffness and fatigue properties of modified asphalt mixes. *Materials and Design*, *61*, pp.8-15.

[96] Moghaddam, T.B., Karim, M.R. and Syammaun, T., 2012. Dynamic properties of stone mastic asphalt mixtures containing waste plastic bottles. *Construction and Building Materials*, *34*, pp.236-242.

[97] Mohammad, L. N., Kim, M., and Elseifi, M., 2012. Characterization of asphalt mixture's fracture resistance using the semi-circular bending (SCB) test. In 7th RILEM International Conference on Cracking in Pavements: Mechanisms, Modeling, Testing, Detection and Prevention Case Histories (pp. 1-10). *Springer Netherlands.*

[98] Mohammadinia, A., Disfani, M. M., Narsilio, G. A., and Aye, L., 2018. Mechanical behaviour and load bearing mechanism of high porosity permeable pavements utilizing recycled tire aggregates. *Construction and Building Materials, 168, 794-804.*

[99] National Association for PET Container Resources (NAPCOR), 2019. PET Recycling Report. Last online access: March 1, 2023. *Available through: https://napcor.com/wp-content/uploads/2021/03/NAPCOR_2019RateReport_FINAL_rev.pdf*

[100] National Association for PET Container Resources (NAPCOR). 2018. Report on Postconsumer PET Recycling Activity in 2018. Last online access: July 12, 2022. *Available through: https://napcor.com/wp-content/uploads/2021/07/Postconsumer-PET-Recycling-Activity-in-2018.pdf*

[101] Nelson, P. K., Li, V. C., and Kamada, T., 2002. Fracture toughness of microfiber reinforced cement composites. *Journal of Materials in Civil Engineering, 14(5), 384-391*.

[102] Ogata, N., Shimada, N., Yamaguchi, S., Nakane, K., and Ogihara, T., 2007. Melt-electrospinning of poly (ethylene terephthalate) and polyalirate. *Journal of Applied Polymer Science, 105(3), 1127-1132*.

[103] Oruç, Ş., Yılmaz, B., and Sancak, K., 2022. Characterization and rheological behavior of asphalt binder modified by a novel cyclic borate ester additive. *Construction and Building Materials, 348, 128673*.

[104] Owida, H. A., Moh'd, B. A. H., and Al Takrouri, M., 2022. Designing an Integrated Low-cost Electrospinning Device for Nanofibrous Scaffold Fabrication. *HardwareX, 11, e00250*.

[105] Pacific Institute, 2007. Fact Sheet: Bottled Water and Energy – Getting to 17 Million Barrels. December 2007. Last online access: June 8, 2021. Available through: https://pacinst.org/wp-content/uploads/2007/12/bottled_water_factsheet.pdf

[106] Papkov, D., Zou, Y., Andalib, M. N., Goponenko, A., Cheng, S. Z., and Dzenis, Y. A., 2013. Simultaneously strong and tough ultrafine continuous nanofibers. *ACS nano, 7(4), 3324-3331*.

[107] Park, P., El-Tawil, S., Park, S. Y., and Naaman, A. E., 2015. Cracking resistance of fiber reinforced asphalt concrete at− 20 C. *Construction and Building Materials, 81, 47-57.*

[108] Peltonen, P., 1991a. Wear and deformation characteristics of fibre reinforced asphalt pavements. *Construction and building Materials, 5(1), 18-22.*

[109] Peltonen, P. V., 1991b. Characterization and testing of fibre-modified bitumen composites. *Journal of materials science, 26, 5618-5622.*

[110] Phan, T. M., Park, D. W., and Le, T. H. M., 2018. Crack healing performance of hot mix asphalt containing steel slag by microwaves heating. *Construction and Building Materials, 180, 503-511*.

[111] Putman, B. J., and Amirkhanian, S. N., 2004. Utilization of waste fibers in stone matrix asphalt mixtures. *Resources, conservation and recycling, 42(3), 265-274*.

[112] Resource Recycling, 2012. A Common Theme. Last online access: November 13, 2020. Available through: http://www.container-recycling.org/assets/pdfs/ACommonTheme.pdf

[113] Sangiorgi, C., Tataranni, P., Simone, A., Vignali, V., Lantieri, C., and Dondi, G., 2016. Assessment of waste bleaching clay as alternative filler for the production of porous asphalts. *Construction and Building Materials, 109, 1-7*.

[114] Santoro, M., Shah, S. R., Walker, J. L., and Mikos, A. G., 2016. Poly (lactic acid) nanofibrous scaffolds for tissue engineering. *Advanced drug delivery reviews, 107, 206-212*.

[115] Senthamizhan, A., Celebioglu, A., and Uyar, T., 2014. Flexible and highly stable electrospun nanofibrous membrane incorporating gold nanoclusters as an efficient probe for visual colorimetric detection of Hg (II). *Journal of Materials Chemistry A, 2(32), 12717-12723*.

[116] Serfass, J. P., and Samanos, J., 1996. Fiber-modified asphalt concrete characteristics, applications and behavior. *Asphalt Paving Technology, 65, 193-230*.

[117] Serin, S., Morova, N., Saltan, M., and Terzi, S., 2012. Investigation of usability of steel fibers in asphalt concrete mixtures. *Construction and Building Materials, 36, 238-244*.

[118] Shukry, N. A. M., Hassan, N. A., Hainin, M. R., Abdullah, M. E., Abdullah, N. A. M., Mahmud, M. Z. H., ... and Mashros, N., 2016. Experimental evaluation of anti-stripping additives on porous asphalt mixtures. *Jurnal Teknologi, 78(7-2).*

[119] Slebi-Acevedo, C. J., Lastra-González, P., Pascual-Muñoz, P., and Castro-Fresno, D., 2019. Mechanical performance of fibers in hot mix asphalt: A *review. Construction and Building Materials, 200, 756-769*.

[120] Smith, R. L., Takkellapati, S., and Riegerix, R. C., 2022. Recycling of Plastics in the United States: Plastic Material Flows and Polyethylene Terephthalate (PET) Recycling Processes. *ACS Sustainable Chemistry and Engineering, 10(6), 2084-2096*.

[121] Spinacé, M. S., and De Paoli, M. A., 2001. Characterization of poly (ethylene terephtalate) after multiple processing cycles. *Journal of Applied Polymer Science, 80(1), 20-25*.

[122] Strain, I. N., Wu, Q., Pourrahimi, A. M., Hedenqvist, M. S., Olsson, R. T., and Andersson, R. L., 2015. Electrospinning of recycled PET to generate tough mesomorphic fibre membranes for smoke filtration. *Journal of Materials Chemistry A, 3(4), 1632-1640*.

[123] Sulyman, M., Haponiuk, J., and Formela, K., 2016. Utilization of recycled polyethylene terephthalate (PET) in engineering materials: A review. *International Journal of Environmental Science and Development, 7(2), 100*.

[124] Sun, Y., Wu, S., Liu, Q., Li, B., Fang, H., and Ye, Q., 2016. The healing properties of asphalt mixtures suffered moisture damage. *Construction and Building Materials, 127, 418-424.*

[125] Tabaković, A., O'Prey, D., McKenna, D., and Woodward, D., 2019. Microwave self-healing technology as airfield porous asphalt friction course repair and maintenance system. *Case Studies in Construction Materials, 10, e00233.*

[126] Tan, S. H., Inai, R., Kotaki, M., and Ramakrishna, S., 2005. Systematic parameter study for ultra-fine fiber fabrication via electrospinning process. *Polymer, 46(16), 6128-6134*.

[127] Tanzadeh, J., and Shahrezagamasaei, R., 2017. Laboratory assessment of hybrid fiber and nano-silica on reinforced porous asphalt mixtures. *Construction and Building Materials, 144, 260-270.*

[128] Tanzadeh, R., Tanzadeh, J., and Tahami, S. A., 2019. Experimental study on the effect of basalt and glass fibers on behavior of open-graded friction course asphalt modified with nano-silica. *Construction and building materials, 212, 467-475.*

[129] Tapkın, S., 2008. The effect of polypropylene fibers on asphalt performance. *Building and environment, 43(6), 1065-1071.*

[130] Thompson, C. J., Chase, G. G., Yarin, A. L., and Reneker, D. H., 2007. Effects of parameters on nanofiber diameter determined from electrospinning model. *Polymer, 48(23), 6913-6922*.

[131] U.S. EPA (United States Environmental Protection Agency), 2020. Advancing Sustainable Materials Management:2018 Fact Sheet, Assessing Trends in Materials Generation and Management in the United States. Report Date: November 2020. Last online access: July 10, 2020. https://www.epa.gov/sites/production/files/2020-11/documents/2018_ff_fact_sheet.pdf

[132] Usman, I. U., and Kunlin, M., 2024. Influence of Polyethylene Terephthalate (PET) utilization on the engineering properties of asphalt mixtures: A review. *Construction and Building Materials, 411, 134439*.

[133] Veleirinho, B., Rei, M. F., and Lopes-DA-Silva, J. A., 2008. Solvent and concentration effects on the properties of electrospun poly (ethylene terephthalate) nanofiber mats. *Journal of Polymer Science Part B: Polymer Physics, 46(5), 460-471*.

[134] Vo, P. P., Doan, H. N., Kinashi, K., Sakai, W., Tsutsumi, N., and Huynh, D. P., 2018. Centrifugally spun recycled PET: Processing and characterization. *Polymers, 10(6), 680*.

[135] Wang, H., Zhang, C., Li, L., You, Z., and Diab, A., 2016. Characterization of low temperature crack resistance of crumb rubber modified asphalt mixtures using semi-circular bending tests. Journal of Testing and Evaluation. *ASTM, doi:10.1520/JTE20150145 / Vol. 44 / No. 2*

[136] Wang, X., Gao, J. P., Zhao, Q. L., Huang, J., Mao, G. L., Wu, W., Ning, Y. N., and Ma, Z., 2013. Polymethylene-block-polystyrene copolymers: A new synthetic approach using a combination of polyhomologation and reversible addition-fragmentation chain-transfer polymerization and their microfibers and microspheres fabricated through electrospinning process. *Journal of Polymer Science Part A: Polymer Chemistry, 51(13), 2892-2899*.

[137] Wang, X., Wu, R., and Zhang, L., 2019. Development and performance evaluation of epoxy asphalt concrete modified with glass fibre. *Road Materials and Pavement Design, 20(3), 715-726.*

[138] Wu, S., Ye, Q., and Li, N., 2008. Investigation of rheological and fatigue properties of asphalt mixtures containing polyester fibers. *Construction and Building Materials, 22(10), 2111-2115.*

[139] Wu, S., Ye, Q., Li, N., and Yue, H., 2007. Effects of fibers on the dynamic properties of asphalt mixtures. *Journal of Wuhan University of Technology-Mater. Sci. Ed., 22, 733-736*.

[140] Xu, Y., Wang, D., Zhang, M., Wang, H., and Wei, Q., 2017. Self-layering behavior of PET fiber deposition in melt-electrospinning process. *Fibers and Polymers, 18(10), 1981-1987*.

[141] Yang, Q., Liu, Q., Zhong, J., Hong, B., Wang, D., and Oeser, M., 2019. Rheological and micro-structural characterization of bitumen modified with carbon nanomaterials. *Construction and Building Materials, 201, 580-589*.

[142] Ye, Q., Wu, S., and Li, N., 2009. Investigation of the dynamic and fatigue properties of fiber-modified asphalt mixtures. *International Journal of fatigue, 31(10), 1598-1602*.

[143] Ye, Z. and Jian, L., 2019. The Effect of Fiber on the Performance of Open Graded Friction Course (An Environmental Survey). *Ekoloji Dergisi*, (107).

[144] Zander, N. E., Gillan, M., and Sweetser, D., 2016. Recycled PET nanofibers for water filtration applications. *Materials, 9(4), 247*.

[145] Zhang, C., Li, Y., Wang, W., Zhan, N., Xiao, N., Wang, S., Li, Y., and Yang, Q., 2011. A novel two-nozzle electrospinning process for preparing microfiber reinforced pH-sensitive nano-membrane with enhanced mechanical property. *European polymer journal, 47(12), 2228-2233*.

[146] Zhang, D., Birgisson, B., Luo, X., and Onifade, I., 2019. A new short-term aging model for asphalt binders based on rheological activation energy. *Materials and Structures, 52, 1-22*.

[147] Zhang, H., Li, H., Zhang, Y., Wang, D., Harvey, J., and Wang, H., 2018. Performance enhancement of porous asphalt pavement using red mud as alternative filler. *Construction and building materials, 160,* 707-713.

[148] Zhang, J., and Seeger, S., 2011. Polyester materials with superwetting silicone nanofilaments for oil/water separation and selective oil absorption. *Advanced Functional Materials, 21(24), 4699-4704*.

[149] Zhang, L., Xing, C., Gao, F., Li, T. S., and Tan, Y. Q., 2016. Using DSR and MSCR tests to characterize high temperature performance of different rubber modified asphalt. *Construction and Building Materials, 127, 466-474*.

[150] Zhu, Y., Li, Y., Si, C., Shi, X., Qiao, Y., and Li, H., 2020. Laboratory evaluation on performance of fiber-modified asphalt mixtures containing high percentage of RAP. *Advances in Civil Engineering, 2020, 1-9.*

[151] Zong, X., Kim, K., Fang, D., Ran, S., Hsiao, B. S., and Chu, B., 2002. Structure and process relationship of electrospun bioabsorbable nanofiber membranes. *polymer, 43(16), 4403-4412*.